Refractometry by Total Reflection

by

Mickey E. Gunter

Dissertation submitted to the Faculty of the

Virginia Polytechnic Institute and State University

in partial fulfillment of the requirements for the degree of

Doctor of Philosophy

in

Geological Sciences

APPROVED:

F. Donald Bloss, Chairman

Susan C. Eriksson

Guy J. Indebetouw

Paul H. Ribbe

J. Alexander Speer

October 1987

Blacksburg, Virginia

Refractometry by Total Reflection

by

Mickey E. Gunter

F. Donald Bloss, Chairman

Geological Sciences

(ABSTRACT)

Refractometry is a means to measure the refractive indices of liquids, gases, and dielectric solids, either isotropic or anisotropic, by observation of light refraction or reflection with a microscope, refractometer or other more specialized equipment. For anisotropic solids, refractometry by total reflection (RTR) is by far the simplest, most rapid, and precise method to determine the refractive indices, provided a polished surface of sufficient size exists. Its precision exceeds that for routine oil immersion techniques but compares less favorably to that for minimum deviation methods. However, minimum deviation requires large crystals and, moreover, specifically oriented prisms, one for each principal refractive index to be measured and, for triclinic crystals, one for each wavelength of measurement.

The phenomenon of polarized light reflection from randomly oriented anisotropic materials has been modeled because, only after a complete understanding of these phenomena could the RTR method be automated. The mathematics and physics required for this stem from theories and equations presented in the literature of ellipsometry, polarized light, and physical optics. These were then modified, rewritten, and unified to suit the requirements of RTR.

RTR, first used by Wollaston (1802a, 1802b), was later perfected for the measurement of the refractive indices and orientation of biaxial minerals in thin section (Viola 1899a, 1899b, 1902; Cornu 1901, 1902). RTR with the Abbe-Pulfrich refractometer yielded refractive indices to a precision of ± 0.0002, or better. Later, Smith (1905a, 1905b) introduced a simpler refractometer, now known as the jeweler's refractometer, which had a precision of ± 0.001 to ± 0.002. This

refractometer is still in use by gemologists. During this century familiarity with the early work has declined; thus several recent papers display a lack of knowledge of aspects of RTR which were already documented in the early 1900s.

A new automated refractometer, designed by Bloss, has precision of ± 0.0002 and will be able to measure the refractive indices and orientation of a biaxial mineral in a petrographic thin section. Even for triclinic crystals, a single polished surface arbitrarily oriented will suffice for measurement of all three principal refractive indices, whatever the wavelength supplied. The design and testing of this refractometer has taken approximately three years. Two prototypes have been built and tested. Results from the second prototype are presented.

Acknowledgements

KDI Electro-Tec of Blacksburg is gratefully acknowledged for their support of my work and this project. I thank the many engineers, administrators, and machinists of Electro-Tec who helped in this project, but Randy Bradley, Tony Martin, Harold Hankins, Kerry Hay, Wendell Hensley, Bill Keeney, Sam Nauman, and Kevin Walsh, in particular. I especially thank Dr. J.A. Speer for all the critical reviews of my writing and thought that he freely rendered, thereby vastly improving my abilities as a scientist.

I thank the members of my committee for critically reviewing and improving this work, especially Dr. G.J. Indebetouw who provided advice on some basic optical, physical, and mathematical questions raised during the course of this work. I am grateful to Dr. S.C. Su, my office mate, for his many conversations and the mathematical help given this work. Enough thanks cannot be bestowed upon my advisor, Dr. F.D. Bloss, for all the support, in many forms, he has given me. I would like to thank him for the opportunity to pursue my education and work with him on this project; he is and always will be a source of inspiration to me.

Lastly, I would like to thank Suzy Aaron, my wife, for the encouragement to return to school for a Ph.D. and the required support to bring that goal to a successful completion.

Table of Contents

List of Illustrations

List of Tables

Chapter 1. Introduction

This chapter briefly introduces problem areas which arose during the course of development of the Bloss Automated Refractometer[1] (BAR). To solve them, a complete understanding of the data acquired from the BAR and a theoretical understanding of light reflection from anisotropic samples was required. The remaining chapters of this dissertation detail the specific topics introduced in this chapter.

The development of the BAR was a team project involving both engineers and scientists. My original involvement with this project was to be use of the BAR to measure the refractive indices of anisotropic samples. However, as the project progressed I became more involved in development and obtaining solutions to problems which arose. The two areas to which I devoted most of my efforts were: 1) unification and development of a mathematical procedure to describe the behavior of polarized light reflection from anisotropic samples and 2) from this treatment better understand the data being obtained from the BAR. To a lesser extent I was also involved in: 1)the development of the optical design of the BAR in conjunction with Randy Bradley, 2) the development of computer algorithms to determine the refractive indices and optical orientation of

[1] U.S. Patent 4692024.

anisotropic materials with F.D. Bloss and S.C. Su, and 3) the computer implementation of these algorithms with Tony Martin.

The BAR

A rediscovery of a forgotten optical method in 1980 led Prof. F.D. Bloss to invent what has since become known as the Bloss Automated Refractometer[2] (BAR) in 1984. The rediscovered technique, modernized by use of laser light, computers, and full automation, permits the three principal refractive indices of a biaxial sample, plus the orientation of its indicatrix, to be determined from a single randomly oriented polished section of a mineral. Like many other refractometers, the BAR works on the principal of total reflection. To distinguish this method from other techniques of measuring refractive index, the phrase "refractometry by total reflection," or RTR for short, was coined. The RTR method has been tested on several anisotropic samples and Davis (1985) used the method to determine all the principal refractive indices of muscovites from a (001) cleavage surface, even α, whose principal vibration is almost perpendicular to (001). Sample size must be at least 1 mm in diameter for use with current refractometers. This limits their usefulness to mineralogists. The main design objectives of the BAR were to reduce the sample size to 0.1 mm in diameter and to automate the process of data collection and data analysis.

Development of the BAR occurred in two distinct phases. The first phase involved the designing and building of two prototypes at Electro-Tec Inc., a KDI company in Blacksburg, Virginia. U.S. patent 4692024 describes the designs of these two prototypes which have become known as the online BAR (Fig. 1, U.S. patent 4692024) and the angular BAR (Fig. 2, U.S. patent 4692024). First the online BAR was built and tested. Although it proved very difficult to align, the results from it were promising. Next the angular BAR was built and tested. Its alignment proved to be less of a problem, and with this device we obtained refractive indices for isotropic samples with

---

[2] U.S. Patent 4692024.

±0.0002 precision. The interpretation of the results from these prototypes was initially hampered because the behavior of light, when reflected from a surface, particularly the surface of an anisotropic medium, was not well understood.

During the first phase of development, it had become apparent that non-normal reflection of light by a mirror or polished crystal surface caused unforeseen but significant changes in the intensity and polarization state of the light. At this point it was decided that the second phase in the development of the BAR should include an effort to understand thoroughly the physics of light reflections and, equally important, to develop the mathematical means to model the behavior of light as it passed through the BAR. Unfortunately, no unified treatment of the behavior of reflected light after non-normal incidence could be located. Instead, the theory was widely spread, as bits and pieces, in the literature of refractometry, of ellipsometry, of ore microscopy, and of physical optics.

The second phase then began with a search of the literature on refractometry, on polarized light, and on ellipsometry. As the search continued it was apparent that most, if not all, of the post-1900 investigators were unaware of the early 19th century literature, which had described some highly quantitative work as well as sophisticated mathematics. By contrast, the post-1900 researchers had become less quantitative and, indeed, raised questions that had already been answered by the earlier works. A detailed review of the literature, both pre- and post-1900, is given in Chapter 2.

The empirical results obtained during phase 1, after study of the literature and obtaining a better mastery of the physics of reflected light, could now be interpreted in terms of: 1) non-normal reflections of polarized light; 2) a thorough understanding of the data collected by the BAR (the Rpl-vs-I scans); 3) developing the algorithms necessary to analyze the data; and 4) improvement of the optical design of the BAR. Each of these topics will now be discussed briefly. More complete discussions will follow in later chapters.

Non-normal reflection of polarized light

Optical crystallographers routinely observe the interaction between transmitted polarized light and crystals to determine the optical properties of minerals and identify them in thin section. In contrast, ore microscopists identify the opaque ore minerals by qualitative or semiquantitative observations of light intensities after the light, normally incident upon polished surfaces of these minerals, is reflected backward. However, even leading textbooks on ore microscopy fail to provide an adequate discussion of the principles underlying this simplest case, reflection of light after normal incidence. On the other hand, RTR involves non-normal reflection of polarized light by the materials under study. In the early stages of development of the BAR it was assumed that the orientation and form (i.e., elliptical, circular, linear, or random) of polarized light would not change significantly upon reflection from the sample or the metal mirrors used in the BAR's optical system (i.e., linearly polarized light reflected from a metallic mirror would essentially retain the same direction of polarization and remain linearly polarized after reflection). Research into the reflection of polarized light from dielectrics and metals later showed these assumptions to be invalid. It then became necessary to understand the polarization-altering characteristics produced by the BAR's optical system and by the samples -- both isotropic and anisotropic. If a mathematical treatment could be developed or found to quantify these polarization changes in terms of the angle of incidence and optical properties of the reflecting surfaces, then it could be determined whether the polarization-altering effects were significant and, if so, how to compensate for them.

A review of polarized light literature yielded many of the equations, in various sources and forms, needed to describe light reflection from isotropic dielectrics and metals. The Fresnel equations serve to calculate the intensity of a reflected light beam as a function of its angle of incidence and of the refractive indices of the reflecting material and of the material in which the incident ray travelled prior to reflection. The results from these equations show that, in general, even when linearly polarized light is reflected from an isotropic dielectric (e.g., a piece of glass or fluorite) the state of polarization of the reflected beam will differ from that of the incident polarized beam.

For metallic reflection, both the extinction coefficient and the refractive index of the metal enter the Fresnel equations. Calculations for metallic reflections show that, in general, when linearly polarized light is reflected from a metal, the reflected beam's orientation is changed and, in addition, it becomes elliptically polarized. The changes in rotation and polarization form depend upon the angle of incidence and optical properties of the material. The greater the angle of incidence the more the incident and reflected beams will differ in polarization state. In ellipsometry, optical devices called ellipsometers serve to measure quantitatively the changes in polarization state of polarized light after its reflectance at non-normal incidence from a sample.

The Jones calculus, which is described in the literature of polarized light and of ellipsometry, constitutes a marvelously succinct means of calculating, and following quantitatively, the alteration in the polarization states of light as it is transmitted or reflected by the optical components of a system. In the Jones method, the required equations can be written in matrix form. Thus, any optical component of the system can be expressed as a 2x2 matrix. Any polarization state of light can be expressed as a 2x1 vector. To model the effect of an optical element on a particular polarization state, the matrix and vector are multiplied. The resulting vector then describes the intensity and polarization characteristics of the reflected beam. The Jones method simplifies the mathematical calculations for polarized light, but more importantly it provides the only practical method to calculate light reflection from a randomly oriented anisotropic material, such reflection involving the mathematical relationships that are considerably more complicated than for isotropic samples.

The theory and equations required to calculate the intensity and polarization state of light reflected by a given surface were modified and unified so they could be applied to our problems in RTR. These equations predicted the effects the metallic mirrors of the BAR would have on the light as it propagated through the system. More importantly, these equations can be used to calculate light intensity and polarization states after reflection from anisotropic samples in random orientations.

Rpl-vs-I scans

The data obtained from the BAR have become known as Rpl-vs-I scans. Rpl is an angle which is mathematically related to the angle of incidence. The I refers to the intensity of the reflected beam. The concept of total reflection -- when the total light energy of a beam is reflected back into the incident media and none crosses the interface to be transmitted -- is the fundamental principle by which RTR works. Originally the point on the Rpl-vs-I scan at which total reflection occurred was to be located; then by using Snell's law the material's refractive index could be calculated. However, the first Rpl-vs-I scans obtained for isotropic samples lacked such sharp inflection points. Thus, as Rpl increased, the intensity rose as expected; however, no sharp change in intensity occurred as the angle of incidence (or Rpl) approached the critical angle for the sample. Consequently, the point on these Rpl-vs-I scans that corresponded to the critical angle was not recognizable. Moreover, at this stage in the investigation, the mathematical relationship between the intensity of the incident beam and that of the reflected beam as the Rpl angle was increased had not been developed to apply to BAR data; thus there was not a complete understanding of the data the BAR produced.

The intensity of the and reflected beam relative to that of the incident beam, as the Rpl angle is varied, can be estimated using the Fresnel equations; indeed, the Rpl-vs-I scans from the BAR were basically equivalent to plots of the Fresnel equations. Despite this equivalence, the Rpl-vs-I scans differed significantly from the Fresnel equations. To illustrate, if the Fresnel equations are graphed as a function of the angle of incidence, the graph would show a sharp change in intensity at the critical angle. By contrast, the empirical Rpl-vs-I scans developed a rounded "knee" rather that a sharp knee at the critical angle. By adding to the Fresnel equations a mathematical expression, which defined the intensity of the laser beam used on the BAR, the measured Rpl-vs-I scans could be reproduced theoretically. Several other factors were found which contributed to the Rpl-vs-I; however, the Fresnel equations, modified to accommodate the laser beam model, proved the most significant.

Prior to the above mathematical developments, the differences between the observed Rpl-vs-I scans for quartz and those for calcite could not be explained. Rpl-vs-I scans for calcite exhibited two "knees", one for ω and one for ε. While quartz only showed one knee. After a thorough understanding of the Rpl-vs-I scans was obtained, the differences between quartz and calcite could be explained by their differences in birefringence and the angular convergence of the focused laser beam used to illuminate the sample. Because the BAR uses a focused laser beam, as mentioned above, there was a rounding of the "knees" for the Rpl-vs-I scans for isotropic and anisotropic samples. Quartz's birefringences is small enough that this effect tended to mask the two "knees".

Rotation of the plane of polarization first became apparent from Rpl-vs-I scans of calcite. With polarizers inserted in the BAR's optical system, we empirically found that linearly polarized light was significantly rotated after reflection. By use of the Jones calculus developed for anisotropic samples, it is easily shown that significant rotations of polarized light can be expected.

Algorithms

Because the BAR is being developed as an automated system, computer algorithms are required to determine the refractive index, for both isotropic and anisotropic samples, from the Rpl-vs-I scans and, for anisotropic samples, to determine all principal refractive indices and the optic orientations.

The first algorithm developed for refractive index determination from the Rpl-vs-I scans was purely empirical, because at that time the theory and equations to model the Rpl-vs-I scans had not yet been developed. Later another method, far superior to first, was developed from the Fresnel equations as modified for a laser source.

It was originally thought that the Rpl-vs-I scans would contain two inflection points which could be used to determine the principal refractive indices and their orientations for an anisotropic

sample. However, as previously explained this is, in general, not the case. Thus another method was devised based on the Joel equations and the EXCALIBR computer program of Bloss (1981). This method assumed that reflected polarized light behaved in a manner similar to transmitted light; however, this is not correct, and thus the method failed. The third method that has been developed takes full advantage of our understanding of the Rpl-vs-I scans and the behavior of reflected light.

BAR optical designs

A new design for the BAR -- called the crystallographic BAR -- was developed based upon the prototype BARs, a complete understanding of the Rpl-vs-I scans, and the theory of reflected light. Many of the optical components of the early BARs were modified or eliminated altogether. An optical design program was used to optimize this new BAR. Currently work is underway to assemble this version of the BAR for testing.

Conclusions

At the beginning of this project we made several assumptions based upon our limited knowledge of RTR and the lack of sophistication of recent articles on the subject. After a literature review it was found that the RTR method had been perfected in the late 1800s and early 1900s, but that during this century the knowledge of the method has declined. Recent authors make incorrect statements and assumptions, much as we did in the early part of this work. However, we devoted a tremendous amount of time and effort in an attempt to understand all aspects of RTR and thus to determine which of our assumptions were incorrect. The main goal was to unify the various aspects of reflected light research and to modify this body of knowledge so it could be applied to RTR. From this new algorithms, based upon theory instead of empirical observations, were de-

veloped. Also the optical design of the BAR was modified and optimized from the original patent because of this newly acquired knowledge.

Chapter 2. Review of RTR

Early RTR

Wollaston (1802a, 1802b) was the first to use RTR and the principle of total reflection to determine the refractive indices and dispersion of several dielectrics.[3] Total reflection, which is discussed in most introductory optical mineralogy textbooks, occurs if a light ray moves from a material of higher to one of lower refractive index at an angle of incidence that equals or exceeds the critical angle (Figure 1). Quantitatively the phenomenon is described by Snell's law (Eqn. 2.1a).

$$n_i \sin \theta_i = n_t \sin \theta_t \qquad [2.1a]$$

where,

n_i = refractive index of incident media
θ_i = angle of incident ray
n_t = refractive index of transmitting media (i.e., unknown)
θ_t = angle of refracted ray

When total reflection is reached, θ_t equals 90° and Snell's law can be rewritten:

$$n_t = n_i \sin \theta_{CA} \qquad [2.1b]$$

---

[3] The term dielectric is used to specify a material, unknown, sample, crystal, etc. whose refractive index can be entirely specified by n, the real part of the refractive index, its imaginary part being zero.

where,

θ_{CA} = critical angle

In RTR the angle of incidence can be measured and if the refractive index of the incident material, the hemicylinder in Figure 1, is known, n_t can be calculated from Eqn. 2.1b.

Figure 1 shows rays labeled I_1 to I_3 which travel from air into a hemicylinder with a high refractive index (commonly 1.8 to 1.9); this is the common design of the jeweler's refractometer (Hurlbut, 1984). A portion of the incident beam is refracted into the unknown material and the remainder simultaneously reflected into the hemicylinder. The angle of the refracted ray (θ_t) is found from Snell's law (Eqn. 2.1a) while the angle of the reflected ray is equal to the angle of the incident ray (θ_i), by the law of reflection (Bloss, 1961, p.8). In Figure 1, I_3 is incident at θ_{CA} the critical angle at which total reflection occurs. For rays with an angle of incidence equal to or greater than θ_{CA} the entire energy of the incident beam is reflected. Rays I_1 and I_2 are partially reflected and partially transmitted; the ratio of the reflected beam's to the incident beam's intensity can be calculated by the Fresnel equations (Hecht and Zajac, 1979, p.74).

$$r_s = \frac{n_i \cos\theta_i - n_t \cos\theta_t}{n_i \cos\theta_i + n_t \cos\theta_t} \qquad [2.2a]$$

$$r_p = \frac{n_t \cos\theta_i - n_i \cos\theta_t}{n_t \cos\theta_i + n_i \cos\theta_t} \qquad [2.2b]$$

where,

r_s = amplitude coefficient normal to plane of incidence

r_p = amplitude coefficient parallel to plane of incidence

The intensity equals the amplitude squared, thus:

$$R_s = r_n^2 \qquad [2.3a]$$

$$R_p = r_p^2 \qquad [2.3b]$$

where,

R_s = reflected ray's intensity normal to plane of incidence

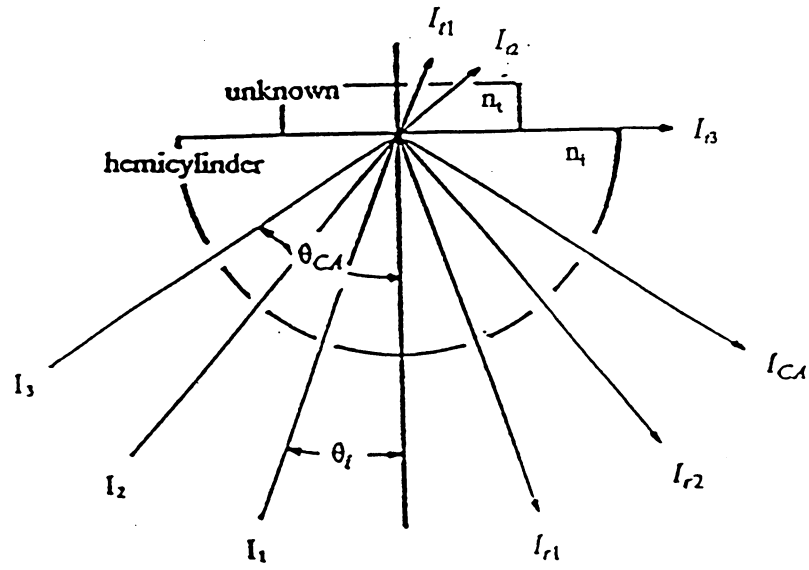

Figure 1. Hemicylinder/unknown interface showing reflection and refraction: The incident rays I_1, I_2, and I_3 are incident upon the unknown at different angles. I_3 is incident at θ_{CA}, thus all of its energy is reflected into ray I_{CA}; the angle of incidence of this ray can be used to determine the material's refractive index. Rays I_1 and I_2 are incident at angles less than θ_{CA} and are partially transmitted as rays I_{t1} and I_{t2}, and partially reflected as rays I_{r1} and I_{r2}. The intensity of these latter two rays can be calculated from Eqns. 2.2 and 2.3.

R_p = reflected ray's intensity parallel to plane of incidence

The principal refractive indices and orientation can be found for any dielectric and its optical class determined (i.e., whether the material is isotropic, uniaxial, or biaxial). By use of Snell's law and measurement of the angle of total reflection, θ_{CA}, the refractive index for an isotropic dielectric can be readily found. The method of total reflection can also be employed in refractive index determination for anisotropic dielectrics by making critical angle measurements while rotating the sample about the normal to the hemicylinder's flat upper surface (Figure 1), and varying the polarization orientation of the incident beam. By analysis of the varying critical angles obtained in this process, the principal refractive indices for an anisotropic dielectric can be obtained.

Two other methods are used to determine the principal refractive indices of solids: 1) minimum deviation and 2) oil immersion. The former can attain six decimal place precision; however, this level of precision can only be attained with the use of large polished prisms of the solid under study. Minimum deviation is used for refractive index and dispersion measurements of some isotropic samples. The sample preparation, cutting and polishing of oriented prisms, precludes its use for anisotropic samples. Oil immersion methods can be used to obtain the refractive indices of transparent solids to third or fourth decimal precision. The former method being more common. Fourth decimal place precision of anisotropic solids can be achieved by oil immersion and use of the spindle stage (Bloss, 1981).

Using an idea from Newton, Wollaston (1802a) made the first refractometric measurements on a prism of glass. With his refractometer he measured the refractive indices of over fifty isotropic materials. He even used RTR to determine if a material found on a Pacific island was bee's wax and to measure the refractive indices and dispersion of calcite to the third decimal place (Wollaston, 1802b). Later, Abbe (1874) developed a refractometer which is still cited in current text books (Phillips, 1971, p. 62). This refractometer was sold by Zeiss up to 1945 at which time it was redesigned and sold in its current form (Höfert, 1962).

High precision RTR with anisotropic crystals

The techniques for the measurement of refractive indices and optical orientation from a single polished section of a biaxial material were refined in the late 1800s. During this time three basic types of refractometers were developed (Tutton, 1922, p. 1016-1035). The first type, the Kohlrausch and Miers' suspended goniometer, submerged a polished crystal section into a high refractive index liquid. A precise knowledge of the liquid's refractive index (n) during the course of the measurements was required for the Miers' refractometer. For precise measurements the liquid's dn/dt must be known and temperature (t) corrections applied as necessary. Soret modified this type of refractometer to simultaneously measure the refractive index of the liquid and the unknown, thus removing the uncertainty of the temperature corrections required for Miers' refractometer. The second type of refractometer, based on Wollaston (1802a), placed a polished crystal surface in optical contact with a high refractive index glass prism. The Liebisch refractometer was of this design. The refractive index and dn/dt of the prism could be better characterized than that for the liquids used above; thus it improved the accuracy of RTR. The third type, commonly known as the Abbe-Pulfrich refractometer, employed a high refractive index hemisphere, upon which the polished sample was placed. The need to rotate anisotropic samples during critical measurements would produce scratches in the prism of the Liebisch refractometer. Use of the hemisphere in the Abbe-Pulfrich refractometer allowed the sample and hemisphere to rotate as a unit, thus reducing the possibility of scratching. All of these refractometers worked on the same principle -- to measure the refractive indices by finding the angle of total reflection and then using Snell's law to find n of the unknown.

Soret (1888a) described the basic method for determining the refractive indices of biaxial minerals with a refractometer. He proposed a method to find α, β, and γ of a biaxial crystal by making critical angle measurements on any polished surface. Four "special" refractive index values were obtained. The highest corresponding to γ, the lowest to α. Of the remaining two values, one is β, the other is an orientation-dependent refractive index called the orientation index and denoted

by n_{oi}. Soret proposed distinguishing the two by repeating the measurements on a different crystal face, in which case the value of n_{oi} will change whereas β, within experimental error, will remain constant.

Perrot (1889) verified Soret's (1888a) method by using the Soret refractometer to make measurements on seven different crystal faces of a tartaric acid crystal. He obtained constant values for three of the four critical angle measurements, while the fourth value -- the n_{oi} -- varied. The standard deviation of the seven measurements he made for α, β, and γ, were 0.00020, 0.00010, and 0.00008, respectively.

Soret (1888b) described the view of the shadow boundaries as seen through the telescope of his refractometer when a biaxial crystal had been cut perpendicular to an optic axis. In this special orientation the interpretation of the shadow boundaries was more difficult than in a random polished section. Nevertheless, even in this orientation all the principal refractive indices could be obtained.

Soret (1889) built on the mathematics derived by Brill (1889) to determine the orientation of the optical indicatrix from measurements made on the refractometer. For this technique, one of the principal vibration directions must be in the polished surface. Lavenir (1889) described a method to find a crystal's orientation by means of two different polished sections oriented with respect to one another.

The Abbe-Pulfrich refractometer, described by Pulfrich (1899) and Viola (1899a), was equipped with a hemisphere and permitted more precise measurement of refractive indices. It could be used both with light incident from below, as in RTR, or with light incident from above, which is referred to as grazing incidence. With grazing incidence the actual wave surface of a biaxial crystal could be imaged and photographed below the hemisphere (Tutton, 1922, p. 1032). Wave surface theory is akin to indicatrix theory; both show the relationship between a material's principal vibration directions and the geometric interpretation of light interaction with them. Thus, given the

wave surface for a material, the magnitude and direction of its principal vibration axes can be determined. The wave surface theory was employed in these earlier works in optical crystallography.

Abbe was responsible for the development of at least two different refractometers which serve different functions and have different forms; but both are called Abbe refractometers. The refractometer invented in 1874 was intended primarily for the measurement of liquids and, even with its redesign in 1945 (Höfert, 1962), it is still used mostly for liquids. This is the common Abbe refractometer in use today. The refractometer described by Pulfrich (1899) is also called an Abbe refractometer but differs considerably in function and design from the earlier model. This refractometer, not commercially available, is also called the Abbe-Pulfrich refractometer and is here referred to as such. The Abbe-Pulfrich refractometer was designed for use with crystals; in fact Drude (1959) refers to it as Abbe's crystal refractometer. The major difference between the two refractometers is that the Abbe refractometer uses a fixed prism while the Abbe-Pulfrich refractometer employs a rotating hemisphere as its measuring element.

Possibly Viola made the greatest contributions to the field of RTR. Viola (1899a) measured a series of refractive indices for calcite and for the Lakos albite. For each material he measured the refractive indices for nine of the Fraunhofer lines, thus determining not only their refractive indices but also their dispersion. To test precision he repeated his measurements seven times for α and β and ten times for γ of the albite. The calculated standard deviations for these observations are 0.00052, 0.00020, and 0.00028, respectively which are somewhat greater than those of Perrot (1889) stated above. Viola comments in a footnote that the probable errors of his measurements are 0.00033, 0.00013, 0.00017 for α, β, and γ. Even the larger errors, however, are much smaller than those commonly accepted in modern day optical crystallography.

In his next paper, Viola (1899b) concentrated more on mathematics and theory than on empirical observations. The major contribution of this work was a plot showing how the two refractive indices observable at any orientation of the polished grain changed as the grain is rotated. These curves (Figure 2), hereafter referred to as the Viola curves, prove very useful in qualitatively

understanding and quantitatively modeling the behavior of anisotropic crystals studied with a refractometer. The maximum of the upper curve, the N curve, is γ while the minimum of the lower curve, the n curve, is α. β and n_{oi} appear on the curves as either the minimum of the N curve or the maximum of the n curve. Because α, β, and γ must be orthogonal, Viola used a stereographic plot to distinguish β from n_{oi}. Thus, he plotted α and γ and then determined whether the direction represents the maximum of the n curve or the minimum of the N curve was orthogonal to them; whichever was orthogonal he assigned to be β. This method differs from that of Soret in that now all the observations necessary to determine all the principal refractive indices can be determined from a single arbitrarily oriented, polished surface through the crystal.

In a later paper Viola (1902) restates his earlier work and adds a description of polarization phenomenon involved in RTR. He uses the vibration direction to distinguish the orientation index from β. The orientation index is discriminated from β because the orientation index will have its vibration direction parallel to the plane of incidence, for a randomly oriented biaxial material; the β direction will never be parallel to the plane of incidence if the crystal is randomly oriented.

Cornu (1901, 1902) significantly contributed to RTR literature by presenting a method to find α, β, and γ, and distinguish between β and n_{oi} from a single random cut through the indicatrix (Cornu, 1901). Cornu (1902) discussed the method to determine the orientation of the biaxial indicatrix from observations made on the refractometer. He presented the necessary mathematics and theory to derive the orientation and states the limitations of the method for finding the orientation. Regardless of the crystal's orientation, all three principal indices can always be observed; however, if the crystal is oriented with a principal vibration direction nearly perpendicular to the hemisphere's flat upper surface, one of the Viola curves becomes almost flat and the data required to calculate the orientation cannot be determined precisely enough to yield the orientation.

Subsequent to the the works of Viola and Cornu, precise work in the RTR of anisotropic crystals halted; Wright (1911) and Tutton (1922) provide the best reviews on the subject of RTR.

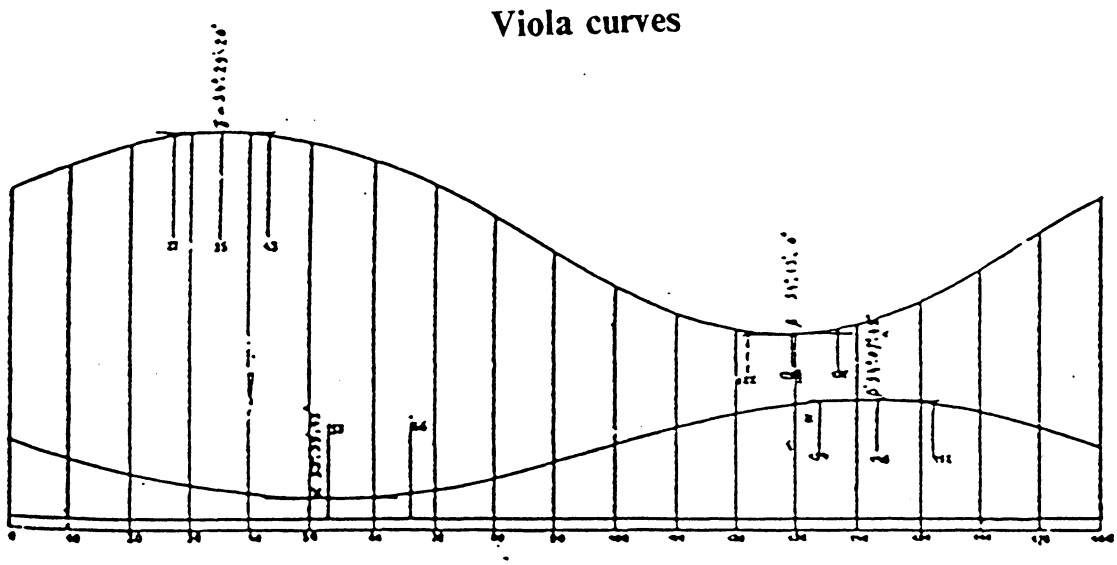

Figure 2. **Viola curves:** The two curves above show how N and n change for an anisotropic crystal during a 180° rotation on the refractometer's hemisphere. The horizontal scale represents a 0° to 180° rotation of the crystal about a normal to its polished surface while the vertical scale represents critical angle in degrees. The upper curve's (the N curve) maximum value is γ while the lower curve's (the n curve) minimum value is α. The minimum on the N curve or the maximum on the n curve corresponds to β and n_{Oi}, Viola explains a method to distinguish between the two.

A review of the mathematical theory involved in RTR was presented in Pockels (1906) and Szivessy (1928). These two sources, both in German, describe all the theories put forth by Brill, Cornu, Soret, and Viola. These two references contain full explanations of partial reflections, polarization phenomenon before and after total reflections, stereographic projections, etc. Ramachandran and Ramaseshan (1961) probably present the most thorough English reference on the subject; however, it falls far short of the more detailed earlier reviews. The Indian authors, writing in a German encyclopedia in English, describe much of the theory of crystal optics and polarization phenomenon in great detail, but have only three paragraphs on total reflection and a few pages on the theory behind it. They refer the interested reader to Pockels and Szivessy for the theoretical details.

Tilton wrote several articles on the precise determination of refractive indices of liquids and isotropic solids. For six-decimal-place precision he used minimum deviation for isotropic solids and wrote several detailed articles on the requirements to achieve this precision. He also wrote two articles (Tilton, 1942; 1943) which detail the requirements for fifth-decimal-place RTR, which he states is the limit of the method.

Low precision RTR - the introduction of the jeweler's refractometer

The refractometers described thus far were all precision laboratory instruments capable, in the right hands, of determining refractive index to a precision of at least ± 0.0002. Smith (1905a) invented a very simple handheld refractometer. His device, based on an idea by Bertrand (1885), who was also the first to suggest the use of a hemisphere, allowed one to measure the refractive indices of crystals at least 1 mm in diameter, within the range of $1.40 < n < 1.76$ with a precision of ± 0.001 to ± 0.002. This refractometer later evolved into the jeweler's refractometer. Although his design served a needed function of both ease of use and portability, which was accomplished, among other things by a reduction in precision, it started the decline of precision RTR. Because

he did not have a rotating hemisphere, as in the earlier Abbe-Pulfrich refractometer, anisotropic samples had to be rotated upon hemisphere's soft glass surface. The hemisphere required repolishing to remove the inevitable scratches resulting from this rotation. Smith (1905b) improved on his earlier design by extending the refractive index range to 1.77 and changing the instrument's geometry so the hemisphere's flat upper surface could be repolished more easily. Tully (1927) modified Smith's refractometer by adding a rotating hemisphere to avoid the scratching problem. His design basically added a rotating hemisphere to the Smith refractometer, as in the Abbe-Pulfrich refractometer, a feature Smith had excluded for simplicity.

Anderson et al. (1940) tried to extend the high refractive index range of gem refractometers by using higher refractive index liquids and hemispheres. All of the high refractive index liquids they cite have "unpleasant" properties. Many of them chemically attack the soft leaded glass hemispheres and are not stable when exposed to the atmosphere. West's liquid (n = 2.00), for example, explodes if not stored correctly. They used it, however, along with a diamond refractometer, to measure the refractive indices of zircons. They concluded no satisfactory liquid exists above n_D = 1.81 and stated "One can only hope that a suitable liquid having a refractive index of over 2.0 and no unpleasant properties will eventually be discovered for use with diamond or blende refractometers." To this day their hope has not materialized.

Instead of the usual soft, leaded glass hemisphere Anderson et al. (1940) employed a diamond prism (n_D = 2.419), because they could not fabricate diamond into a hemisphere. They also made a refractometer with spinel (n_D = 1.7266), which had the advantage of using white light, because spinel's low dispersion yielded sharp boundaries and not the usual spectrum boundary which occurred in white light for refractometers with hemispheres of a higher dispersion. Both diamond and spinel solved the problem of scratches which resulted from the soft glass. The latest material used for the hemisphere of a refractometer is cubic zirconia (CZ) (Hurlbut, 1981). Zirconia (ZrO_2) is anisotropic but by addition of yttria (Y_2O_3) the structure becomes isotropic (Gunter, AR-1986a).[4]

---

[4] References prefixed with AR- refer to Automated Refractometer reports written at Electro-Tec during BAR development. A list of the reports is given in the Appendix.

CZ is the perfect material because of its high hardness (approximately 8.5), high refractive index (approximately 2.16), its ability to be machined, and its chemical resistance.

•

Current trends in RTR of anisotropic crystals - uses in gemology

Burbage and Anderson (1941) discussed "movement of shadow-edges" of gemstones, which was in essence a rediscovery of the Viola curves (Viola, 1899b). A mathematical approach was presented to calculate the Viola curves and a formula was included which allows one to discriminate between β and n_{oi}. An example of a Viola curve is shown for topaz in a random orientation, also two sets of Viola curves are presented for uniaxial positive and negative crystals oriented with their c-axis normal to the hemisphere's upper surface and three sets of curves are drawn for biaxial minerals with X, Y, and Z, respectively, normal to the hemisphere's surface. In their paper they did not cite any of the earlier literature on the subject of RTR. If they had reviewed the early literature they would not have made the statement "... it might be possible, for instance, to develop a technique for the ascertainment of the optical orientation of any facet of a gemstone from a set a refractive index readings derived from it." The ability to determine fully a biaxial crystal's orientation from refractometer readings had already been discussed by Cornu (1902). Burbage and Anderson (1941) cite precision of their observations as ± 0.001 to ± 0.005.

Another apparent rediscovery of the Viola curves was made by McKague (1971). He presented three examples of uniaxial crystals and ten of biaxial, thus giving all the possible random and special orientations for anisotropic crystals. McKague, like Burbage and Anderson, does not cite any of the early literature on the subject. It is obvious that he did not consult the existing literature, not even Burbage and Anderson, because he believed that before one can discriminate between a uniaxial and a biaxial mineral and determine the mineral's optical sign, its orientation must be known prior to its examination on the refractometer. This of course is not true because the orientation can be found from refractometer data. In regard to discriminating between β and n_{oi} he

stated in his conclusions "... there is no method of distinguishing if it is the high point on the lower curve or the low point on the upper curve." A method to distinguish between β and n_{oi} is given in the recent literature by Burbage and Anderson, and of course, is contained in the older literature. A final point he missed, along with almost every other author on this subject, is that rays are partially reflected before the critical angle (see Figure 1, rays I_{r1} and I_{r2}).

Hurlbut and Switzer (1979) presented a six-page introductory description on RTR of gemstones. In their Figure 6.12 showing the phenomenon of total reflection, they excluded any of the partially reflected rays, just as McKague did. This expression conveys the false impression that all the light is transmitted (refracted) into the crystal until the critical angle is achieved. In their discussion of RTR of biaxial gems, they provided a very good qualitative description of the phenomenon. However, like the early two papers, they failed to cite any of the classic older papers. Because of this oversight they gave an improper analysis of the movements of the shadows during grain rotation. They stated, starting in the last paragraph of p. 78, that the maximum value attained is γ and the minimum is α; however, they erroneously conclude that the maximum on the lower curve (the n curve) and the minimum of the upper curve (the N curve) on Figure 2 both equal β, when in fact, in a random orientation, these two values are not equal, one of them being β the other n_{oi}.

The most recent paper on RTR, and best of this series is Hurlbut (1984). In this paper Hurlbut referred to Wright (1911) for the early work with the Abbe-Pulfrich refractometers and their higher precision than the jeweler's refractometer. Hurlbut believed the oil immersion method caused abandonment of RTR. He referred to the problems in the McKague paper and explained how to distinguish β from n_{oi} by the orientation of n_{oi} being parallel to the plane of incidence, the same method as discussed by Viola (1902), which he did not cite. Hurlbut also described and used the Viola curves without citing Burbage and Anderson (1941) or Viola (1899a). He corrected the statement about the dissimilarity of β and n_{oi} made in the Hurlbut and Switzer book did not include any partially reflected rays on his Figure 1.1 showing total reflection. Hurlbut stated for anisotropic

crystals at the critical angle two rays, which would represent N and n, have a common wave normal, at total reflection; this statement only applies if N and n are equal (i.e., the mineral is isotropic).

Errors, omissions, and oversights naturally occur in research. But, the number and prevalence of mistakes and lack of reference to earlier literature seem to be very high in the area of RTR. The early optical crystallographers, Cornu, Soret, Viola, etc., understood the theory and made very precise measurements. In the more recent work of the gemologist, the theory is poorly understood, at best, and the precision is at least an order of magnitude less. However, RTR has been kept alive by the gemologist and their empirical use of it meets their needs -- the rapid non-destructive identification of gemstones. Were it not for the gemologist, this method would be totally lost, as is seen in the following review of optical mineralogy texts.

Status of RTR

The subject of RTR does not receive adequate coverage in the optical mineralogy textbooks. Winchell (1937) describes the Smith refractometer (Smith, 1905a), but does not mention that it can be used for the measurement of refractive indices of anisotropic solids. Bloss (1961), although he and Wahlstrom (1969) are the only mineralogy authors found who correctly illustrated the phenomenon of partial reflection of rays prior to total reflection, did not mention RTR. Bloss (1981, p. 180) described the use of a refractometer for the measurement of refractive indices of liquids. Wahlstrom (1969, p. 127) discussed RTR at length, mentioning nothing of anisotropic samples but illustrating the partially reflected rays correctly. Phillips (1971, p. 62) described the Abbe refractometer used for measurements of liquids but not for solids of any kind. Kerr (1977, p. 59) presents an eleven page description of RTR, and must be credited for pointing out that refractometers can be used for the measurement of refractive indices of anisotropic samples. He does not, however, give any details and omits the partially reflected rays in his Figure 4-5 (p. 66).

The refractometer, and the method of RTR, currently finds use in industry, testing labs and chemistry measuring the refractive index of liquids, and to a lesser extent of solids. In these areas a correlation between refractive indices and composition is required. For example the sugar content of water/sugar mixtures is measured by using a refractometer to determine the refractive index of the solution which in turn is correlated to the sugar content of the mixture. In mineralogy the refractometer is commonly used to check or calibrate the refractive indices of the liquids used in the oil immersion method. The refractometer is an important part of the spindle stage methods (Bloss, 1981). In this technique the refractometer is required to calibrate the refractive index liquids. It is only after the liquids have been correctly calibrated that immersion methods can be performed with fourth-decimal-place accuracy (Su et al., 1987).

Return to high precision RTR

In the summer of 1981 a student worker (Laura Davis) of Dr. Bloss, while measuring β and γ of mica flakes on a refractometer also observed, in certain orientations, the α value. To verify that a principal refractive index not in the plane of the refractometer's measuring prism could be measured, a calcite rhomb face was placed on the refractometer by the author and, indeed, ε was observed. We proceeded to measure ω, ε', and ε for calcite with a precision of approximately ± 0.0001. Next, a sample of topaz was obtained and polished on a random face and all three indices measured. At this point we thought we had made a great discovery, but later, like so many of the previous authors, we found we had just rediscovered an old method which had been lost in the literature. Davis (1985) went on to use this method to measure the refractive indices for twenty five muscovites.

From these observations originated the idea to produce a new refractometer, incorporating lasers and computers, to fully automate the process of refractive index measurements. Not only could all three principal refractive indices from a mineral in thin section be determined, but we

could also determine the orientation of its optical indicatrix. By using a focused laser beam we could make these measurements on grain diameters down to 100 μm; in comparison the jeweler's refractometer requires diameters of at least 1.0 mm. Moreover, precision was significantly increased.

Chapter 3. Automated RTR

Basic requirements for RTR

RTR is based upon the physical phenomenon of total reflection; given the angle of total reflection and the refractive index of the incident media, the refractive index of the unknown is calculated by Snell's law (Eqn. 2.1). To measure total reflection, an unknown is placed in optical contact with a material of higher refractive index, commonly a hemisphere (Figure 1). The sample is illuminated from below with light incident at various angles. The angle of incidence is varied until total reflection is reached and the critical angle measured. For anisotropic samples the above procedure is repeated while rotating the sample about a normal to the hemisphere's upper surface. The critical angle is measured at several positions during this rotation producing the Viola curves and Figure 2 and defining the material's principal refractive indices.

Sample requirements: RTR requires the use of polished flat surfaces of the material to be examined. Only a single surface is required for either isotropic or anisotropic materials. No quantitative information has been found describing either the "flatness" required or the quality of the polish (i.e., the scratch and dig terminology used in optical finishes). In routine work samples are commonly ground flat and polished by working through a series of successively finer grades of abrasive com-

pounds on a lapidary wheel; the final polish is performed with 0.3 μm to 0.05 μm Al_2O_3 powder on a felt wheel. Petrographic thin sections of rocks, with the cover slip removed, can be used provided the minerals to be examined are large enough. The jeweler's refractometer requires samples sizes at least 1 mm in diameter. Davis (1985) used 14 mm x 14 mm cleavage flakes of muscovite for her refractive index measurements. Obtaining a suitable polished surface presents no problem, however the sample size required for current use on the available refractometers greatly reduces the usefulness of RTR to mineralogists and petrologists. Ideally a refractometer should be able to measure grains as small as 50 μm to be useful for measuring refractive indices and determining petrofabric of minerals in thin section.

Refracting element: A refractometer's refracting element must have an index refraction higher than the unknowns to be measured. The majority of refractometers employ leaded glass, either in the form of a prism (the Zeiss-Abbe refractometer), hemicylinder (the current jeweler's refractometer), or hemisphere (the Abbe-Pulfrich crystal refractometer). However, the Kohlrausch refractometer employs a liquid for this purpose. One major problem in current refractometers is the widespread use of soft leaded glass (approximately 4 on the Moh's scale). When used for anisotropic samples, which must be rotated upon the hemisphere to generate data to produce the Viola curves, the upper flat surface becomes scratched and unusable. Also, certain refractive index liquids will chemically attack the leaded glass, equally rendering it useless. To alleviate this problem more resistant materials have been sought.

Gunter (AR-1986a) presents a list of possible materials to use for the refracting element. The desired requirements are: 1) high refractive index ($n > 2.00$), 2) hardness > 8 on the Moh's scale, 3) chemical inertness, 4) optical isotropy, 5) homogenous 6) ease of optical fabrication, and 7) low cost. He concluded yttria-stabilized zirconia (so called cubic zirconia or CZ) meets these requirements. Eight to fifteen mole percent Y_2O_3 is added to ZrO_2 to transform its structure from monoclinic to cubic. Its refractive index and hardness are approximately 2.16 and 8.5, respectively,

and both decrease with the addition of Y_2O_3. CZ was proposed for use in the jeweler's refractometer by Hurlbut (1981).

Contact liquid: The polished flat surface of the sample must make optical contact with the hemisphere. In other words, no air film greater than a small fraction of a wavelength in thickness should occur between them. There are two ways to facilitate optical contact: 1) use a liquid of appropriate refractive index and 2) prepare optically flat surfaces. The latter method is used for work in the IR, but for work in the visible, with shorter wavelengths, very high optical tolerances are required. Wollaston (1802a), the first to do RTR, used a liquid to make optical contact between his prism and the unknowns he wished to measure. The refractive index of the liquid used must exceed the refractive index of the unknown but, according to current literature, be less than that of the hemisphere. In the older literature, however, it is suggested that the refractive index of the liquid should be higher than that of the hemisphere; the point is moot because no suitable liquids exist with a refractive index higher than that for CZ. Indeed liquids above 1.81 have serious problems for routine uses in RTR. They are non-stable, corrosive, carcinogenic, explosive, opaque, etc. Ideally a stable, non-corrosive liquid with a refractive index similar to CZ needs to be found. Until this occurs, the upper limits of routine RTR will be limited by the index of the liquid.

Optics: Lenses and mirrors are used in refractometers to shape (image) and direct the incident and reflected light beams. The jeweler's refractometer and, indeed, most refractometers possess very simple optics. In the jeweler's refractometer, light reflected from the unknown/hemicylinder interface is incident upon a mirror. A lens is used to form the image of the light/dark boundary from the mirror into the eye. Other refractometers include Amici prisms to compensate for differences in dispersion between the refracting element and the unknown. These produce a sharper light/dark boundary, instead of the colored boundary, even if white light is used to illuminate the sample. The colored boundary results from differences in the dispersion between the hemisphere and the unknown. If smaller samples are to be measured, then a means to focus the light must be found; this may be accomplished by use of an expanded, collimated, and focused laser beam (Gunter,

AR-1986g). If lenses are to be used to perform this task, they must be achromatic over the range of wavelength of interest so that the focused beam size remains constant.

Polarization control/observation: The polarization state of the incident or reflected light must be determined to ascertain fully the optical properties of an anisotropic material. Three methods can be used to achieve this: 1) a rotating polarizer in conjunction with a randomly polarized light source, the polarizer being placed either before or after the light reflects from the sample; 2) a rotating polarized light source (e.g., a polarized laser); or 3) a rotating $\lambda/2$ plate in conjunction with a polarized light source. The jeweler's refractometer has a rotating cap polarizer which is placed over the eyepiece; light incident into the refractometer is unpolarized. Using this polarizer while rotating the crystal on the hemicylinder, one can determine if the crystal is uniaxial or biaxial and also its optic sign. The same observations could be made if linearly polarized light was incident upon the sample, provided the direction of linear polarization can be varied and controlled by, for instance, a rotating half-wave plate. If a laser is used as a light source, then the latter method must be chosen because the polarization characteristics of randomly polarized lasers are not temporally stable (Duardo et al., 1976). If a half-wave plate is used for polarization control, it must be achromatic over the desired wavelength range; new achromatic half-wave plates are available as discussed in Gunter (AR-1986e). A rotating laser would present mechanical difficulties in construction because of the precise alignment required for the incident laser beam.

Light source: Several types of possible light sources exist for use in RTR. Light sources can be broadly classed into coherent (lasers) and incoherent (gas discharge and tungsten bulbs). The coherent sources have the advantage of ease of collimation and better focusing characteristics. Diffraction-limited focusing, resulting in very small focused spot sizes, is achievable with lasers (Gunter, AR-1987g). Incoherent light cannot be as "tightly" focused; thus larger spot sizes would result and limit the spatial resolution of RTR. Smaller spot sizes can be obtained by first expanding, then collimating, and finally focusing the laser (Gunter, AR-1987g).

In the early days of RTR, sodium metal was burned to produce Na light or the sun's rays were used and the Fraunhofer lines isolated from it (Viola, 1899a). More recently Su et al. (1987) use a variety of gas discharge bulbs and the appropriate filters to isolate various wavelengths in the visible. Tungsten bulbs can also be used along with the appropriate filters to isolate different portions of the visible and near IR spectrum. Monochromatic light isolated from tungsten bulbs in this manner, is far less intense than monochromatic light from gas discharge bulbs. Lasers have been used by Moreels et al. (1984) for the measurement of liquids on a Pulfrich refractometer.

Several wavelengths must be used to measure dispersion. Newer He-Ne lasers are being manufactured which are designed to emit at Ne transitions other than the normal 632.8 nm wavelength. Currently, He-Ne lasers can be purchased with 1.5 μm, 632.8 nm, 611.9 nm, 594.0 nm, and 543.0 nm outputs. Ideally the light source for a refractometer should be stable over the period of measurements and produce a range of wavelengths wide enough for dispersion analysis.

Detection: Refractometers commonly use the eye to determine the light/dark boundary between partial and total reflection. Newer refractometers use some sort of electro-optic device which outputs a voltage as a function of light input. The advantage of these devices is the user is no longer involved in the decision of light/dark boundary location and, if the instrument is calibrated correctly, the entire process could be automated. Moreover, solid state detectors exist that are sensitive to certain wavelengths outside as well as within the visible. The normal eye's peak sensitivity is approximately at 550 nm. By contrast, detectors exist with peak sensitivities at various wavelengths.

For RTR a solid state detector can be used. The detector's sensitivity should be constant throughout the desired wavelength range. Its output is analyzed by a computer and thus the changes in the reflected beam's intensity can be monitored.

Mechanical components: One of the problems of high precision RTR was the demanding alignment tolerances required to perform fourth-decimal-place RTR. The determination of the critical angle, in general, requires some moving apparatus, such as a telescope or mirror. The critical angle

must be measured to within approximately 1 minute of arc; thus, for example, a mirror would require very precise positioning. When measuring anisotropic samples, the stage the sample rests upon must be rotated, also some rotating device is required to control or monitor the polarization orientation.

The only moving part in the jeweler's refractometer is the rotating polarized eyepiece. In the Abbe-Pulfrich refractometer the hemisphere/stage combination is rotated and the critical angle is measured by a moving telescope to within 1 minute of arc. A detailed discussion of the required adjustments for the Abbe-Pulfrich refractometer is given in Wright (1908).

If a laser is used in automated RTR, then its angle of incidence must be controllable. To vary this angle a rotating mirror could be used to reflect the beam onto the sample. The angle of incidence this mirror produces must be known to within 1 minute of arc if fourth-decimal precision is desired.

The Bloss automated refractometer (BAR)

The Bloss automated refractometer (BAR),[5] invented by Professor F. Donald Bloss, and being developed by KDI Electro-Tec, Inc. of Blacksburg Virginia, will make automated measurements of refractive indices and determine the orientation of anisotropic crystals. The BAR works on the basic principles of RTR, but its design and data manipulation drastically depart from normal refractometers. The schematic design of the BAR (Bloss, 1985) is discussed next. Data manipulation is discussed, in detail, in Chapters 5 and 6, for anisotropic and isotropic samples respectively.

The current design of the BAR requires polished samples of approximately 200 μm diameter. Its refracting element is a hemicylinder of CZ with a refractive index of 2.1646. A Cargille liquid

[5] U.S. Patent 4692024.

with n = 1.698 has been routinely used to make optical contact between the hemicylinder and the unknown. The BAR's optical system consists of a series of lenses and mirrors, explained in detail below, which focus and guide a laser beam through the system. A 632.8 nm He-Ne laser is used and its direction of polarization controlled by a rotating achromatic half-wave plate. A solid state detector is used to measure the reflected light intensity. A rotatable stage serves for sample rotation of anisotropic materials. The entire process of motion control, data collection, and data manipulation is performed by a computer.

The BAR's optical system makes it unique in its ability to measure the optical properties of 200 μm grains. To accomplish this task the BAR's optical system is more complicated than that of most other refractometers. In essence the BAR measures the intensity of the reflected component of an incident laser beam (Figure 1, rays I_{r1} and I_{r2}). The critical angle is determined when 100 percent of the incident beam is reflected. The angle of incidence is controlled by a rotatable mirror (Figure 3).

Two elliptical mirrors form the major beam-focusing and beam-directing optical elements of the BAR. The original reasons for using elliptical mirrors were: 1) their achromaticity and 2) their ability to direct and refocus the light from the first rotatable mirror to the hemicylinder. By placing the rotatable mirrors and hemicylinder at the focal points of these elliptical mirrors the beam's angle of incidence onto the sample can be controlled by adjustment of the rotatable mirrors. A basic geometrical property of an ellipse is, that a ray drawn from one focal point to the ellipse's surface will be reflected to the ellipse's second focal point. The laser reflects from the first rotatable mirror (RM1), which controls the angle of incidence onto the sample, to the first elliptical mirror (EM1) and is then reflected onto the hemicylinder. From the hemicylinder the beam is reflected onto the second elliptical mirror (EM2) and then to the second rotatable mirror (RM2) and finally onto the detector. EM1's two focal points coincide with RM1 and the hemicylinder's center of curvature, and EM2's focal points coincide with RM2 and this same center of curvature of the hemicylinder. The detector is positioned about 10 mm from the center of RM2.

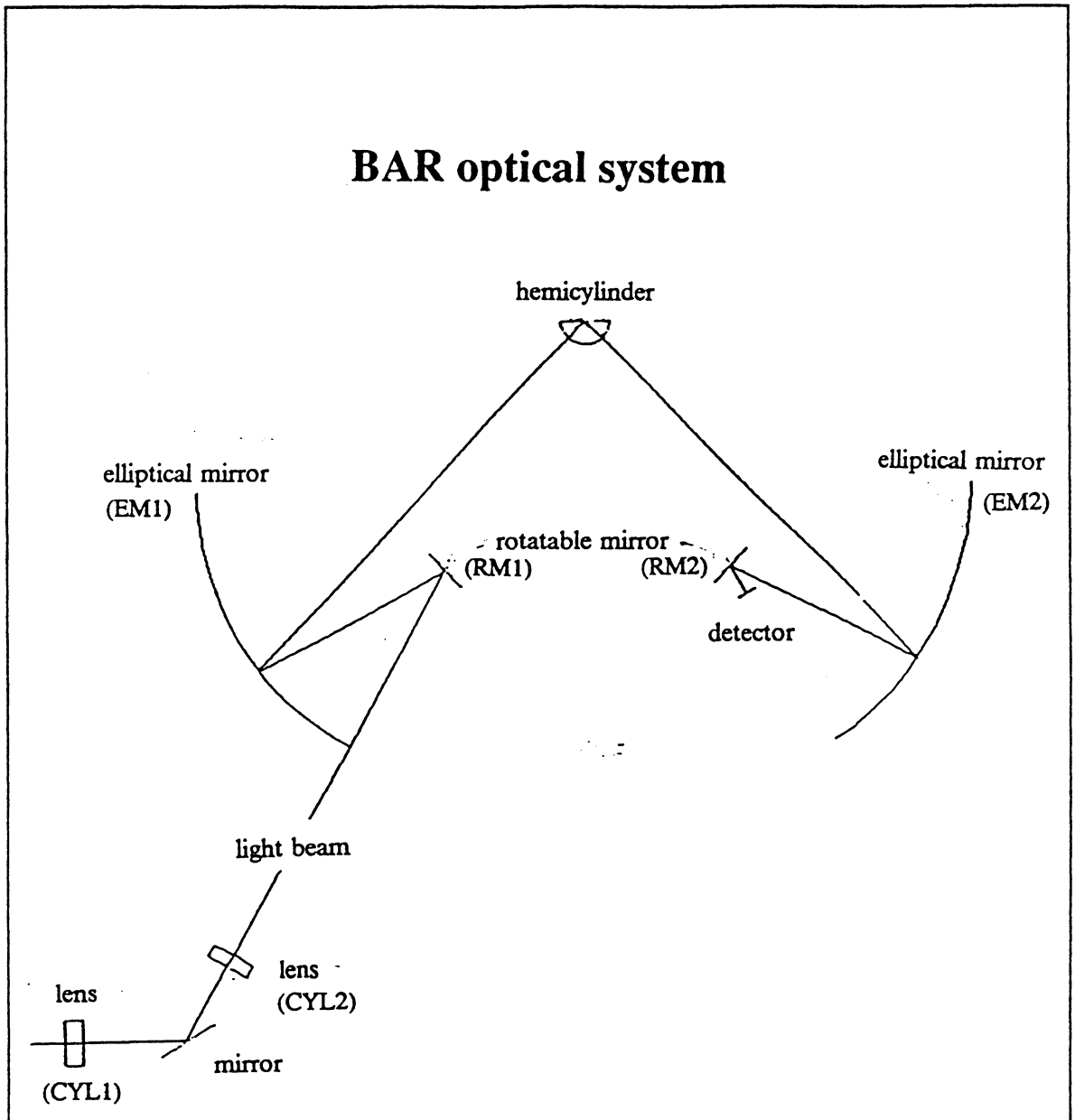

Figure 3. The BAR's optical system: The laser beam, incident from the left, is guided through the system by three planar mirrors and two elliptical mirrors. The planar mirrors, RM1 and RM2, rotate and control the angle of incidence of the beam onto the sample. Two lenses, CYL1 and CYL2, focus the laser beam onto the hemicylinder's flat upper surface. The detector collects intensity data as the rotatable mirrors change the angle of incidence.

Two cylindrical lenses are used to focus the laser beam's size from approximately 800 μm to 200 μm diameter spot on the hemicylinder's upper surface. The first lens, CYL1, has a focal length of 300 mm and produces a line focus on the hemicylinder within the plane of the figure. The second lens, CYL2, has a focal length of 100 mm and forms a line focus on RM1 normal to the plane of the drawing. The combination of these two lenses results in an approximate point focus on the hemicylinder's upper surface.

In operation, a drop of contact liquid is placed on the upper surface of the hemicylinder. The liquid's refractive index must be greater than that of the unknown but less than that of the hemicylinder, preferably closer to the latter. The sample is placed on the hemicylinder/liquid surface. The liquid forms the thin film necessary for optical contact. A computer controls the rotations of RM1 and RM2 about an axis normal to the drawing and simultaneously collects intensity data from the detector. As RM1 rotates, it changes the angle of incidence of the laser beam onto the sample. The laser beam is partially reflected from the sample, and this beam is directed into the detector by EM2 and RM2. When the intensity reaches a maximum (i.e., all the incident beam is being reflected), the critical angle has been reached. The intensity prior to total reflection can be theoretically determined based upon on the Fresnel equations (Eqns. 2.2). With prior knowledge of the refractive index of the hemicylinder and the measured critical angle, the unknown's refractive index can be calculated using Snell's law (Eqn. 2.1b).

The BAR varies the angle of incidence, θ, by rotating RM1; thus θ is controlled by the angular position, Rpl, of RM1. Rpl is defined as the angle between the incidence laser beam and the normal to RM1's surface. The mathematical relationships between θ, n, and Rpl are given below. (See Appendix for derivation.)

$$n = nhc \times \sin\left(\cos^{-1}\frac{[k1 + k2\ \cos 2Rpl]}{[k2 + k1\ \cos 2Rpl]} + \beta\right) \qquad [3.1a]$$

$$Rpl = \frac{\cos^{-1}\dfrac{[k1 - k2\ \cos\alpha]}{[k2\ \cos\alpha - k1]}}{2} \qquad [3.1b]$$

where,

n = refractive index of unknown

Rpl = angle between the normal RM1 and the laser beam

nhc = refractive index of the hemicylinder

k1 = 2ac

$k2 = a^2 + c^2$

a = semi-major axis of the elliptical mirror

b = semi-minor axis of the elliptical mirror

$c = \sqrt{a^2 - b^2}$

$\alpha = \sin^{-1}\frac{n}{nhc} - \beta = \theta - \beta$

β = angle between normal to hemicylinder's flat surface and a

The relationship between n and Rpl is more linear than that between n and θ, thus the precision of measurement is almost constant over the BAR's entire measurement range. As suggested by Gunter (AR-1986b), a, b, and β could be optimized in Eqn. 3.1 to yield a near-linear relationship between n and Rpl, which would simplify the calibration of the instrument. A graph of Rpl-vs-n for three different b values (see Appendix) demonstrates this point.

Raw intensity data collected from the BAR for an isotropic sample and for an anisotropic sample appear in Figure 4 and Figure 5, respectively. In both scans the Rpl angle is plotted horizontally while intensity, in arbitrary units, is plotted vertically. For the isotropic scan, the intensity of the reflected beam increases with increasing Rpl until the critical angle is reached at approximately 19.5°, which, by use of Eqn. 3.1a, could be used to find an approximate refractive index, n, of the sample. Figure 5 shows two separate Rpl scans, each possessing a different critical Rpl value, corresponding to the two different refractive indices present for an anisotropic sample in a random orientation. The different curves are produced by changing the polarization of the incident linearly polarized light. The theory, computer modeling, and algorithms used to extract the refractive index from these Rpl scans will be discussed in the remaining chapters.

In the lower portion of each figure is shown the position of the refracted wave-normal at total reflection. For the isotropic material there is only a single refracted wave-normal. For the

anisotropic material two refracted wave-normals occur corresponding to the two different observable refractive indices, N and n, present in a random section through a anisotropic crystal. Hurlbut (1984) stated that these wave-normals coincided for anisotropic crystals, but clearly this cannot be the case; they are separated by an amount equal to their birefringence. Also shown in these figures is the assignment of a right-handed cartesian coordinate system used for the BAR.

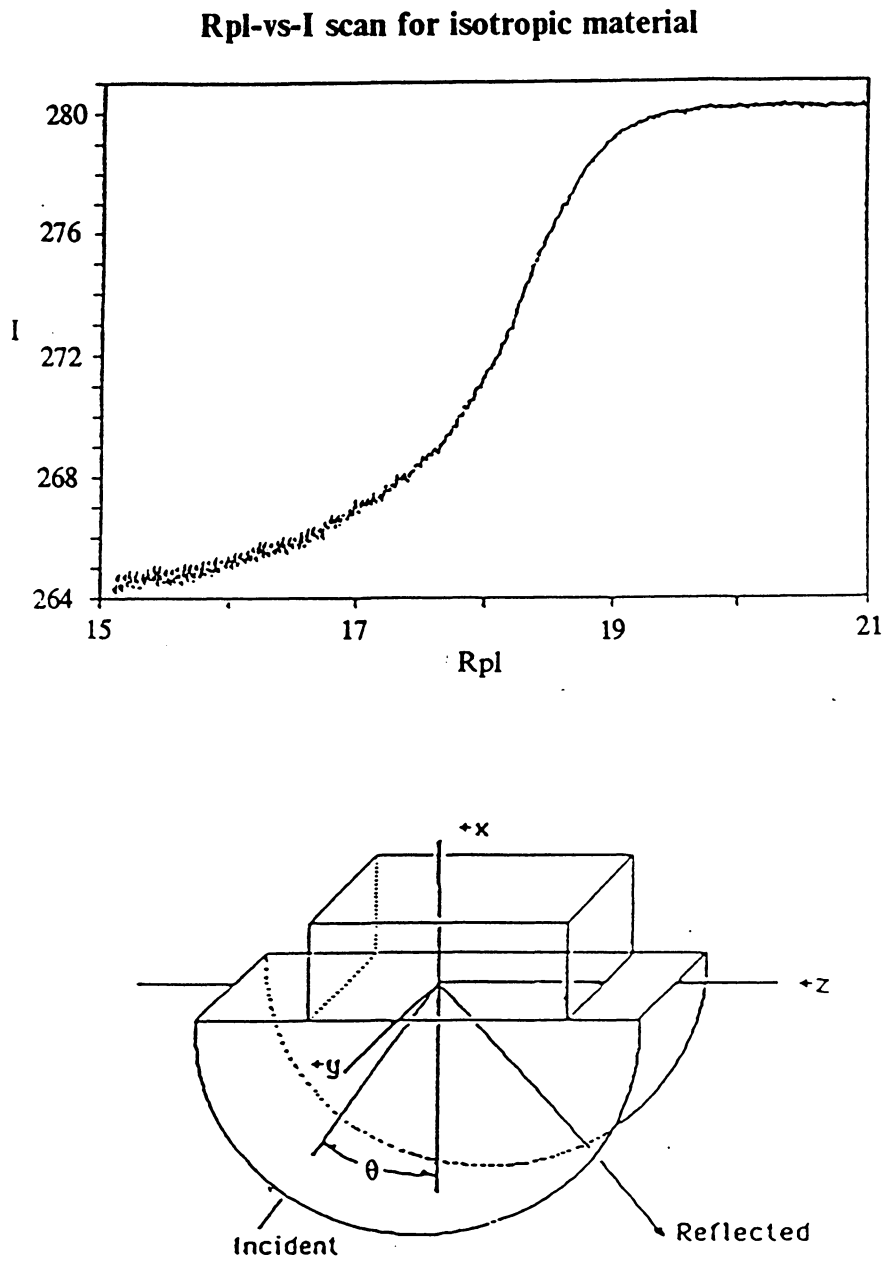

Figure 4. **Data from the BAR for an isotropic sample:** The intensity increases with increasing Rpl until the critical Rpl is reached at approximately 19.5°. From this value an approximate refractive index can be calculated. The lower portion of the figure shows the refracted wave-normal at the critical angle and the coordinate system used by the BAR.

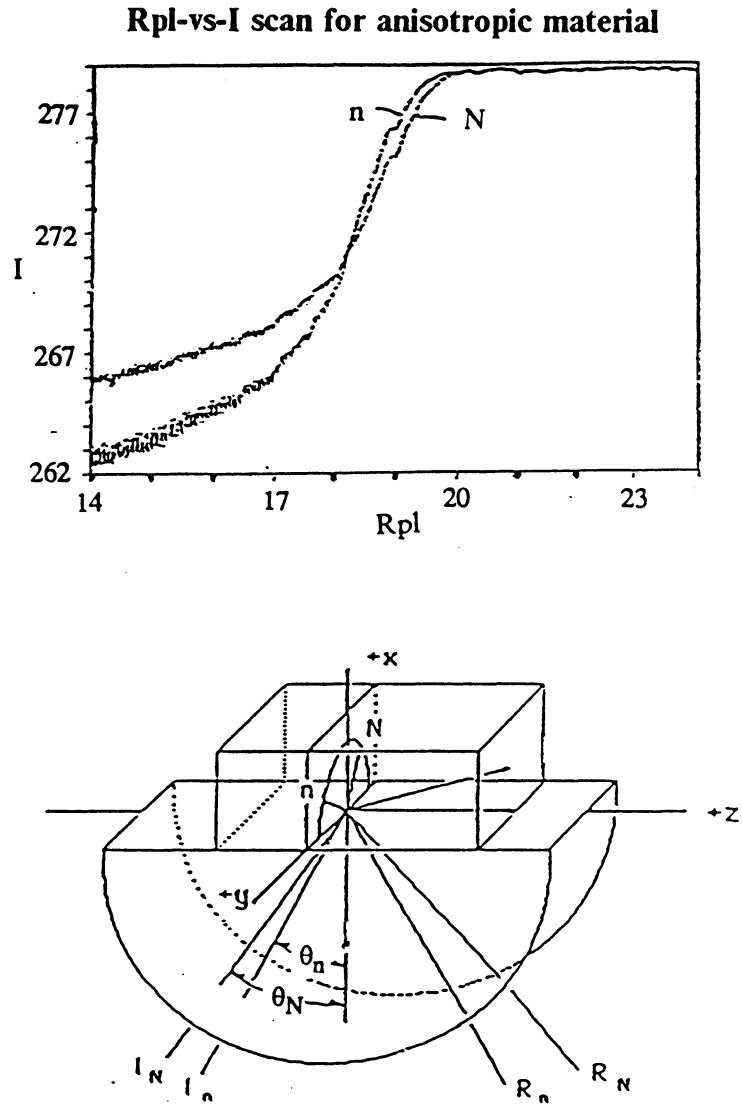

Figure 5. Data from the BAR for an anisotropic sample: Two separate Rpl-vs-intensity scans are shown for an anisotropic crystal. The curves were produced by varying the orientation of the incident lasers plane of polarization. The lower part of the figure shows the refracted wave-normals. The two wave-normals are separated by an amount equal to their birefringence.

Chapter 4: Polarized Light Reflection and Jones Calculus

Introduction

In general the polarization properties of light are altered when it is reflected from any surface. The effect the reflecting surface will have on an incident beam depends on the optical properties of the surface and the angle of incidence. Optical materials are divided into dielectrics and metals, and each group contains both isotropic and anisotropic materials. After reflection from a dielectric, randomly polarized light will become partially polarized, linearly polarized light will be rotated, and, in the case of reflection from a metal, linear polarization will be transformed into elliptical polarization. There are two cases when the light is not altered: 1) when the angle of incidence is 0° (i.e., normal incidence) and 2) when light is incident in a particular polarization state which corresponds to one of the two so called eigenpolarization states of the system.

Most manual refractometers analyze the polarization characteristics of the light after it has been reflected from the sample; these refractometers commonly use a randomly polarized light source and contain no polarization-altering optics (e.g. metallic mirrors). Thus only the sample

alters the polarization properties of the incident light. The BAR uses a linearly polarized light source and metallic mirrors to direct and focus the laser beam. The BAR's optical system will have an effect on the polarization characteristics of the linearly polarized laser. These effects must be known so we can interpret the polarization-altering effects of the samples independently from those effects introduced by the BAR's optical system.

To measure refractive indices of anisotropic materials, the BAR must determine: 1) the intensity of the reflected beam and 2) the polarization state of the reflected beam. Intensity data is used to determine the refractive index, while the polarization information is required to calculate the orientation of anisotropic materials. Changes in both intensity and polarization state of a polarized beam will occur as the laser beam propagates through the BAR's optical system. These changes can be calculated as a function of the: 1) angle of incidence, 2) polarization state of incident beam, and 3) optical properties of reflecting surfaces (i.e., the mirrors). Jones calculus can be used to calculate the polarization characteristics of any optical system. A Jones vector can be written to describe any polarized light beam. Each optical element can be represented by a Jones matrix. After all the components have been modeled by a matrix, the polarization characteristics of the system are easily calculated by matrix multiplication. For the BAR, the reflection matrices are formed and recalculated at various Rpl angles and input polarization states.

Polarization-altering by the BAR and by samples placed upon it can be calculated. If only slight changes occur in the polarized beam as it propagates through the BAR's optical system, then they can be ignored and the properties of the reflected polarized beam used to aid in determining the optical properties of the sample. If, on the other hand, the BAR causes major changes in the polarization characteristics of the beam, these changes will have to be mathematically removed from the reflected beam before use could be made of the beam's polarization properties.

A quantitative approach can be developed to determine the behavior of polarized light in any optical system. Polarized light is represented mathematically by specifying its amplitude and phase in vector form. The effects on polarized light of each optical component can be represented by a

2x2 matrix. To model polarized light behavior for a particular optical system like the BAR, a 2x2 matrix needs to be written for each of its polarization-altering components. The matrices for the mirrors contain information which must be obtained from an understanding of the optical properties of metals, specifically, the intensity and phase of the reflected beam. To obtain all the necessary information to calculate the effects on polarized light of the optical system, a considerable amount of introductory material is briefly presented; the references may be consulted for additional information. The material presented herein details the behavior of reflected polarized light from isotropic dielectrics and isotropic metals and gives the necessary mathematics to quantify it. The more complicated case for anisotropic materials is presented in the next chapter.

Polarized light

Polarized light exists in three forms: linear, circular, and elliptical, the two former being special cases of the latter. In any form of polarized light, the direction of the electric field (E-field), which is normal to the propagation direction, is nonrandom. Light is linearly polarized when the E-field vector remains in a single plane. In elliptically and circularly polarized light the E-field vector sweeps out either an ellipse or a circle. For a detailed explanation of polarized light refer to: Azzam and Bashara (1977, the first two chapters), Bennett and Bennett (1978), Clarke and Grainer (1971), Hecht and Zajac (1979), Jenkins and White (1976), Shurcliff (1962), and Shurcliff and Ballard (1964).

Several parameters must first be defined to describe polarized light quantitatively. Figure 6 shows elliptically polarized light and the associated parameters needed to define it. A system of right-handed cartesian axes is used. The x direction corresponds to the p-state, the direction parallel to the plane of incidence, because the x direction is, by definition, in the plane of incidence. In general the plane of incidence is defined as the plane which contains the incident and reflected ray and the normal to the reflecting surface. Specifically, for the BAR the plane of incidence is the

meridional plane, as defined by geometrical optics and by the GENII[6] optical design program, or the xz plane of Figure 4. The y direction corresponds to the s-state; the direction normal to the plane of incidence. The direction of light propagation, not shown, is toward the observer in the positive z direction.

The parameters shown in Figure 6 are defined as follows:

1. The semi-major and semi-minor axes of the ellipse are represented by a and b, respectively.

2. The azimuth, α, denotes the angle between the semi-major axes and x; the angle is positive when measured counterclockwise from x.

3. The ellipticity is defined as the tan ε, (where ε is defined in Figure 6, and Eqn. 4.8) when this value is positive the light is right elliptically polarized, when negative left elliptically polarized.

Jones calculus: Jones calculus is a very concise method to perform calculations involving polarized light (Hurwitz and Jones, 1941; Jones, 1941, 1942, 1947, 1948, and 1956). Any form of polarized light can be expressed as a 2x1 matrix (= Jones vector). Any optical element can be described by a 2x2 Jones matrix, even an anisotropic crystal in a random orientation (Chapter 5). To determine the effect an optical element has on the particular form of polarized light, their matrices are multiplied. The result can then be analyzed mathematically to determine quantitatively the polarization characteristics of the output beam. Azzam and Bashara (1977), Hecht and Zajac (1979), and Shurcliff (1962) all provide an introduction to Jones calculus and some examples for representing polarized light by Jones vectors and performing operations with Jones matrices.

---

[6] GENII is an optical design program which performs ray tracing of complex optical systems. The program does not perform any polarization calculations and treats every surface as a perfect reflector or refractor.

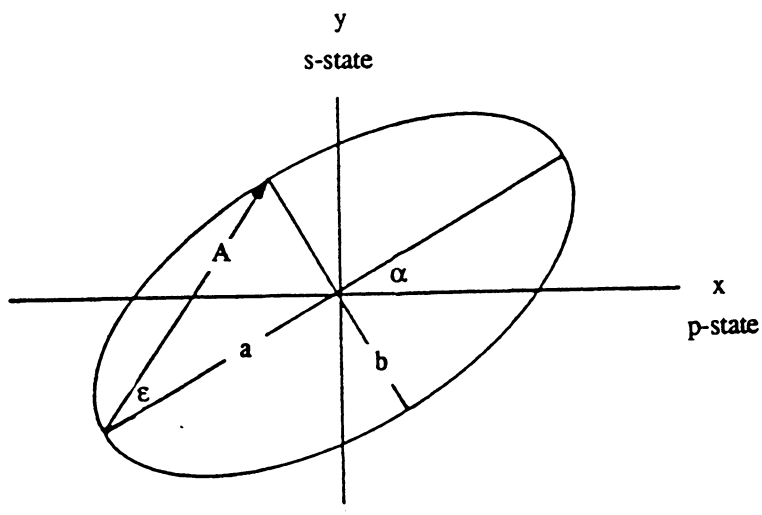

Figure 6. Symbols used in polarized light: A right handed system of cartesian axes is used to describe polarized light. The x direction coincides with the p-state, and y coincides with the s-state. The orientation of the major axis is defined by α. The ellipse is defined by a and b, its semi-major and semi-minor axes. Ellipticity is defined by tan ε. The total amplitude of the light is A.

A Jones vector for polarized light is shown in Eqn. 4.1. The E_x and E_y values represent the component of the light amplitude along the x and y cartesian axes, which are used to calculate the intensity of the light. If phase information is required the complex quantities must be added. For linearly polarized light the complex component will simply equal one, thus the expression on the left side of the arrow would be applicable. For the general case of elliptically polarized light the complex phase information must be retained. Thus, depending upon the situation, either form of Eqn. 4.1 may be applicable.

$$\begin{bmatrix} E_x \\ E_y \end{bmatrix} \rightarrow \begin{bmatrix} E_x\ e^{i\delta_x} \\ E_y\ e^{i\delta_y} \end{bmatrix} \qquad [4.1]$$

where,

E_x = amplitude of x component

E_y = amplitude of y component

δ_x = phase of x component, in degrees

δ_y = phase of y component, in degrees.

By use of Eqn. 4.1, the 2x1 Jones vector for linearly polarized light parallel to x can be written in column form as {1 0}, the {} notation being a means to write the vector horizontally. The E_x value of Eqn. 4.1 equals 1 because all the light is parallel to the x direction and no y component exists, thus the E_y value is zero. The phase for linearly polarized light, δ_x, can be given as either 0 or 2π; regardless of the choice, $E_x\ e^{i\delta x}$ evaluates to 1. For light linearly polarized parallel to y, the Jones vector would be written as {0 1}. For any orientation of linear or elliptically polarized light, Eqn. 4.2 can be used to express its Jones vector.

$$\begin{bmatrix} E_x\ e^{i\delta_x}\ \cos\alpha \\ E_y\ e^{i\delta_y}\ \sin\alpha \end{bmatrix} \qquad [4.2]$$

where,

α = orientation of the polarized light (Figure 6).

An optical element can be represented by a 2x2 Jones matrix. Equations 4.3a and 4.3b define the incident and output beams for the x and y directions. The output beam, the polarized form after passage through or reflection from an optical element, is obtained from the input beam by use of the T values. These T values take on different forms depending upon the polarization-altering properties of the optical element. Basically, the T values can be thought of as the quantitative relation between the incident and output beam. These values map the input into the output beam based upon the properties of the optical element. These two equations can be written in matrix form (Eqn. 4.4). All that remains is to find correct expressions for the T's in this matrix. Shurcliff (1962) and Azzam and Bashara (1977) list several such optical element matrices.

$$E_{rx} = T_{11}E_{ix} + T_{12}E_{iy} \qquad [4.3a]$$

$$E_{ry} = T_{21}E_{ix} + T_{22}E_{iy} \qquad [4.3b]$$

or in matrix form

$$\begin{bmatrix} T_{11} & T_{12} \\ T_{21} & T_{22} \end{bmatrix} \begin{bmatrix} E_{ix} \\ E_{iy} \end{bmatrix} = \begin{bmatrix} E_{ox} \\ E_{oy} \end{bmatrix} \qquad [4.4]$$

where,

E_{ix} = amplitude of x component of incident light

E_{iy} = amplitude of y component of incident light

E_{rx} = amplitude of x component of output light

E_{ry} = amplitude of y component of output light

T_{11} = matrix component that maps E_{ix} onto E_{ox}

T_{12} = matrix component that maps E_{iy} onto E_{ox}

T_{21} = matrix component that maps E_{ix} onto E_{oy}

T_{22} = matrix component that maps E_{iy} onto E_{oy}.

Two Jones matrices are presented in Eqns. 4.5 and 4.6. Equation 4.5 represents the Jones matrix for a $\lambda/2$ plate (Shurcliff, 1962). The matrix for a $\lambda/2$ plate requires as input the angle between the $\lambda/2$ plate's fast axes and the x direction, called ρ. The T_{11} entry for this matrix has a phase angle of π. This π phase shift will retard the y component behind the x component after passage through the plate. This retardation results in a 2ρ rotation of α.

$$\begin{bmatrix} \cos 2\rho\ e^{i\pi} & \sin 2\rho \\ \sin 2\rho & -\cos 2\rho \end{bmatrix} \qquad [4.5]$$

where,

ρ = angle between the fast axes of the $\lambda/2$ plate and x.

Equation 4.6, taken from Azzam and Bashara (1977), defines the Jones matrix for metallic reflection. The amplitude components for this matrix are calculated from the generalized Fresnel equations (Eqns. 4.9a and b). The phase angle information is obtained from Eqns. 4.10a and b. These values, computed at a specific angle of incidence, form the entries for the reflection matrix:

$$\begin{bmatrix} |\, r_x \,| e^{i\delta_x} & 0 \\ 0 & |\, r_y \,| e^{i\delta_y} \end{bmatrix} \qquad [4.6]$$

where,

r_x = Fresnel amplitude coefficient for the p-state

r_y = Fresnel amplitude coefficient for the s-state

Both the p- and s-states will be used interchangeably with the x and y cartesian axes to define orientations.

Calculations with polarized light: Any Jones vector representing a polarized beam can be quantitatively analyzed to determine its polarization characteristics. By use of Eqns. 4.7 and 4.8, and the components of the Jones vector, the polarization characteristics of the beam can be evaluated for polarization form (ε) and orientation (α).

$$\alpha = \frac{1}{2}\tan^{-1}[(\tan 2\psi)(\cos\gamma)] \qquad [4.7]$$

$$\varepsilon = \frac{1}{2}\sin^{-1}[(\sin 2\psi)|\sin\gamma|] \qquad [4.8]$$

where,

α = orientation for linearly polarized light or the major axes' orientation for elliptically polarized light

ε = elliptical angle, $\tan\varepsilon$ = b/a or the ellipticity

$\psi = \tan^{-1}\frac{E_y}{E_x}$ from the Jones vector

γ = the phase difference = $(\delta_y - \delta_x)$ from the Jones vector.

In general the Jones vector will carry both phase and amplitude information and correspond to elliptically polarized light. In special cases (i.e., linearly polarized) only amplitude information will exist in the Jones vector. By use of Eqn. 4.7 the orientation of linearly polarized light, or the major axes of the ellipse for elliptically polarized light, can be calculated. From Eqn. 4.7 it can be seen that linearly polarized light reflected at any nonnormal incidence or non p- or s-state will be rotated. The rotation will occur because $r_p \neq r_s$, thus $E_x \neq E_y$ and tan ψ is nonunity. If the phase difference, γ, is a multiple of π, Eqn. 4.8 will yield a zero value for ellipticity. If the phase difference is not a multiple of π then ε is no longer zero and the light is elliptically polarized. Equations 4.7 and 4.8 are used to determine the polarization characteristics of the output of the BAR's optical system.

Optical properties of isotropic metals

Metals, unlike dielectrics, reflect a large amount of incident light. But like dielectrics, the intensity of the light reflected from a metal is a function of the angle of incidence, polarization orientation, and optical properties of the material. The generalized Fresnel equations are used to determine the reflectance of a metal, as a function of the above parameters (Hunter, 1965). To calculate the reflection for the p- and s-state orientations of polarized light at any angle of incidence, Eqns. 4.9a and b are used. The optical properties of the material must be known before the equations can be solved. The optical properties of a metal are defined by its refractive index, n, and its extinction coefficient, k. If the extinction coefficient equals zero, the material behaves as a dielectric, and Eqns. 4.9a and b reduce to Eqns. 2.3a and b; if k is nonzero, the material will have metallic properties.

$$R_s = \frac{(a - \cos\theta)^2 + b^2}{(a + \cos\theta)^2 + b^2} \qquad [4.9a]$$

$$R_p = R_s \times \frac{(a - \sin\theta\tan\theta)^2 + b^2}{(a + \sin\theta\tan\theta)^2 + b^2} \qquad [4.9b]$$

where,

R_p = reflected light's intensity parallel to the plane of incidence

R_s = reflected light's intensity normal to the plane of incidence

$|r_p| = \sqrt{R_p}$ = Fresnel amplitude coefficient parallel to the plane of incidence

$|r_s| = \sqrt{R_s}$ = Fresnel amplitude coefficient normal to the plane of incidence

$a^2 = 0.5 \times \{[(n^2 - k^2 + \sin^2\theta)^2 + 4n^2k^2]^{\frac{1}{2}} + (n^2 - k^2 - \sin^2\theta)\}$

$b^2 = 0.5 \times \{[(n^2 - k^2 + \sin^2\theta)^2 + 4n^2k^2]^{\frac{1}{2}} - (n^2 - k^2 - \sin^2\theta)\}$

θ = angle of incidence

n = refractive index of the material

k = extinction coefficient.

The reflected intensity variation, as a function of angle of incidence, θ, is less for metals than for dielectrics. Figure 7a is a plot of intensity variation vs. θ for a dielectric with n = 1.5. Both the p- and s-states are shown; the p-state has zero intensity at the Brewster angle. Figure 7b shows a plot of R_p and R_s from normal to grazing incidence for aluminum, n = 0.97 and k = 6.00. R_p reaches a minimum, at the principal angle (Jenkins and White, 1976), which is equivalent to the Brewster angle for dielectrics. However, in metals R_p does not reach zero as in dielectrics and occurs at a much higher angle of incidence than Brewster's angle.

In dielectrics the phase change upon external reflections (n incident < n material - the so called "hard reflection") is either zero or π. See Jenkins and White (1976, p. 528) or Hecht and Zajac (1979, p. 77) for a complete discussion of phase changes for both internal (n incident > n material) and external reflections for dielectrics and metals. Disagreement exists in the literature over the phase shifts. Azzam and Bashara (1977) describe the phase shift as either π or 2π, replacing the zero phase shift of Hecht and Zajac with 2π. The 2π phase shift is used herein because it sim-

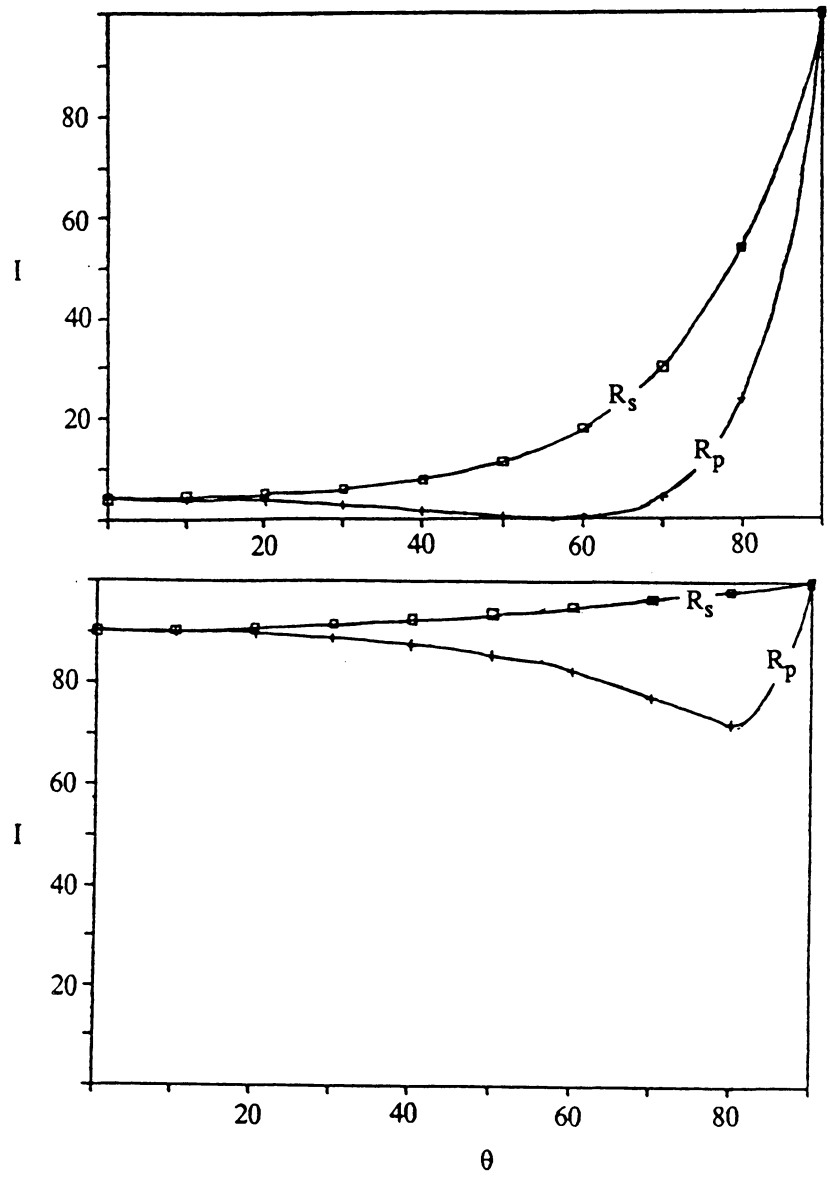

Figure 7. **Plot of intensity vs. θ for a dielectric and metal:** a) (top) A plot of reflected light intensity variation for a dielectric with n = 1.5. Both the p- and s-states are shown. The p-state has zero intensity at Brewster's angle, θ_{BA}, which for this sample equals 56.3°. b) (bottom) This plot shows the reflected light intensity for a metal (Al) with n = 0.97 and k = 6.00. The intensity is much higher at lower angles than for the dielectric above. R_p reaches a nonzero minimum at the 80.14°, the principal angle.

plifies phase-change calculations in metals. Phase changes must be considered for both the p- and s- states. In dielectrics an abrupt π phase change occurs at Brewster's angle for the p-state. After this change the p- and s-state phase values are equal; the s-state remains constant at any incident angle. In a metal, the phase changes are gradual and occur as a function of the angle of incidence. The p-state undergoes a phase change until its value equals that of the s-state; however, the p-state change is not abrupt. For a metal the s-state is not constant but varies with incident angle. Both phase values must be determined quantitatively, for any angle of incidence, to fully model the polarization characteristics of the beam. Equations 4.10a and b describe the phase change, δ, for both the p- and s-state as a function of angle of incidence and the optical properties of the metal (Bennett and Bennett, 1978).

$$\tan \delta_s = \frac{2\eta_{os} b}{\eta_{os}^2 - a^2 - b^2} \qquad [4.10a]$$

$$\tan \delta_p = \frac{-2\eta_{op} d}{c^2 + d^2 - \eta_{op}^2} \qquad [4.10b]$$

where,

δ_s = phase change for the normal component, the actual phase of this component equals 180° - δ_s

δ_p = phase change for the parallel component, the actual phase of this component equals 360° - δ_p

$\eta_{os} = n_o \cos\theta$

$\eta_{op} = \frac{n_o}{\cos\theta}$

θ = angle of incidence

n_0 = refractive index of the incident material

$a^2 - b^2 = n_1^2 - k^2 - n_0^2 \sin^2\theta$

$a^2 + b^2 = [(a^2 - b^2)^2 + 4n_1^2k^2]^{\frac{1}{2}}$

$c^2 + d^2 = \frac{(n_1^2 + k^2)^2}{a^2 + b^2}$

$b = -\sqrt{\frac{a^2 - b^2}{2} + \frac{a^2 + b^2}{2}}$

$d = b(1 - \frac{n_0^2 \sin^2\theta}{a^2 + b^2})$

k = material's extinction coefficient

n_1 = material's refractive index.

The p- and s-state phase changes for a dielectric with n = 1.5 are shown in Figure 8a for external reflection. Compare Figure 8a to Figure 8b which shows the phase changes for aluminum, n = 0.97 and k = 6.00. For metals the phase shifts are not multiples of π; thus they change gradually as a function of the angle of incidence. From Eqn. 4.8, the value of γ will yield a nonunity value for the cosine term, which will yield a nonzero value for ε. Thus at nonnormal incidence linearly polarized light, not in the p- or s-state, becomes elliptically polarized after reflection. The magnitude of ellipticity is a function of the angle of incidence, orientation of polarized light, and optical properties of the metal.

The BAR's optical system

Description of optical system: Polarization changes in the laser beam will be induced by the BAR's optical system as a function of the: 1) optical properties of the mirrors, 2) angle of incidence of the beam (Figure 9, and Eqns. 4.11a-c), 3) azimuth of the linearly polarized beam (Figure 6) and, 4) the characteristics of the sample (which at this time are ignored, but will be discussed in detail in Chapter 5). The optical parameters for the mirrors at 600 nm are n = 0.97 and k = 6.00 (Schulz and Tangherlini, 1954: and Schulz, 1954).

Equations 4.11a-c are used to calculate the angles of incidence for the rotatable mirrors (RM1 and RM2, Figure 9), the elliptical mirrors (EM1 and EM2, Figure 9), and the hemicylinder (HE, Figure 9). All three equations use the value of Rpl. Equation 4.11a is the definition for the Rpl setting. Equation 4.11b was derived by S.C. Su and defines the angle of incidence on the elliptical mirrors. Equation 4.11c has been previously defined (Eqn. 2.1a) and equals the angle of incidence onto the sample. Because of the BAR's symmetry, $\theta_{RM1} = \theta_{RM2}$ and $\theta_{EM1} = \theta_{EM2}$; these relations simplify the calculations:

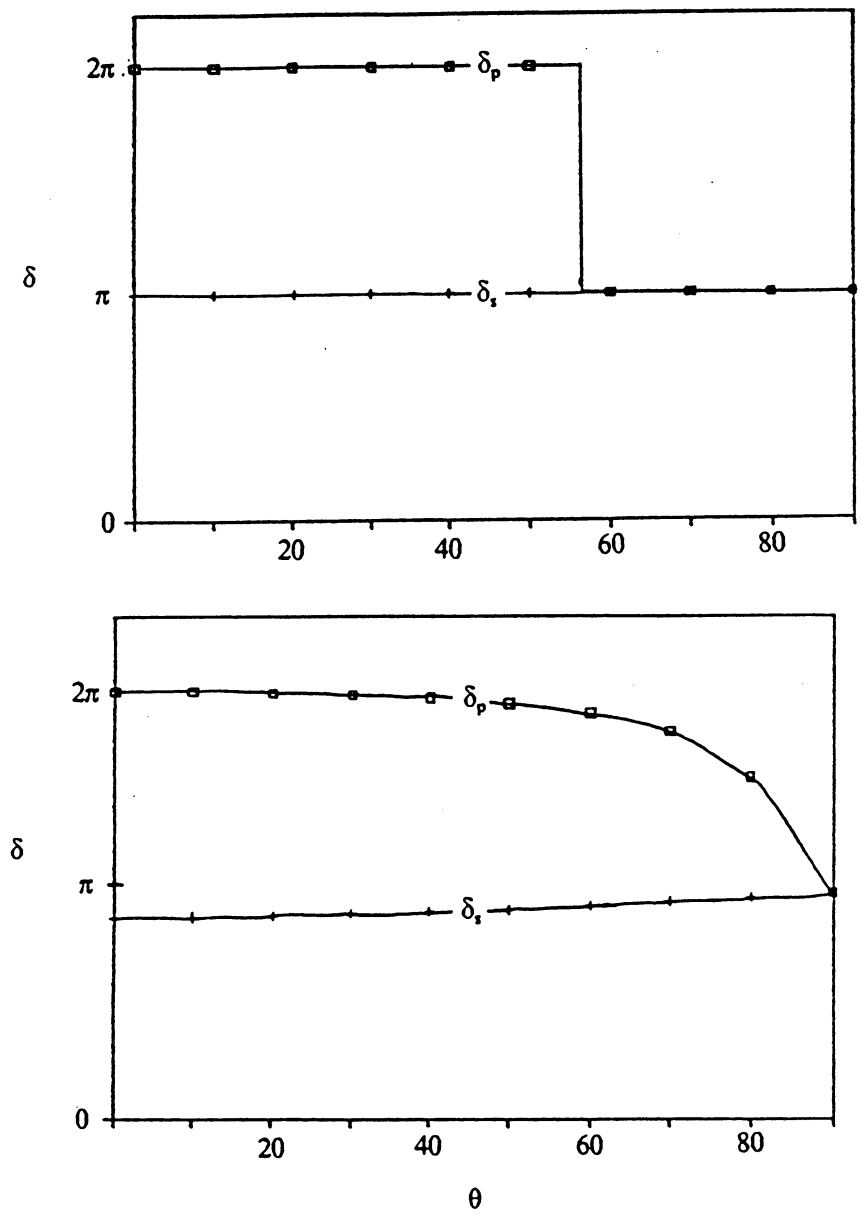

Figure 8. **Plots of phase changes vs. θ for a dielectric and a metal:** a) (top) This plot shows the phase changes for a dielectric with n = 1.5. The R_S phase is constant regardless of angle of incidence. R_p has a stepwise π phase shift at Brewster's angle. b) (bottom) For Al, n = 0.97 and k = 6.00, the phase changes are gradational and can be calculated from Eqns. 4.10a and b. At the principal angle, 80.14°, the phase difference, γ = 90°.

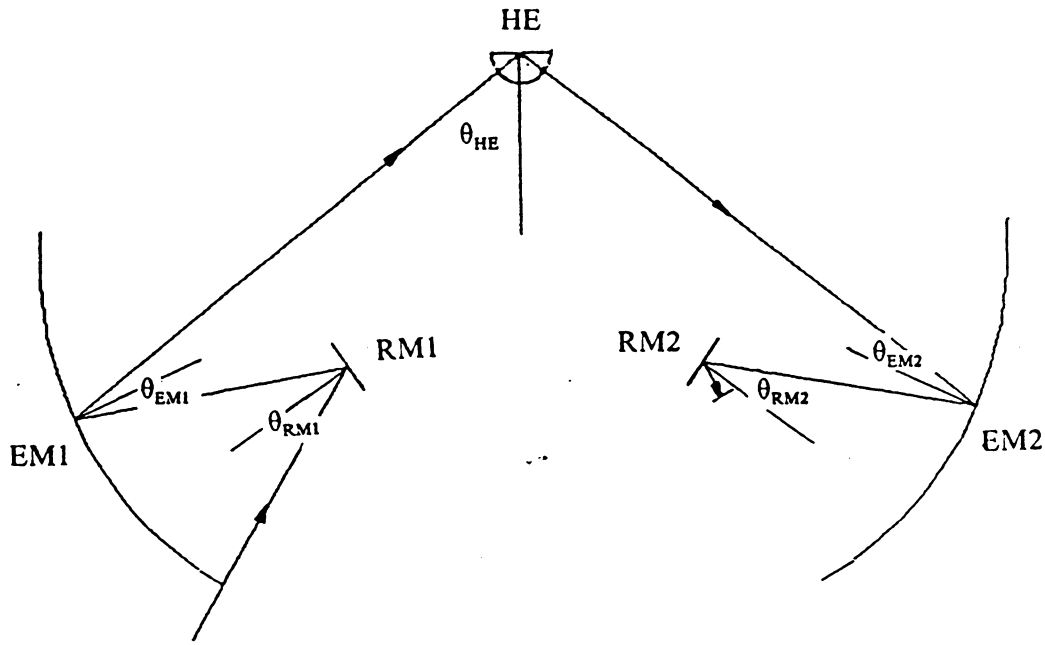

Figure 9. **Angles of incidence for the reflecting elements of the BAR:** The three angles required to make polarization calculations are shown in the above diagram of the BAR. Only the angles θ_{RM}, θ_{EM}, and θ_{HE} are required because $\theta_{RM1} = \theta_{RM2}$ and $\theta_{EM1} = \theta_{EM2}$. See Eqn. 4.11 a-c for quantitative definitions of these angles.

$$\theta_{RM} = \text{Rpl} \qquad [4.11a]$$

$$\theta_{EM} = 0.5 \sin^{-1}\left(\frac{2}{Q + Q^{-1}}\right) \qquad [4.11b]$$

$$\theta_{HE} = \sin(\beta + \cos^{-1} U) \qquad [4.11c]$$

where,

θ_{RM} = angle of incidence for rotatable mirrors

θ_{EM} = angle of incidence for elliptical mirrors

θ_{HE} = angle of incidence for hemicylinder

$$Q = \frac{a + c \cos 2\text{Rpl}}{c \sin 2\text{Rpl}}$$

$$U = \frac{k1 + k2 \cos 2\text{Rpl}}{k2 + k1 \cos 2\text{Rpl}}.$$

The halfwave plate controls the azimuth of the linearly polarized beam. The input laser beam is written as {1 0} for a beam which is vertically linearly polarized light -- the p-state. Orthogonal to {1 0} is {0 1}, the s-state. These two polarization orientations are called the eigenstates or the eigenpolarization states (Shurcliff and Ballard, 1963) for the BAR. All optical devices have two eigenstates, when light is input along them the output and input are equivalent in terms of polarization characteristics. For all other azimuths (i.e., when α is not equal to 0° or 90°) the BAR will affect the polarization state of the beam.

Jones matrix representation of the BAR's optical system: To quantify the polarization-altering characteristics of the BAR, a 2x2 matrix must be written for each polarization-altering optical component. These matrices, representing each optical component of the BAR, can then be multiplied by the input polarization form to determine what the output polarization form will be. Equation 4.12 provides the Jones matrix representation for the BAR. The matrices are multiplied from right to left. By varying Rpl, which causes angle of incidence changes, and halfwave settings, creating changes in the azimuth, α, any input linear polarization form can be modeled at any Rpl setting. Thus,

$$[RM2][EM2][HE][EM1][RM1]\left[\frac{\lambda}{2}\right][IN] \qquad [4.12]$$

where,

EM2 and EM1 = reflection matrix for the elliptical mirrors, see Eqn. 4.6

RM2 and RM1 = reflection matrix for the rotatable mirrors, see Eqn. 4.6

HE = reflection matrix for the unknown atop the hemicylinder, here written as the identity matrix

$\lambda/2$ = matrix representation for the $\lambda/2$ plate, see Eqn. 4.5

IN = input polarization form, for the BAR {1 0}.

The vector labelled "IN" represents the input laser beam. This vector can be written {1 0} which represents the output of a linearly polarized laser beam oriented vertically. The general Jones vectors will have both amplitude and phase components; however, no phase information is required in this vector because the light is linearly polarized.

The first polarization-altering element the beam encounters is the halfwave plate. To vary the azimuth of polarization the angle ρ (Eqn. 4.5) is changed. When $\rho = 0°$, the input and output polarization forms would be {1 0}. If $\rho = 45°$ the input and output polarization forms would be orthogonal, namely, input = {1 0}, output = {0 1}. In Eqn. 4.5 the T_{11} element contains phase information. The induced π phase shift is a function of the $\lambda/2$ plate. Thus if ρ is not equal to 0° or 45°, the output beam will contain phase information.

All four mirrors have the same type of matrix representation. A general reflection matrix is presented in Eqn. 4.6. The reflection matrix requires both amplitude and phase information. To calculate these values for RM1, EM1, EM2, and RM2, first the angles of incidence are found from Eqns. 4.11a-c. Next the generalized Fresnel Eqns. 4.9a and b are used with the appropriate values for n, k, and θ, to provide the amplitude information. Lastly, the phase information is calculated from Eqns. 4.10a and b.

At the present time, the hemicylinder, HE Eqn. 4.12, is represented by the identity matrix. In Chapter 5 a method is described to write a general Jones reflection matrix for an anisotropic sample in a random orientation placed on the hemicylinder's upper surface. The Fresnel equations are modified in Chapter 6 to describe more accurately the actual Rpl-vs-intensity data; these modified equations could be substituted into the Jones matrix representation of an anisotropic or isotropic sample to better model data from the BAR.

Results: By use of Eqn. 4.12 the output polarization form can be calculated for any input polarization form at any Rpl and α setting. Two Rpl settings have been chosen: Rpl = 16.45° and 25.02°. These Rpl values correspond to refractive index values of 1.5 and 1.7. The $\lambda/2$ plate was set to ρ = 22.5°, which produced an α value of 45° for the light incident upon RM1. The 45° orientation was chosen because it departs equally from the BAR's two eigenstates. Preliminary calculations indicate maximum polarization alteration will occur at, or near, this value. Equation 4.12 was solved at these two Rpl settings and one $\lambda/2$ setting (see Table 1, and the Appendix for a sample calculation of metallic reflection).

As the linearly polarized beam propagates through the BAR's optical system, its orientation and state of polarization both change upon reflection from the metallic mirrors. After a single reflection, at RM1, α has been changed by approximately 90°. After each mirror reflection α changes by approximately 90°. This change is a result of the phase value from Eqns. 4.7 and 4.10a and b. The ellipticity increases after each reflection, again this is due to phase shifts calculated from Eqns. 4.10a and b. If the mirrors were dielectrics, the α values would still vary but the ε values would remain zero.

Input and output α values differ by 0.36° for n = 1.5 and by 0.78° for n = 1.7. In general, any vibration direction measurements made will require corrections which are a function of Rpl and $\lambda/2$ setting. The p- and s-states will require no corrections whereas intermediate orientations must

Table 1. Polarization changes in the BAR's optical system

optical component	azimuth (α)	ellipticity (ε)
	n = 1.5 (Rpl = 16.46°)	
laser beam	0.00°	0.00
$\lambda/2$	45.00°	0.00
RM1	-44.87°	0.77
EM1	44.80°	1.09
RM2	-44.78°	1.34
EM2	44.64°	2.07
	n = 1.7 (Rpl = 25.02°)	
laser beam	0.00°	0.00
$\lambda/2$	45.00°	0.00
RM1	-44.70°	1.78
EM1	44.60°	2.39
RM2	-44.54°	2.99
EM2	44.22°	4.78

be corrected. Increasing ellipticity cannot be removed in calculations. Its effect can be determined only after a Jones matrix has been determined for the sample.

Conclusions

In general, the state of polarization of a linearly polarized beam is changed as it propagates through the BAR's optical system except for two specific orientations: the p-state (parallel to the plane of incidence), and the s-state (normal to the plane of incidence). Changes consist of a rotation of the vibration direction and a change from linear to elliptical polarization. The magnitude of these changes increases with higher angles of incidence (i.e., larger Rpl values) and with degree of departure from p- and s-state polarization orientations. For a beam polarized at 45° to the p- and s-states, the rotation of the vibration direction after passage through the BAR's optical system is 0.4° for Rpl = 16.5° and 0.8° for Rpl = 20.0° The corresponding changes in ellipticity are 2.07 and 4.78. The 45° orientation was chosen because it was assumed to have the maximum polarization-alteration ability; preliminary calculations tend to verify this assumption. The calculations in this chapter do not include the effects of polarization alteration by the isotropic and anisotropic samples. A description of Jones matrices for them is presented in Chapter 5.

Chapter 5. Anisotropic Materials: Jones matrices and Rpl-vs-I scans

Introduction

To calculate light reflection from anisotropic samples, both the sample's orientation and its optical properties must be known. Jones reflection matrices can be written to calculate polarized light changes after reflection from an anisotropic sample in a random orientation. This mathematical process is presented in detail and a numerical example is shown in the Appendix. The necessary mathematical rigor to form a Jones matrix simplifies considerably when non-random sections of an anisotropic material or isotropic materials are modeled. Also the process is less complicated for dielectrics than for metals. The Jones matrices presented herein can be used to calculate the reflected intensity and polarization form for any anisotropic dielectric or metal in any orientation.

To determine the refractive indices of an anisotropic sample, it is rotated about the BAR's x axis and N and n determined at several S settings. From the N,n values, the Julian-Bloss method[7] (Bloss, AR-1987a, and Gunter, 1987f) can be used to determine the principal refractive indices and orientation for an anisotropic sample. All of the necessary data can be collected from a single polished section for a randomly oriented sample. The RTR method thus differs from other more common techniques used to determine the principal refractive indices of anisotropic samples. For example, both the U-stage and spindle stage are used to orient a sample so a principal refractive index can be measured by the oil immersion method. However, in RTR all principal refractive indices can be measured regardless of the orientation and, through the use of Jones matrices, the reflected light's intensity and polarization can also be calculated.

BAR scans on anisotropic samples

As the plane of polarization of the incident light is changed, the resulting Rpl-vs-I scan for anisotropic samples differs from that for isotropic samples in two ways: 1) the critical Rpl varies, and 2) the scan may show more than one inflection point. In Figure 10 the BAR's stage and hemicylinder are shown; also shown in this figure is an ellipse whose major and minor axes correspond to N and n. If the incident linearly polarized light is parallel to either N or n, an Rpl-vs-I scan will yield the corresponding refractive index value. Thus, Rpl-vs-I scans for quartz yield different curves, which are a function of the orientation of the incident polarized light (Figure 11). For materials of high birefringence, in certain orientations, the Rpl-vs-I scans show an inflection (Figure 12). Before anisotropic samples can be analyzed with the BAR (i.e., N and n values determined), the theory for light reflection from randomly orientated anisotropic samples must be understood, along with the discrepancy between Figure 11 and Figure 12. In other words the fine-structure of the Rpl-vs-I curves for anisotropic samples must be understood.

---

[7] The Julian-Bloss method is explained in detail in the Appendix.

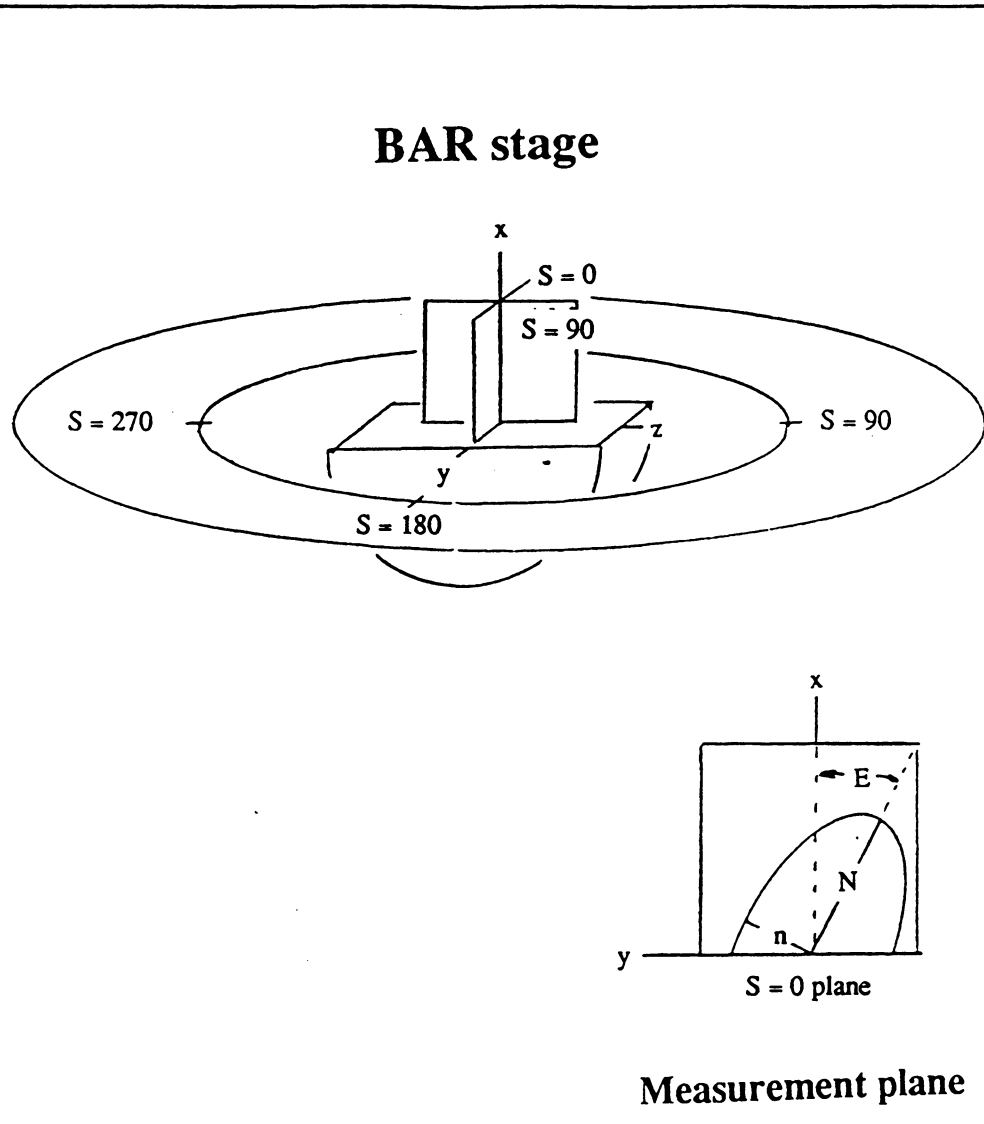

Figure 10. **Illustration of the BAR's stage with an enlarged view of an anisotropic crystal:** The observable refractive indices for anisotropic samples occur in the BAR's xy plane. In this plane the two refractive indices, N and n, are the semi-major and semi-minor axes of an ellipse which represent the intersection between the BAR's xy plane and the optical indicatrix of a biaxial crystal. When the plane of polarization of the incident light is made parallel to one of these vibration directions its corresponding refractive index value can be determined. By measuring N,n pairs as the sample is rotated about the BAR's x-axis, the Viola curves are formed and the material's optic properties can be determined. S represents the angular position of the BAR's stage and E is the angle between a vibration direction and the BAR's x-axis.

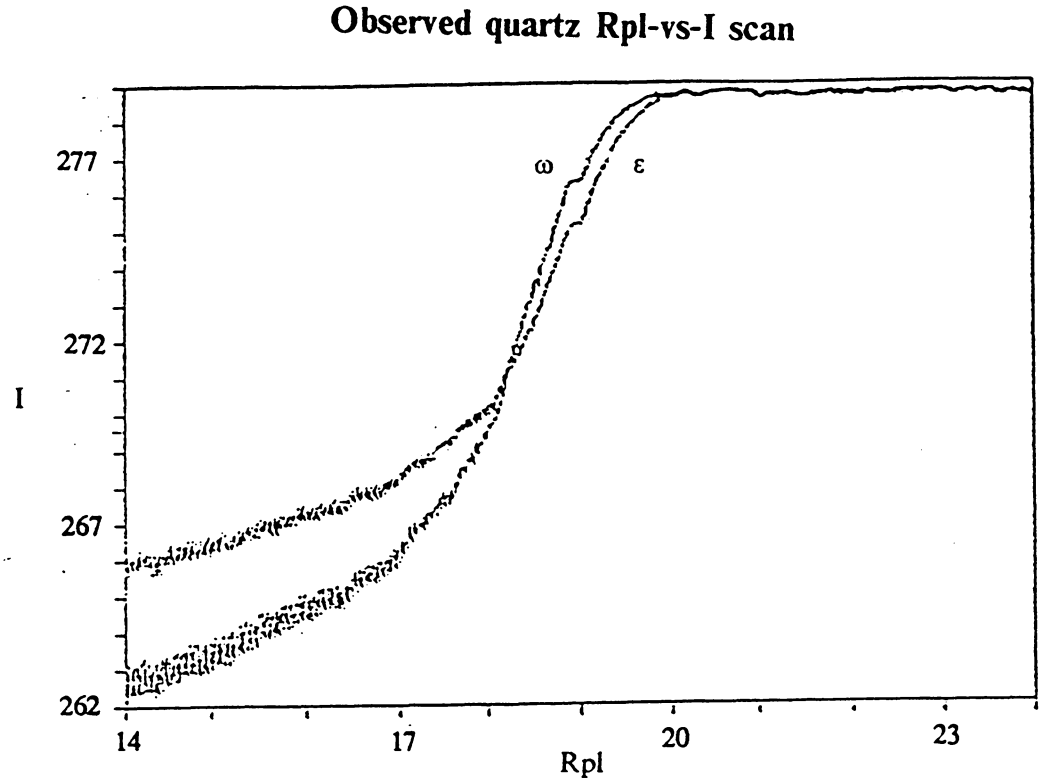

Figure 11. BAR scan of quartz: The two Rpl-vs-I scans represent N and n, ε and ω, for a quartz crystal. The separate curves result by aligning the plane of polarization of the incident light parallel to N's and n's vibration direction. As the plane of polarization is varied a family of Rpl-vs-I scans would occur and would be bounded by these two curves.

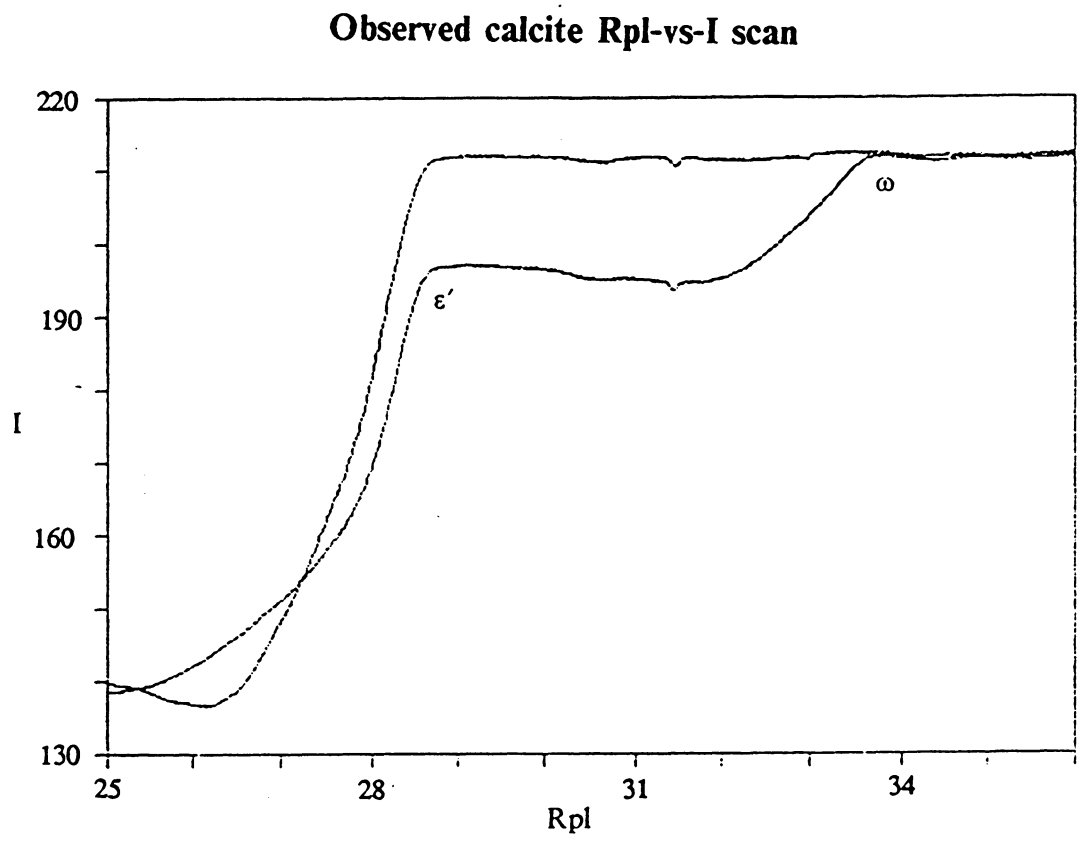

Figure 12. **BAR scan of calcite:** The same method was used to produce these pair of curves for calcite as for quartz (Figure 11). However, these curves appear significantly different from those for quartz. Calcite's principal refractive indices could be determined from these curves, but the algorithm would differ from that which would be used for quartz.

Jones reflection matrices for anisotropic samples

Anisotropic samples used on the BAR produced two previously unexplained phenomenon: 1) rotation of the plane of polarization of the input polarized light after reflection from the sample and 2) different forms of the Rpl-vs-I scans for quartz and calcite. To understand these phenomena and to understand better the behavior of reflected polarized light, a mathematical approach was sought to describe quantitatively the behavior of polarized light when reflected from optical elements. The polarization characteristic's of the BAR were described in the last chapter. There the Jones calculus method was introduced to model the interaction of polarized light with polarization-altering optical components. In this section Jones reflection matrices are developed for anisotropic materials.

Discussion

Polarized light reflection from dielectrics is best expressed by the use of Jones matrices. Once the Jones matrix has been defined, the reflected intensity and polarization alteration upon reflection can be calculated for various angles of incidence and, for anisotropic samples, in various orientations. To model samples on the BAR, the cone angle effect, explained in detail in the next chapter, is added and its effect on the calculations for anisotropic samples can be modeled. It is added to the Fresnel equations to model the Gaussian energy profile of a focused laser beam; the finer the focus of the laser beam, the larger the cone angle.

General case - biaxial sample, random orientation: The derivation of the Jones matrices begins with the results from Maxwell's equations which relate the displacement vector and the magnetic induction to the electric field and magnetic field by the dielectric and magnetic permeability tensors respectively. Several papers in the ellipsometry literature proceed with this derivation and describe

the mathematical methods to calculate the reflected light properties from anisotropic samples: Aspenes (1980), Azzam and Bashara (1977), Berreman (1972, 1973), DeSmet (1975, 1976), Lin-Chung and Teitler (1984), and Teitler and Henvis (1970). The basic approach used by each author does not differ greatly and the method described by Azzam and Bashara is followed. In their method the 4x4 matrix scheme devised by Teitler and Henvis (1970) and Berreman (1972) is modified to calculate a Jones reflection matrix for reflection from a semi-infinite biaxial material (i.e., a crystal plate) in a random orientation. The 4x4 method was originally developed by Billard (1966) and Teitler and Henvis (1970) to calculate a Jones reflection matrix for a finite biaxial material (i.e., a thin film).

The 4x4 method requires creation and mathematical manipulation of a series of matrices. The final matrix, prior to the Jones matrix, has the dimensions of 4x4, hence the method's name. The series of required matrices are given below in the order of their creation, the arrows indicate some form of mathematical treatment, explained later, to arrive at the next matrix in the series:

dielectric tensor (DT) → optical matrix (OM) → propagation matrix (PM) → reflection matrix (RM)

A numerical example of the above outlined procedure is presented in the Appendix. The example follows the equations given below to arrive at the general Jones reflection matrix for an anisotropic dielectric in a random orientation, thus permitting calculation of the intensity and polarization characteristics of a polarized light beam reflected at an angle θ from it.

Transformation equations: Before the dielectric tensor can be formed, the spherical coordinates used to denote a crystal's orientation on the BAR must be transformed into cartesian coordinates. The following equations transform the S,E spherical coordinates (Figure 10) into x,y,z cartesian coordinates.

$$x = \cos E \qquad [5.1a]$$

$$y = \sin E \cos S \qquad [5.1b]$$

$$z = \sin E \sin S \qquad [5.1c]$$

$$S = \tan^{-1}\frac{z}{y} \qquad [5.2a]$$

$$E = \cos^{-1}x \qquad [5.2b]$$

where,

x,y,z = cartesian coordinates for the BAR

S,E = spherical coordinates for the BAR.

Dielectric tensor: The dielectric tensor, (DT), defines the optical properties of a dielectric material in a specific orientation. From the dielectric tensor the optical properties and orientation of a biaxial material can be found, similarly to that described in Bloss (AR-1987a, Appendix). Unfortunately, there exists two tensors which are closely related: the index tensor (Ramachamdran and Ramaseshan, 1961) and the dielectric tensor. In the physics literature the dielectric tensor is used and calculated based upon the square of the refractive indices; in the Julian-Bloss method (Bloss, AR-1987a and Gunter, AR-1987f) the index tensor is used and written based upon the inverse squares of the refractive indices, which more closely defines their geometrical objective of determining the shape of the optical indicatrix. For Jones matrix calculations, the dielectric tensor will be used. The dielectric tensor is written as follows.

$$\begin{bmatrix} DT_{11} & DT_{12} & DT_{13} \\ DT_{21} & DT_{22} & DT_{23} \\ DT_{31} & DT_{32} & DT_{33} \end{bmatrix} \qquad [5.3]$$

where,

$$DT_{11} = \alpha^2 \cos^2\theta_{11} + \beta^2 \cos^2\theta_{21} + \gamma^2 \cos^2\theta_{31}$$

$$DT_{22} = \alpha^2 \cos^2\theta_{12} + \beta^2 \cos^2\theta_{22} + \gamma^2 \cos^2\theta_{32}$$

$$DT_{33} = \alpha^2 \cos^2\theta_{13} + \beta^2 \cos^2\theta_{23} + \gamma^2 \cos^2\theta_{33}$$

$$DT_{12} \equiv DT_{21} = \alpha^2 \cos\theta_{11} \cos\theta_{12} + \beta^2 \cos\theta_{21} \cos\theta_{22} + \gamma^2 \cos\theta_{31} \cos\theta_{32}$$

$$DT_{13} \equiv DT_{31} = \alpha^2 \cos\theta_{11} \cos\theta_{13} + \beta^2 \cos\theta_{21} \cos\theta_{23} + \gamma^2 \cos\theta_{31} \cos\theta_{33}$$

$$DT_{23} \equiv DT_{32} = \alpha^2 \cos\theta_{12} \cos\theta_{13} + \beta^2 \cos\theta_{22} \cos\theta_{23} + \gamma^2 \cos\theta_{32} \cos\theta_{33}$$

and,

α, β, γ = principal refractive indices
x,y,z = cartesian axis for the BAR
X,Y,Z = orientations of α, β, γ
θ_{11} = angle between X and x
θ_{12} = angle between X and y
θ_{13} = angle between X and z
θ_{21} = angle between Y and x
θ_{22} = angle between Y and y
θ_{23} = angle between Y and z
θ_{31} = angle between Z and x
θ_{32} = angle between Z and y
θ_{33} = angle between Z and z.

The eigenvectors of the dielectric tensor define the orientation of the principal vibration axes of the optical indicatrix. The eigenvalues permit calculation of the principal refractive indices, through a reverse transformation. For the method presented above, the square root of the eigenvalues will correspond to the principal refractive indices. For the method presented in Bloss (AR-1987a, Appendix) the inverse square root of each eigenvalue is the desired refractive index. To test the derivation of Eqn. 5.3, the data used in Bloss (AR-1987a, Appendix) were used and the same refractive index values and orientations resulted. The numerical results are presented in the Appendix.

Equation 5.3 presents the dielectric tensor written in terms of the refractive index, n, for the sample. A modified "dielectric tensor" can be written for metals. Similarly to the generalized Fresnel equations presented earlier, the refractive index of the metal is defined by replacing n with (n - ik), where k is the material's absorption coefficient. Anisotropic materials will possess different values of both n and k for different orientations in the material, inclusion of these n and k values in Eqn. 5.3 will allow calculations to be performed for anisotropic metals.

Optical matrix: The optical matrix is the first of several matrices required to calculate the reflected intensity; each matrix is based upon information obtained from an earlier matrix with the final re-

sultant matrix being the general Jones reflection matrix. The optical matrix (OM) is a 6x6 matrix formed from the overall optical properties and orientation of the material under study. It consists of four 3x3 matrices, which are the tensors that define the optical properties of any material under study. Equation 5.4 represents the optical matrix, (OM), written in abbreviated form. Each entry in OM is a 3x3 matrix, thus the overall dimension of OM is 6x6.

$$\begin{bmatrix} DT & \rho \\ \rho' & \mu \end{bmatrix} \qquad [5.4]$$

where,

DT = dielectric tensor (Eqn. 5.3)

ρ and ρ' = optical-rotation tensors, null matrices for reflection

μ = magnetic permeability tensor, for non-magnetic materials it is the identity matrix.

For dielectrics with zero magnetic permeability, OM simplifies considerably. The magnetic permeability tensor is simply the identity matrix. In reflected light analysis, the optical-rotation matrices simplify to null matrices; these matrices only become non-zero for light transmission in optically active media (i.e., media that rotate the plane of polarization).

If the materials under study exhibit non-zero magnetic permeability, then the magnetic permeability tensor could be calculated. The procedure to calculate this tensor is similar to that for the dielectric tensor. Detailed discussion of the magnetic permeability tensor is presented in Nye (1986) and Bloss (1971).

Propagation matrix: Berreman (1972) discusses the necessary boundary conditions for reflection of light from an anisotropic material. By satisfying these boundary conditions, a set of simultaneous equations results which upon solution yields the propagation matrix. The propagation matrix (PM) is formed by numerical manipulation of the optical matrix and can be written as follows:

$$\begin{bmatrix} PM_{11} & PM_{12} & PM_{13} & PM_{14} \\ PM_{21} & PM_{22} & PM_{23} & PM_{24} \\ PM_{31} & PM_{32} & PM_{33} & PM_{34} \\ PM_{41} & PM_{42} & PM_{43} & PM_{44} \end{bmatrix} \qquad [5.5]$$

where,

$$PM_{11} = OM_{51} + (OM_{53} + \eta)\,A_1 + OM_{56}\,A_5$$
$$PM_{12} = OM_{55} + (OM_{53} + \eta)\,A_4 + OM_{56}\,A_8$$
$$PM_{13} = OM_{52} + (OM_{53} + \eta)\,A_2 + OM_{56}\,A_6$$
$$-PM_{14} = OM_{54} + (OM_{53} + \eta)\,A_3 + OM_{56}\,A_7$$
$$PM_{21} = OM_{11} + OM_{13}\,A_1 + OM_{16}\,A_5$$
$$PM_{22} = OM_{15} + OM_{13}\,A_4 + OM_{16}\,A_8$$
$$PM_{23} = OM_{12} + OM_{13}\,A_2 + OM_{16}\,A_6$$
$$-PM_{24} = OM_{14} + OM_{13}\,A_3 + OM_{16}\,A_7$$
$$-PM_{31} = OM_{41} + OM_{43}\,A_1 + OM_{46}\,A_5$$
$$-PM_{32} = OM_{45} + OM_{43}\,A_4 + OM_{46}\,A_8$$
$$-PM_{33} = OM_{42} + OM_{43}\,A_2 + OM_{46}\,A_6$$
$$PM_{34} = OM_{44} + OM_{43}\,A_3 + OM_{46}\,A_7$$
$$PM_{41} = OM_{21} + OM_{23}\,A_1 + (OM_{26} - \eta)\,A_5$$
$$PM_{42} = OM_{25} + OM_{23}\,A_4 + (OM_{26} - \eta)\,A_8$$
$$PM_{43} = OM_{22} + OM_{23}\,A_2 + (OM_{26} - \eta)\,A_6$$
$$-PM_{44} = OM_{24} + OM_{23}\,A_3 + (OM_{26} - \eta)\,A_7$$

and,

$$\eta = n_i \sin\theta$$
θ = angle of incidence
n_i = refractive index of incident media
$$A_1 = (OM_{61}\,OM_{36} - OM_{31}\,OM_{66}) / A_9$$
$$A_2 = [(OM_{62} - \eta)\,OM_{36} - OM_{32}\,OM_{66}] / A_9$$
$$A_3 = (OM_{64}\,OM_{36} - OM_{34}\,OM_{66}) / A_9$$
$$A_4 = [OM_{65}\,OM_{36} - (OM_{35} + \eta)\,OM_{66}] / A_9$$
$$A_5 = (OM_{63}\,OM_{31} - OM_{33}\,OM_{61}) / A_9$$
$$A_6 = [OM_{63}\,OM_{32} - (OM_{62} - \eta)\,OM_{33}] / A_9$$
$$A_7 = (OM_{63}\,OM_{34} - OM_{33}\,OM_{64}) / A_9$$
$$A_8 = [(OM_{35} + \eta)\,OM_{63} - OM_{33}\,OM_{65}] / A_9$$
$$A_9 = OM_{33}\,OM_{66} - OM_{36}\,OM_{63}$$

The above equations can be simplified for the case of light reflection from a non-magnetic dielectric as follows:

$$PM_{11} = PM_{22} = -\eta(OM_{31}/OM_{33})$$
$$PM_{12} = 1 - \eta^2/OM_{33}$$
$$PM_{13} = PM_{42} = -\eta(OM_{32}/OM_{33})$$
$$PM_{21} = OM_{11} - OM_{13}^2/OM_{33}$$
$$PM_{23} = PM_{41} = OM_{12} - OM_{13}(OM_{32}/OM_{33})$$
$$PM_{34} = 1$$
$$PM_{43} = OM_{22} - OM_{23}^2/OM_{33} - \eta^2$$
$$PM_{14} = PM_{24} = PM_{31} = PM_{32} = PM_{33} = PM_{44} = 0.$$

Jones reflection matrix: The general Jones reflection matrix (RM) is found by calculating the four eigenvalues and their four corresponding eigenvectors of the propagation matrix. Of the four eigenvectors, two represent the reflected light and two represent transmitted light. The reflected and transmitted eigenvectors are distinguished based upon the sign of their associated eigenvalue. The two eigenvectors whose associated eigenvalues have a positive imaginary part, if the eigenvalues are complex, or a positive real part, if the eigenvalues are real, represent the eigenvectors associated with the reflected beam. These two eigenvectors can then be mathematically manipulated to arrive at the Jones matrix as follows:

$$RM = (S_1 + S_2)^{-1}(S_2 - S_1) \qquad [5.6]$$

where,

$$S_1 = \cos\theta \begin{bmatrix} \psi_{11} & \psi_{12} \\ \psi_{41}/n_i & \psi_{42}/n_i \end{bmatrix}^{-1}$$

$$S_2 = \begin{bmatrix} \psi_{21}/n_i & \psi_{22}/n_i \\ \psi_{31} & \psi_{32} \end{bmatrix}^{-1}$$

RM = general Jones reflection matrix

ψ_{k1} = four components of one eigenvector

ψ_{k2} = four components of the other eigenvector

After RM is found, it can be substituted into the following equation to find the reflected amplitudes for the p- and s-states:

$$\begin{bmatrix} E_{rx} \\ E_{ry} \end{bmatrix} = \begin{bmatrix} r_{11} & r_{12} \\ r_{21} & r_{22} \end{bmatrix} \begin{bmatrix} E_{ix} \\ E_{iy} \end{bmatrix} \qquad [5.7]$$

where,

E_{ix} = amplitude of x component of incident light

E_{iy} = amplitude of y component of incident light

E_{rx} = amplitude of x component of reflected light

E_{ry} = amplitude of y component of reflected light

r_{11} = matrix element that maps E_{ix} onto E_{rx}

r_{12} = matrix element that maps E_{iy} onto E_{rx}

r_{21} = matrix element that maps E_{ix} onto E_{ry}

r_{22} = matrix element that maps E_{iy} onto E_{ry}

Next, the following two equations (Eqns. 5.8 and 5.9) can be used to analyze the intensity (I) and polarization (α) characteristics of the reflected beam:

$$I = E_{rx}^2 + E_{ry}^2 \qquad [5.8]$$

where,

I = intensity of the reflected beam

$$\alpha = \tan^{-1}\frac{E_{ry}}{E_{rx}} \qquad [5.9]$$

where,

α = orientation of the linearly polarized light after reflection

Equation 5.9 applies only to dielectrics and is a simplified form of Eqn. 4.7. An example calculation for an anisotropic sample in a random orientation is presented in the Appendix, along with the simpler case of an isotropic sample.

Explicit Jones matrix representation for five special cases

The above mathematical procedure to calculate a general Jones reflection matrix for a randomly oriented anisotropic dielectric can be simplified for particular classes and orientations of materials. Five examples follow in which the equations required to calculate the Jones matrix can be written in simpler form, thus significantly reducing the amount of mathematical rigor necessary to derive the desired Jones matrix.

Isotropic material: For an isotropic material the Jones matrix simplifies to a diagonal matrix, $r_{12} = r_{21} = 0$. The diagonal terms in the matrix reduce to the Fresnel coefficients for p- and s-states. Equation 5.10 represents this simplified matrix.

$$\begin{bmatrix} r_{11} & 0 \\ 0 & r_{22} \end{bmatrix} \qquad [5.10]$$

where,

$$r_{11} = (n_t \cos\theta_i - n_i \cos\theta_t) / (n_t \cos\theta_i + n_i \cos\theta_t)$$
$$r_{22} = (n_i \cos\theta_i - n_t \cos\theta_t) / (n_i \cos\theta_i + n_t \cos\theta_t)$$

The above Jones matrix is identical to the following equation (Eqn. 5.11) normally used to calculate the intensity of linearly polarized light at an angle α reflected from an isotropic material.

$$R = r_p^2 \cos^2\alpha + r_s^2 \sin^2\alpha \qquad [5.11]$$

where,

R = intensity of the reflected light
r_p = r_{11} Eqn. 5.10, amplitude parallel the plane of incidence
r_s = r_{22} Eqn. 5.10, amplitude normal to the plane of incidence
α = angle between the plane of incidence and the polarization vibration direction.

Uniaxial material with optic axis parallel to x axis of BAR: Azzam and Bashara (1977) present a set of equations to calculate the reflected intensity from a uniaxial crystal in a preferred orientation. If the crystal's optic axis is parallel to the x axis of the BAR, Eqns. 5.3 to 5.6 reduce to Eqn. 5.12.

In Eqn. 5.12, as in Eqn. 5.11, the off diagonal elements of the 2x2 Jones matrix are zero, $r_{12} = r_{21} = 0$.

$$r_{11} = \frac{\omega\varepsilon\cos\theta - n_i(\varepsilon^2 - n_i^2\sin^2\theta)^{\frac{1}{2}}}{\omega\varepsilon\cos\theta + n_i(\varepsilon^2 - n_i^2\sin^2\theta)^{\frac{1}{2}}} \qquad [5.12a]$$

$$r_{22} = \frac{n_i\cos\theta - (\omega^2 - n_i^2\sin\theta)^{\frac{1}{2}}}{n_i\cos\theta + (\omega^2 - n_i^2\sin\theta)^{\frac{1}{2}}} \qquad [5.12b]$$

where,

r_{11} and r_{22} = diagonal elements of Jones matrix

ω and ε = two principal refractive indices for a uniaxial material

Uniaxial material with optic axis in yz plane of BAR: If the optic axis of a uniaxial material lies in the flat surface of the hemisphere, the following Jones matrix can be written (Sosnowski, 1972):

$$r_{11} = \frac{F_1G_4 + F_2G_3}{F_1 + F_2} \qquad [5.13a]$$

$$r_{12} = \frac{F_1F_2(G_2 - G_1)}{F_1 + F_2} \qquad [5.13b]$$

$$r_{21} = \frac{G_4 - G_3}{F_1 + F_2} \qquad [5.13c]$$

$$r_{22} = \frac{F_1G_1 + F_2G_2}{F_1 + F_2} \qquad [5.13d]$$

where,

ϕ = angle between the optic axis and the z axis of the BAR

$F_1 = J / (n_i\sin^2\theta + J\cos\theta)\tan\phi$

$F_2 = \omega\tan\phi(I + n_i\omega\cos\theta) / (I\omega\cos\theta + n_iJ^2)$

$G_1 = (n_i\cos\theta - J) / (n_i\cos\theta + J)$

$G_2 = (n_i\omega\cos\theta - I) / (n_i\omega\cos\theta + I)$

$G_3 = (\omega^2\cos\theta - n_iJ) / (\omega^2\cos\theta + n_iJ)$

$G_4 = (I\omega\cos\theta - n_iJ^2) / (I\omega\cos\theta + n_iJ^2)$

and,

$$I^2 = \omega^2\varepsilon^2 - \omega^2 \sin^2\theta(\omega^2 \sin^2\phi + \varepsilon^2 \cos^2\phi)$$
$$J^2 = \omega^2 - n_i \sin^2\theta \ .$$

Unlike Eqns. 5.11 and 5.12, Eqn. 5.13 contains non-zero elements in the off diagonal entries. These non-zero values reduce the symmetry of the polarization characteristics of the BAR-material combination. For any diagonal Jones matrix, the eigenpolarization states of the BAR correspond to the p- and s-states, the x and y axes, respectively, of the BAR. The eigenpolarization states of an optical instrument define two orthogonal orientations in which the input polarization characteristics are identical to the output polarization characteristics. In general, when working with arbitrarily oriented anisotropic materials, the eigenpolarization states of the BAR-material combination will no longer be the p- and s-states, thus any input polarization will be modified (i.e., rotated) upon output and this rotation can be calculated from Eqn. 5.9.

Biaxial material with optical indicatrix oriented along the cartesian axes of the BAR: Graves (1969) derived the equations necessary to calculate the forms of the Jones reflection matrix for a biaxial material when its indicatrix is orientated along the cartesian axes of the BAR. Equation 5.14 lists his equations. As in Eqns. 5.11 and 5.12, the Jones reflection matrix is diagonal, $r_{12} = r_{21} = 0$. Thus, as described above, the eigenpolarization states for a biaxial material in this preferred orientation correspond to the p- and s-states of the BAR.

$$r_{11} = \frac{n_x n_z \cos\theta - n_i(n_z^2 - n_i^2 \sin^2\theta)^{\frac{1}{2}}}{n_x n_z \cos\theta + n_i(n_z^2 - n_i^2 \sin^2\theta)^{\frac{1}{2}}} \qquad [5.14a]$$

$$r_{22} = \frac{n_i \cos\theta - (n_y^2 - n_i^2 \sin^2\theta)^{\frac{1}{2}}}{n_i \cos\theta + (n_y^2 - n_i^2 \sin^2\theta)^{\frac{1}{2}}} \qquad [5.14b]$$

where,

n_x = principal refractive index parallel to the x axis of the BAR
n_y = principal refractive index parallel to the y axis of the BAR
n_z = principal refractive index parallel to the z axis of the BAR

The two equations (Eqn. 5.12 and 5.14) for anisotropic materials in preferred orientations will both simplify to the isotropic case (Eqn. 5.10). For the biaxial case the simplification results if the three principal refractive indices are set equal to a single value. Similarly by allowing the two principal refractive indices for a uniaxial material to become equal, Eqn. 5.12 reduces to Eqn. 5.10.

Biaxial material with a principal vibration direction parallel to the BAR's y axis: Recently DeSmet (1987) derived a set of closed form equations that can be used to calculate the Jones matrix if one of the three axes of the optical indicatrix is parallel to the y axis of the BAR. His method requires use of the dielectric tensor (Eqn. 5.3). In this special orientation the dielectric tensor has five non-zero entries. These entries are used in Eqn. 5.15 to arrive at the Jones matrix. Because of the symmetry of this orientation, the off diagonal elements of the Jones matrix are: $r_{12} = r_{21} = 0$.

$$r_{11} = \frac{(DT_{11} - DT_{13}^2/DT_{33})^{\frac{1}{2}} \cos\theta - n_i(1 - \eta^2/DT_{33})^{\frac{1}{2}}}{(DT_{11} - DT_{13}^2/DT_{33})^{\frac{1}{2}} \cos\theta + n_i(1 - \eta^2/DT_{33})^{\frac{1}{2}}} \qquad [5.15a]$$

$$r_{22} = \frac{n_1 \cos\theta - (DT_{22} - \eta^2)^{\frac{1}{2}}}{n_1 \cos\theta + (DT_{22} - \eta^2)^{\frac{1}{2}}} \qquad [5.15b]$$

where,

$$\eta = n_i \sin\theta.$$

Comparison of observed and calculated Rpl-vs-I scans for anisotropic material

To obtain calculated Rpl-vs-I scans of anisotropic materials, Eqn. 5.12 was used to model uniaxial materials with their optic axis normal to the hemisphere's flat surface. Of the various equations and methods discussed above this orientation was chosen for the following reasons: 1)

we have collected data on uniaxial materials in this orientation on the BAR and 2) the calculations are considerably simplified without loss of ability to compare calculated and observed Rpl-vs-I scans. The computer program listed in Appendix A of Gunter (AR-1987a) was modified by replacing the equations for isotropic samples (Eqn. 5.10), used in the next chapter, with those for a uniaxial material with its c axis vertical (Eqn. 5.12). Given this modification the program could produce Rpl-vs-I scans at varying cone angles, input polarization orientations, and sample birefringence. These scans could be visually compared to data already collected from the BAR to determine the effect sample anisotropy has on Rpl-vs-I scans.

Three separate birefringences were selected to perform the modeling. The smallest birefringence (0.009, representing a difference of approximately 0.4° in Rpl) corresponds to quartz, a uniaxial positive mineral. The largest birefringence (0.172, representing a maximum difference of approximately 7.2° in Rpl) corresponds to calcite, a uniaxial negative mineral. The intermediate sample (0.048, approximately 2.0° difference in Rpl) is a fictitious uniaxial positive material. Rpl-vs-I scans were generated for each of these three materials at 4 separate cone angles, which define the angular convergence of the focused laser beam, and 3 different input polarization angles. The four cone angles chosen were based upon the current and future design of the BAR plus a cone angle of 0° to model the theoretical case based upon geometrical optics. The three polarization states were chosen to correspond to the p- and s-states, the eigenpolarization states of the BAR, and a polarization orientation between them at $\alpha = 45°$. The results of these calculated data sets appear in Figure 13 through Figure 19.

Figure 13 and Figure 14 show the calculated Rpl-vs-I scans for quartz based upon Eqn. 5.12 and four separate cone angles. For these calculations the optic axis is parallel to the BAR's x axis; thus, linearly polarized light in the p-state ($\alpha = 0°$) will yield the principal refractive index ε. Likewise, polarized light in the s-state ($\alpha = 90°$) will yield ω. Polarized light in any non p- or s-state will yield a hybrid of ε and ω. In Figure 13a the three separate curves represent light in the p- and s-state plus an intermediate state ($\alpha = 45°$). The p- and the s-state show ε and ω, respectively and the 45° state shows a mixture of the two. Figure 11 is a scan of quartz taken on the

BAR. The scans in Figure 11 were performed at two α angles and do not appear similar to Figure 13a; however, as previously discussed the cone angle effect must be taken into consideration. Figure 13b was calculated in the same manner as Figure 13a except a cone angle of 2° was added. The addition of the cone angle makes these calculated Rpl-vs-I scans appear similar to the observed ones shown in Figure 11. Figure 14a and b show calculated scans similar to Figure 13b except with larger cone angles.

The same set of calculations were performed for calcite as for quartz. Calcite is negative, so its N ($=\omega$) is measurable whenever the incident light is in the s-state. Figure 15a shows the three Rpl-vs-I scans for the three separate orientations of polarized light. Unlike quartz, Rpl-vs-I scans for calcite taken on the BAR reveal two distinct "knees" in certain orientations of the crystal and the polarized light (Figure 12). These two knees appear on the calculated Rpl-vs-I scan shown in Figure 15b which incorporates a 5° cone angle. In Figure 16a and Figure 16b larger cone angles are used; in Figure 16b the "knees" finally disappear from the α = 45° scan. From these calculations on quartz and calcite we conclude that for materials whose birefringence is smaller than the cone angle any Rpl-vs-I scan will appear as though it came from an isotropic sample. For materials whose birefringence is greater than the cone angle a distinct inflection will occur on Rpl-vs-I scans when the incident polarized light is not parallel to one of the principal vibration directions. If the cone angle is increased, a consequence of focusing the laser to smaller spot sizes, as proposed for the next BAR, all anisotropic samples will behave as quartz currently does, thus allowing for more efficient handling of the data, because the modified Fresnel-fit (MFF) algorithm, to be discussed in the next chapter, can then be used for both isotropic and anisotropic samples.

Figure 17 and Figure 18 are for a positive uniaxial crystal of intermediate birefringence. The birefringence for this material correlates to a difference in Rpl of 2°. For a cone angle of 2° the α = 45° scan still shows an inflection due to the sample's anisotropism. However, for a cone angle of 5°, or higher, the inflection has disappeared.

By increasing the cone angle, as proposed for future BARs, the effect of anisotropism will disappear in the Rpl-vs-I scans. This will be an advantage because all the Rpl-vs-I data can use the MFF. The disadvantage of an increased cone angle will be reduced precision as discussed latter, however several methods can be used to improve precision at these higher cone angles.

Bloss (AR-1987a) proposed a method to determine N and n at each S setting of the BAR, a requirement for anisotropic materials. In this method two refractive indices are determined from each Rpl-vs-I scan; each scan is done at different α angles and the maximum refractive index is assigned to N and the minimum to n. If this procedure is performed at S settings from 0, 10, ..., 180, the Viola curves will result and the refractive indices and crystal orientations can be gleaned from these curves or the S,N,n data set can be processed by the Julian-Bloss method (Bloss, AR-1987a and Gunter, AR-1987f) to yield the same information more quantitatively. Figure 19a demonstrated this method with data collected by him and Gunter on a quartz sample. In their data collection it was observed that to determine n the polarized light had to be very close to the n vibration direction; however, to determine N, the polarized light orientation did not need to coincide so closely with the N vibration direction. Figure 19b is based upon the crystal with intermediate birefringence and shows a series of Rpl-vs-I curves calculated at different α angles. These calculated curves bear out their observations; the rate of change of refractive index, if calculated from these curves, would be less in the vicinity of N than n as a function of α.

Conclusions

Rotation of linearly polarized light occurs whenever the input polarization is not coincident with one of the two orthogonal eigenpolarizations of an optical system. The BAR's two eigenpolarizations states correspond to the p- and s-state when: 1) no sample is on the hemisphere, 2) an isotropic sample is on the hemisphere, or 3) an anisotropic sample in a special orientation is

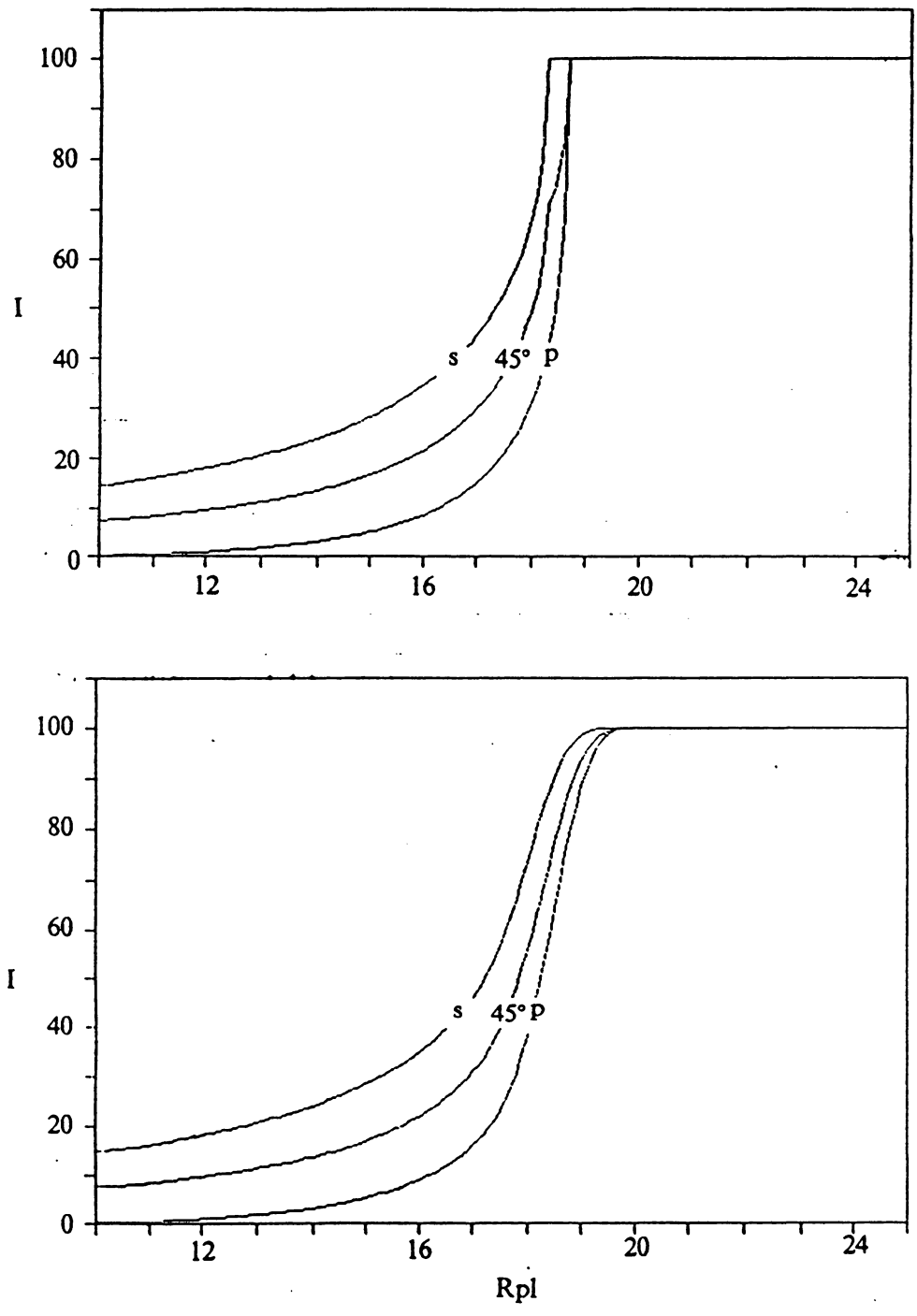

Figure 13. Calculated Rpl-vs-I scan as a function of cone angle and sample birefringence: a) (top) Calculated Rpl-vs-I scans for quartz with its optic axis vertical, 0° cone angle, for p- and s-states plus a 45° orientation of the incident linearly polarized light. b) (bottom) Same as Figure 13a except the cone angle has been increased to 2° and the inflection on the 45° scan has vanished.

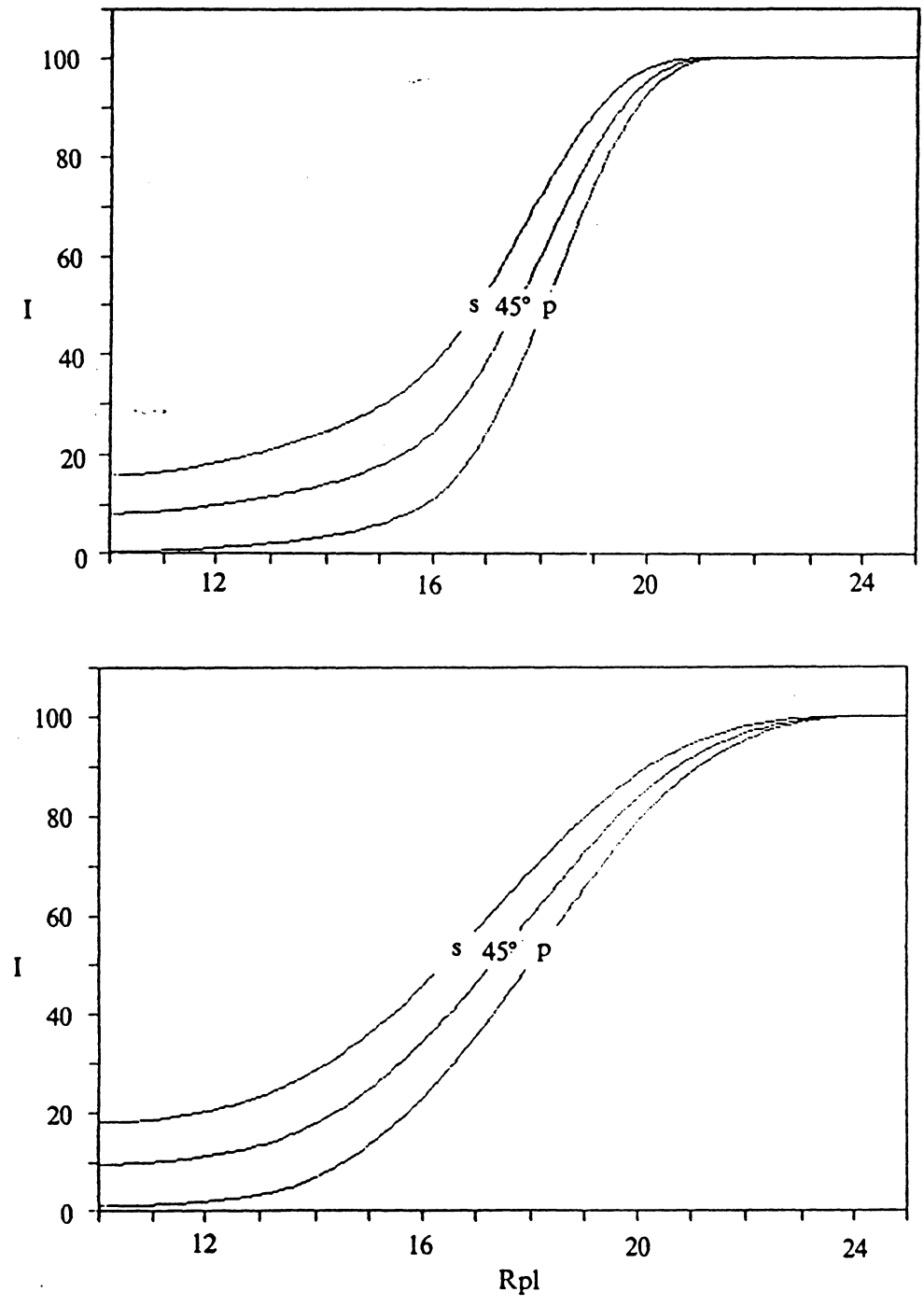

Figure 14. **Calculated Rpl-vs-I scan as a function of cone angle and sample birefringence:** a) (top) Same as Figure 13a except cone angle increased to 5°, the curves are skewed more to the right than in Figure 13a and Figure 13b. b) (bottom) Same as Figure 13a except cone angle increased to 10°, approximately the value to be used for the future BAR.

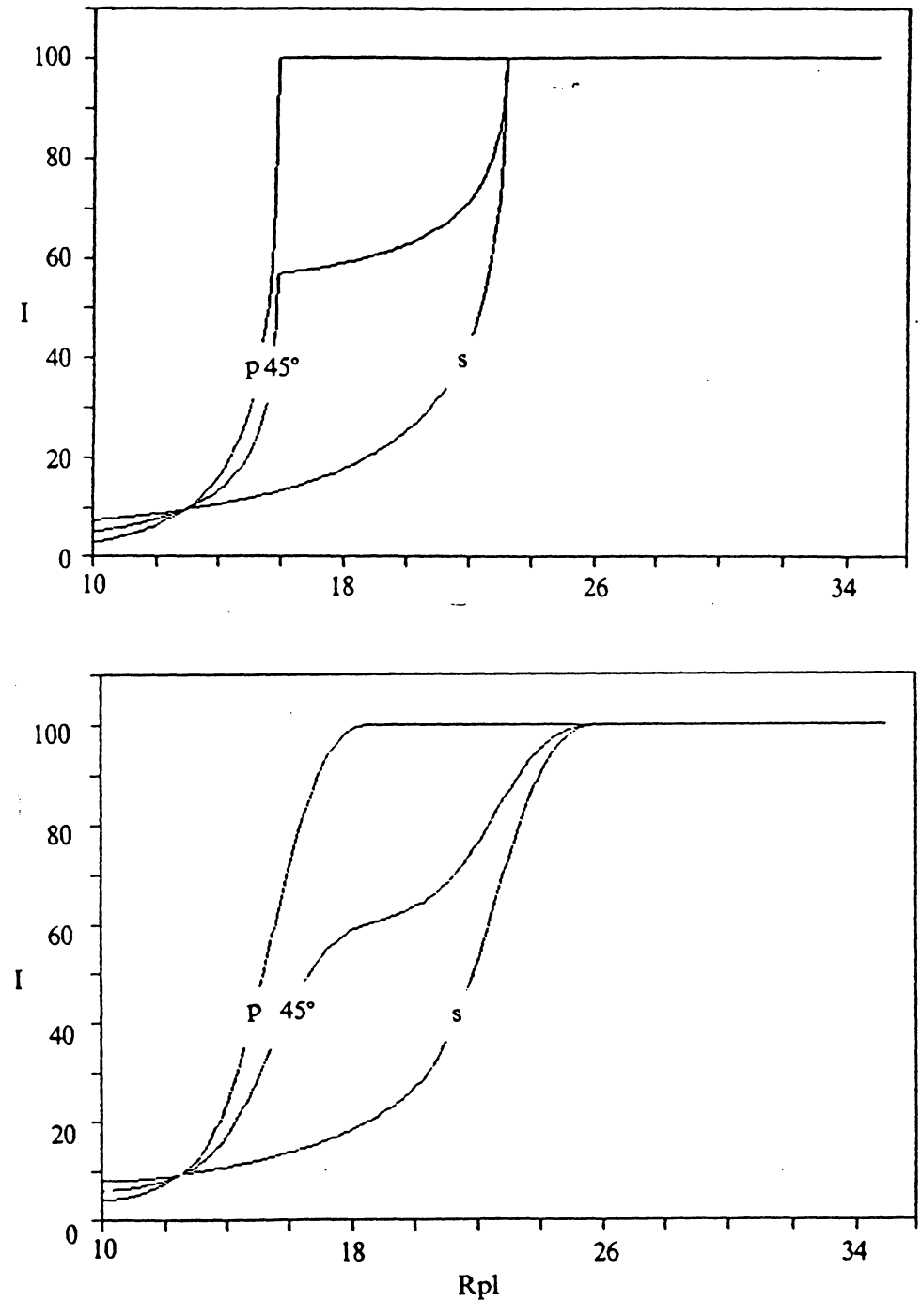

Figure 15. **Calculated Rpl-vs-I scan as a function of cone angle and sample birefringence:** a) (top) Calculated Rpl-vs-I scans for calcite, optic axis vertical and 0° cone angle. b) (bottom) Same as Figure 15a except cone angle increased to 5°. An inflection still occurs for the 45° scan.

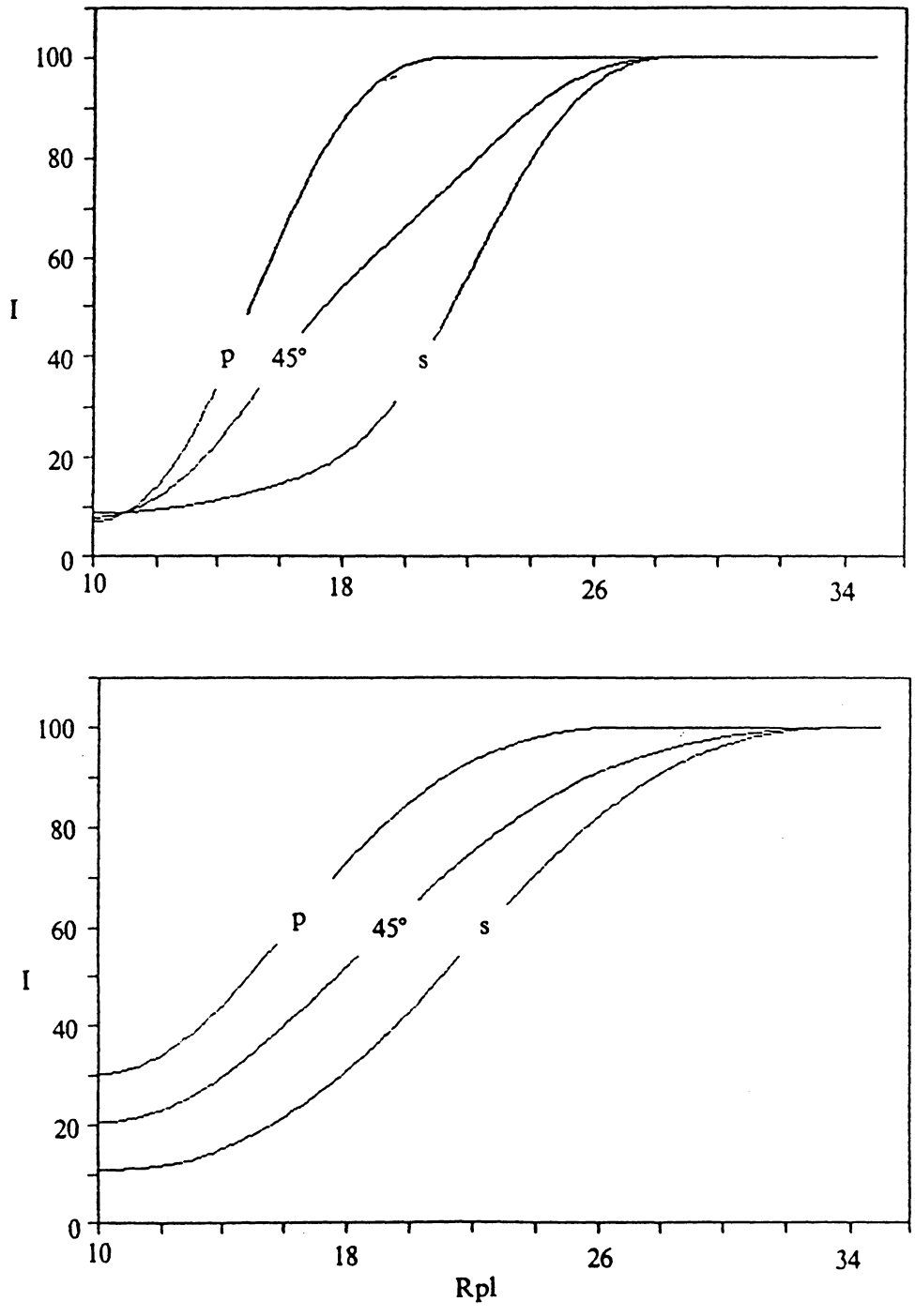

Figure 16. Calculated Rpl-vs-I scan as a function of cone angle and sample birefringence: a) (top) Same as Figure 15a except cone angle increased to 10°; only a slight inflection remains on the 45° scan. b) (bottom) Same as Figure 15b except cone angle increased to 20°; the inflection has now totally vanished from the 45° scan.

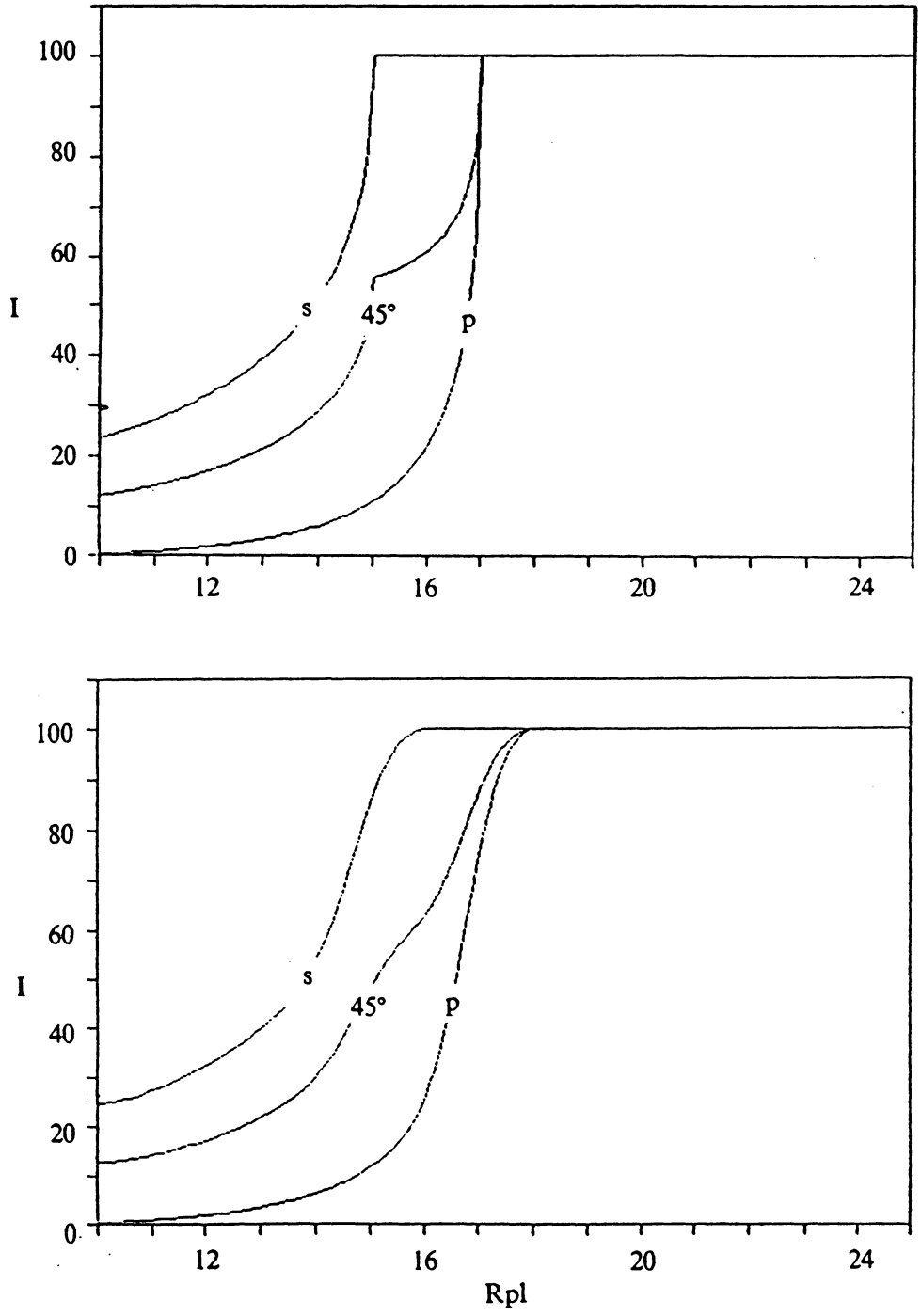

Figure 17. **Calculated Rpl-vs-I scan as a function of cone angle and sample birefringence:** a) (top) Calculated Rpl-vs-I scans for a uniaxial positive crystal with its c axis vertical and a birefringence of 0.048. b) (bottom) Same as Figure 15a except cone angle increased to 2°; the inflection on the 45° scan is still present.

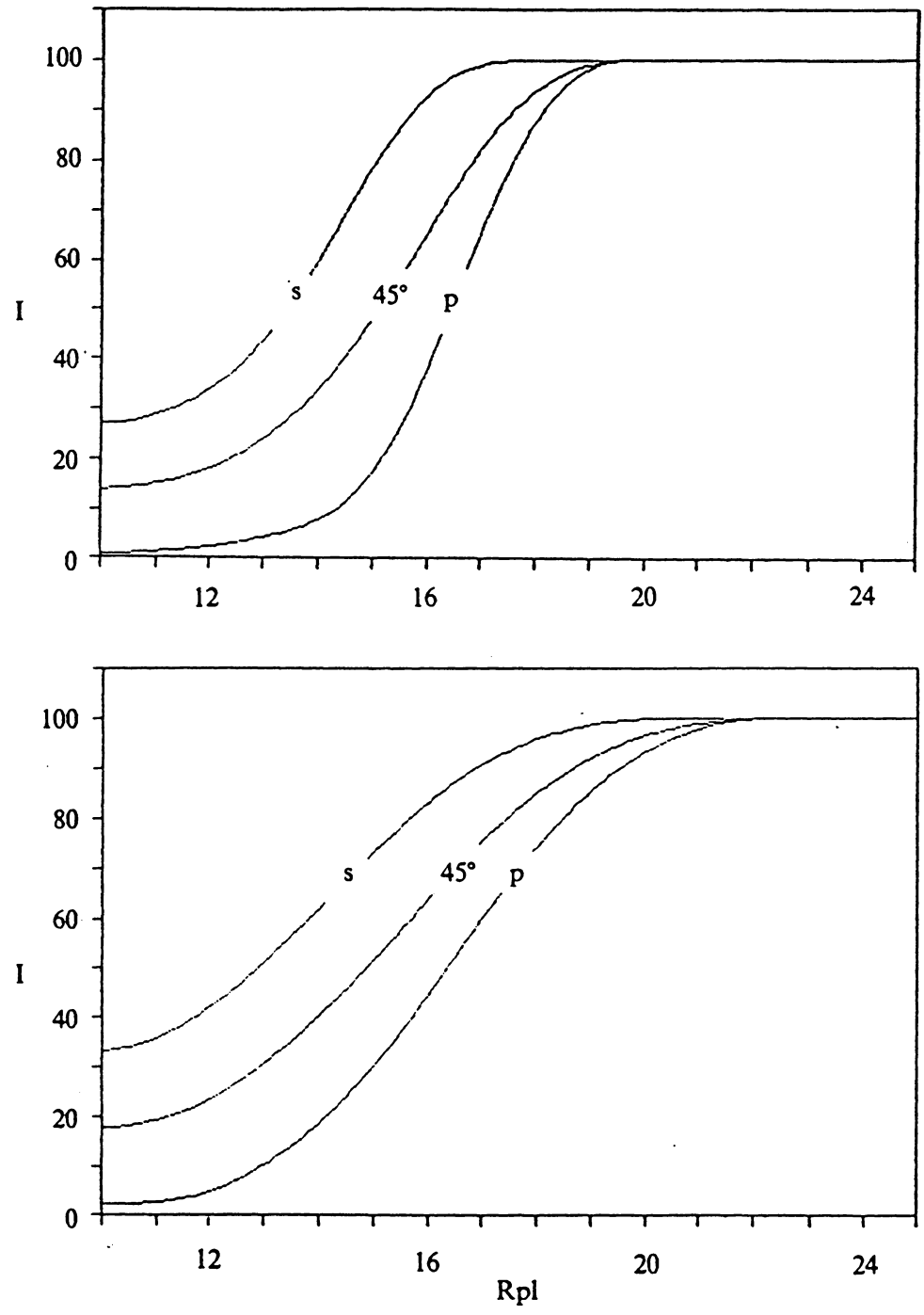

Figure 18. **Calculated Rpl-vs-I scan as a function of cone angle and sample birefringence:** a) (top) Same as Figure 17a except cone angle increased to 5°; the inflection on the 45° scan as disappeared. b) (bottom) Same as Figure 13a except cone angle increased to 10°.

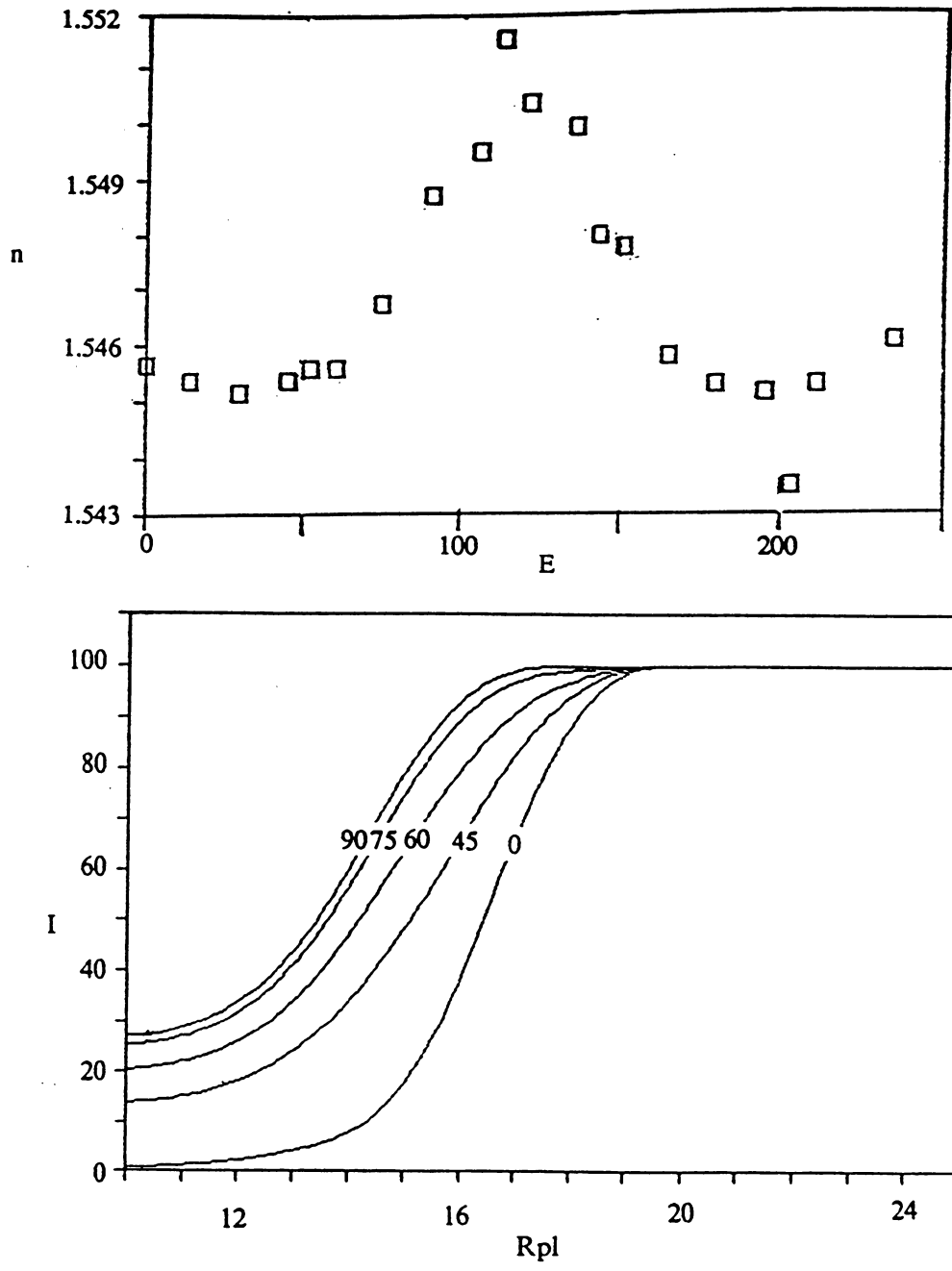

Figure 19. Observed and calculated values as a function of polarization angle: a) (top) By varying the orientation of the plane of polarization of the incident light N and n for a quartz crystal can be found. The polarization angle was varied 15°, and in the areas of N and n by 7.5°. From this curves it appears that to find n the orientation is more critical than for N. b) (bottom) Calculated Rpl-vs-I scan as a function of cone angle and sample birefringence. Same as Figure 17a except α angles of 60° and 75° have been added.

on the hemisphere (i.e., a principal vibration direction parallel to the BAR's y axis); under any other conditions the eigenpolarization states do not coincide with the p- and s-state. The difference in the appearance of the quartz and calcite Rpl-vs-I scans is due to their differences in birefringence and the cone angle of the focused laser. If the cone angle is greater than the birefringence, as true for quartz, all Rpl-vs-I scans are similar and resemble isotropic scans, except they are shifted in Rpl to designate the different refractive indices of the anisotropic sample. For calcite the cone angle is less than the Rpl difference corresponding to the birefringence; thus for certain orientations, an inflection occurs on the Rpl-vs-I curves. This inflection vanishes if the cone angle is increased. To determine the refractive indices and orientation for anisotropic crystals N,n pairs are obtained at several S settings and the Julian-Bloss method applied to this data.

Chapter 6: Detailed Examination of Rpl-vs-I scans

Introduction

This chapter is broken into two main sections. The first section attempts to explain all the factors contributing to the Rpl-vs-I scans. Once all the factors are understood, mathematical models can be developed to produce Rpl-vs-I scans similar to those obtained on the BAR. The second section of the chapter builds on the mathematical modeling of Rpl-vs-I scans. Rpl-vs-I scans are generated under different operating conditions of the BAR. A method is then tested to extract the refractive index of the sample from these scans. Finally, this new theoretical method is tested on actual BAR scans and the results compared to a former empirical algorithm that had been used in development work.

Rpl-vs-I scans from the BAR differ from idealized calculations based upon the Fresnel equations; however, the Fresnel equations can be modified to more closely resemble the observed Rpl-vs-I scans obtained from the BAR. If all the significant effects on these curves can be understood and mathematically described, better algorithms can then be developed for refractive index determination for isotropic and anisotropic samples. In this chapter a theoretical development

based upon mathematical modeling of isotropic samples and empirical observations of data are used to explain the deviation of the Rpl-vs-I scans from the Fresnel equations. From this modeling, an algorithm was developed to determine the refractive index from Rpl-vs-I scans.

Cone angle effect

Instead of the idealized infinitely small single ray used by the Fresnel equations (Gunter, AR-1986a) the BAR uses a focused laser beam, which produces a cone-shaped family of rays incident upon the sample. This causes the Rpl-vs-I scans to become more "rounded" in the area of the critical angle. Indebetouw (AR-1986b) derived the necessary modification to the Fresnel equations to compensate for this effect. This section examines how changes in the cone angle affect calculated Rpl-vs-I scans based upon the Fresnel equations.

The Fresnel equations (Eqns. 2.2) contain the variable θ, which defines a light ray's angle of incidence onto the sample. In these equations it is assumed that the incident beam could be defined as an infinitely small single ray of light. This assumption is invalid when a focused laser beam, with a finite width and convergence angle, is used. To model Rpl-vs-I scans more accurately, the size and shape of the incident laser beam can be modeled and added to the Fresnel equations.

The BAR uses a laser beam focused to a minimum spot size at the hemicylinder's upper surface. A bundle of rays converges to this focus (Gunter, AR-1986f). The convergence angle of this ray bundle is called the cone angle. For a cone angle of 0° the Fresnel equations are applicable. However for nonzero cone angles, the realistic case for the BAR, the Fresnel equations require modification.

The theoretical energy distribution of a laser beam can be modeled by the following Gaussian distribution:

$$I_r = I_0 e^{-2\frac{r^2}{w^2}} \qquad [6.1]$$

where,

I_r = resultant intensity

I_0 = original intensity

r = distance from beam center

w = beam radius.

To add the cone angle effect to the Fresnel equations, the intensity of the light whose central ray is incident at the angle θ, for a focused laser beam, is modeled by a Gaussian distribution calculated over the beam's convergence angle (= cone angle). The procedure is as follows:

1. Select a cone angle (which is a function of the spot size).

2. Select the angle of incidence (which is a function of Rpl).

3. Calculate the integrated intensity from the Fresnel equations.

To perform the integration in step 3, the cone angle could be divided into 0.1° increments. Thus, for a 2° cone angle there were 21 separate beams. Two parameters were used to calculate the intensity for an Rpl value: 1) the beam's θ angle and 2) an energy-distributive weighting factor derived from Eqn. 6.1. Given these two parameters, the intensity for an Rpl value corresponding to the angle of incidence for the central ray of the cone could be calculated by using the Fresnel equations and summing the calculated intensities. For a cone angle of 2° the Fresnel equations must be calculated 21 times and these 21 values summed and normalized to determine the intensity for this 2° cone centered at a particular angle of incidence. By this method the intensity for a cone of rays, the realistic model, could be calculated. This set of calculations performed at each Rpl setting in a scan yielded Figure 20. An example of the above procedure is presented in the Appendix.

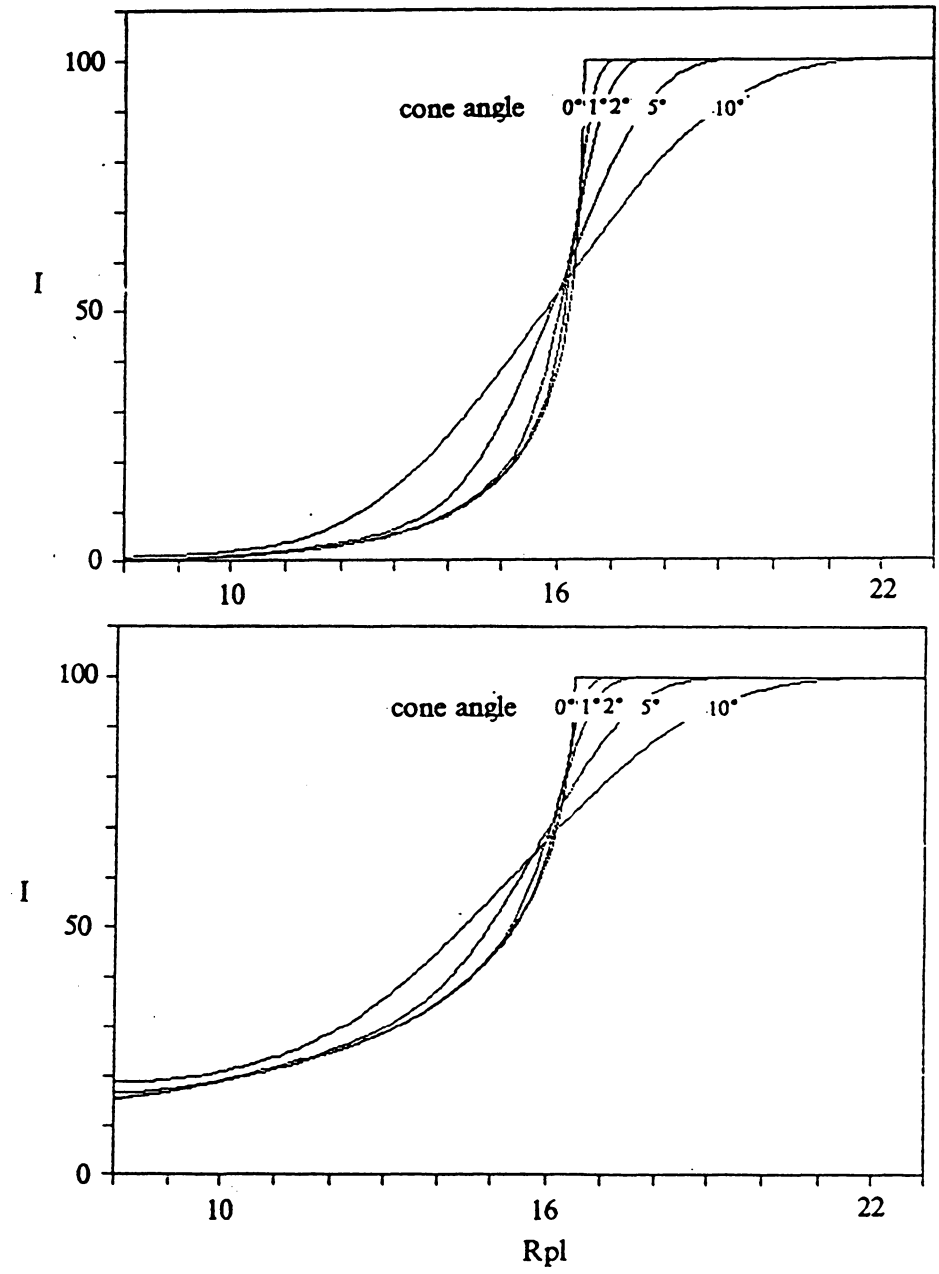

Figure 20. **Calculated Rpl-vs-I curves based on the cone angle effect:** a) (top) The top graph shows five calculated Rpl-vs-I curves, based on five cone angles (0°, 1°, 2°, 5°, and 10°), for an isotropic material with a refractive index of 1.5 using linearly polarized light in the p-state. b) (bottom) The bottom graph is identical to the top except the s-state is used.

For Figure 20 five separate cone angles were chosen: 0°, 1°, 2°, 5°, and 10°. The addition of a non-zero cone angle to the Fresnel equations causes the critical angle, as determined from an Rpl-vs-I scan, to increase by one half the cone angle in θ, where θ represents the angle of incidence and is related to Rpl and n by Eqns. 3.1a and b.

Figure 21 shows a data set recently collected by the BAR for a glass. The other curve on the graph represents a calculated curve using the Fresnel equations incorporating a cone angle of 2°. It was experimentally determined that an Rpl correction of 1.1° was required to correct the value of this glass. This 1.1° value is further confirmation that the current BAR has a cone angle of approximately 2°. From Figure 20 and Figure 21 it is apparent that the cone angle contributes significantly to the form of the Rpl-vs-I scans and should be included in modeling them.

By modifying the Fresnel equations, Rpl-vs-I scans from the BAR can be more accurately modeled than by simply using the Fresnel equations alone. By addition of the cone angle, the calculated Rpl-vs-I plots appear very similar to those obtained experimentally from the BAR. For glasses whose refractive indices are known accurately, comparison of their calculated Rpl-vs-I scans with experimental ones for various cone angles suggests that the BAR has a cone angle of approximately 2°. Thus the scan levels off at an angle that exceeds the critical angle by approximately 1°. Addition of the cone angle parameter to the Fresnel equations (Eqns. 2.2) improves their ability to model Rpl-vs-I scans for isotropic samples taken on the BAR.

In focusing the light beam on the sample, the cone angle increases with decreasing spot size on the hemicylinder's upper surface. A larger cone angle tends to "round" the critical angle knee in the Rpl-vs-I scans.

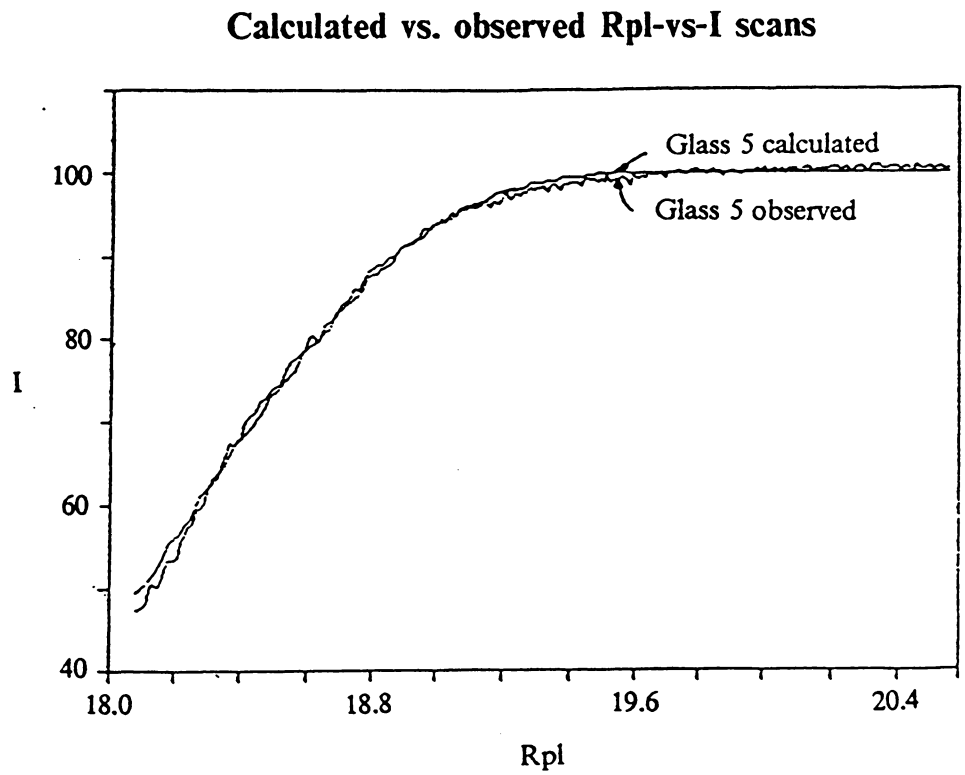

Figure 21. Calculated vs. observed Rpl-vs-I scan for a glass: Comparison of a calculated Rpl-vs-I scan for a glass with a cone angle of 2°, to an observed scan obtained from the BAR.

Contact liquid effect

When a coherent light beam reflects from two parallel surfaces of differing optical properties, which are separated by a finite thickness, interference of the two reflecting beams may occur. The path difference of the two reflecting beams will determine if constructive or destructive interference occurs. Constructive interference will take place if the path difference is some multiple of the wavelength, (λ), of reflecting light; while destructive interference occurs for odd numbered multiples of $\lambda/2$. If the path separation is on the order of a few hundredths λ, then no significant interference will occur.

A liquid film must be used to form optical contact between a sample and the BAR's hemicylinder surface. Because of this film's finite thickness, two reflected beams occur in an Rpl-vs-I scan. If the film is too thick, one beam, reflected from the sample/liquid interface interferes with the other, reflected from the hemicylinder/liquid interface. Some Rpl-vs-I scans from previous BARs (e.g., the BAR equipped with the "yellow" leaded glass hemicylinder) yielded a sinusoidal intensity variation before the critical angle was reached (Gunter, AR-1986b; Figure A4). This phenomenon was attributed to the interference of beams reflected from the sample/liquid interface and the liquid/hemicylinder interface. The effect of these interfering beams can be calculated based upon thin-film equations presented by Indebetouw (AR-1986b) and Hecht and Zajac (1979). These equations are used to calculate the intensity of the reflected and transmitted beam at the first interface. Next, the intensity of the reflected beam from the second interface, which results from the transmitted beam from the first interface, is calculated. Also, the phase of each beam is calculated based upon the path difference, where the path difference is a function of the separation of the two surfaces plus the angle of incidence of the beam. Finally, these beams were combined and their resultant plotted as a function of Rpl.

The Fresnel equations for linearly polarized light describe the theoretical Rpl-vs-I scans on the BAR for isotropic samples. However, two main departures from this theoretical treatment need

be considered for the BAR, they are: 1) the cone angle effect, as previously described and 2) the contact-liquid effect. The contact liquid produces perturbations in the intensity values of the Rpl-vs-I scans because of repeated reflection and refraction of the laser beam within the liquid film between the sample and the hemicylinder. Observations from past Rpl-vs-I scans indicate this effect is composed of two separate components. The first is based upon interference from two separate beams; one from the sample/liquid interface, the second from the liquid/hemicylinder interface. The second is a "waveguide" effect first observed on the BAR after the replacement of the leaded hemicylinder with the cubic zirconia hemicylinder. This second effect, and several other phenomena contribute, to a lesser extent, to the Rpl-vs-I scans and are addressed in the next section.

To calculate the interference between the two separate reflected beams, the thin film equations were programmed by S.C. Su. The code was then used to calculate the interference of these two beams based upon the refractive index of the hemicylinder, liquid, and sample and the thickness of the liquid film in λ.

The film thickness was estimated to be approximately 1λ. This estimate was based upon the following suggestion made by Su. A drop of the immersion liquid was placed upon a glass slide and weighed, then a one inch diameter epoxy plug containing glass samples was placed over the liquid and the flattened liquid's area observed. Next the density of the liquid was determined so that the liquid's thickness could be calculated from its measured area and weight. The thickness thus calculated was approximately 1λ. However, the glasses embedded in the one inch epoxy plug tend to stand above the surrounding epoxy matrix, thus the 1λ estimate more closely relates to the film's thickness in contact with the epoxy rather than with the glass. The film thickness between the glass samples and the slide was probably less than 1λ.

Four different film thicknesses were chosen to model: 0λ, 0.1λ, 1λ, and 10λ. The refractive index of the liquid was chosen to be 1.7 and two different refractive index samples were used, 1.5 and 1.69. All calculations were performed with linearly polarized incident light in both the p- and s-state. The calculations were performed at a cone angle of 0°, to ascertain the effect of film-

thickness for a cone angle of 0°, as well as for a cone angle of 2° to simulate the current BAR's cone angle (Gunter, AR-1987a). The results of these calculations are presented in graphical form in Figure 22 through Figure 27.

Figure 22a shows the resultant curves when the sample's index equals 1.5, the cone angle is 2°, and the light is in the p-state for the four different liquid thicknesses. From these curves it can be concluded liquid thickness has a small effect on the Rpl-vs-I scans. Figure 22b is similar to Figure 22a except the incident light is in the s-state. These four scans show more variation than those in Figure 22a; however, most of the variation occurs at Rpl values low enough to be excluded in the Fresnel-fit refinement method, described in the last section of this chapter. Figure 23 is similar to Figure 22 except the sample's index has been chosen closer to that of the liquid's, n = 1.69. In Figure 23 the variation of these curves as a function of liquid thickness is very small.

To determine the effect of various liquid thicknesses in the absence of the cone angle effect, Figure 24 through Figure 27 were calculated. In this family of graphs two curves appear on each. One curve is the Fresnel equation with the liquid modification and a cone angle of 0°, while the other contains both the liquid modification and a cone angle of 2°. For Figure 24 and Figure 25 the liquid thickness is 1λ, but the refractive index of the sample and the orientation of the incident polarized light has been changed. All four of these graphs show no significant effects from the 1λ liquid film.

Figure 26 and Figure 27 are similar to Figure 24 and Figure 25, except the liquid thickness has been set to 10λ, probably an over-estimate, but a situation which may occur for samples which are not flat or not parallel to the hemicylinder's surface. These four graphs show two interesting phenomena. In each graph the curve with a cone angle of 0° shows a sinusoidal intensity variation, which can be attributed to interference of the beam reflected from the sample/liquid interface and the beam reflected from the liquid/hemicylinder interface. The second interesting feature of these graphs is that when a 2° cone angle is added, the sinusoidal variation is almost totally removed. The non-zero cone angle is thus performing a smoothing of the data.

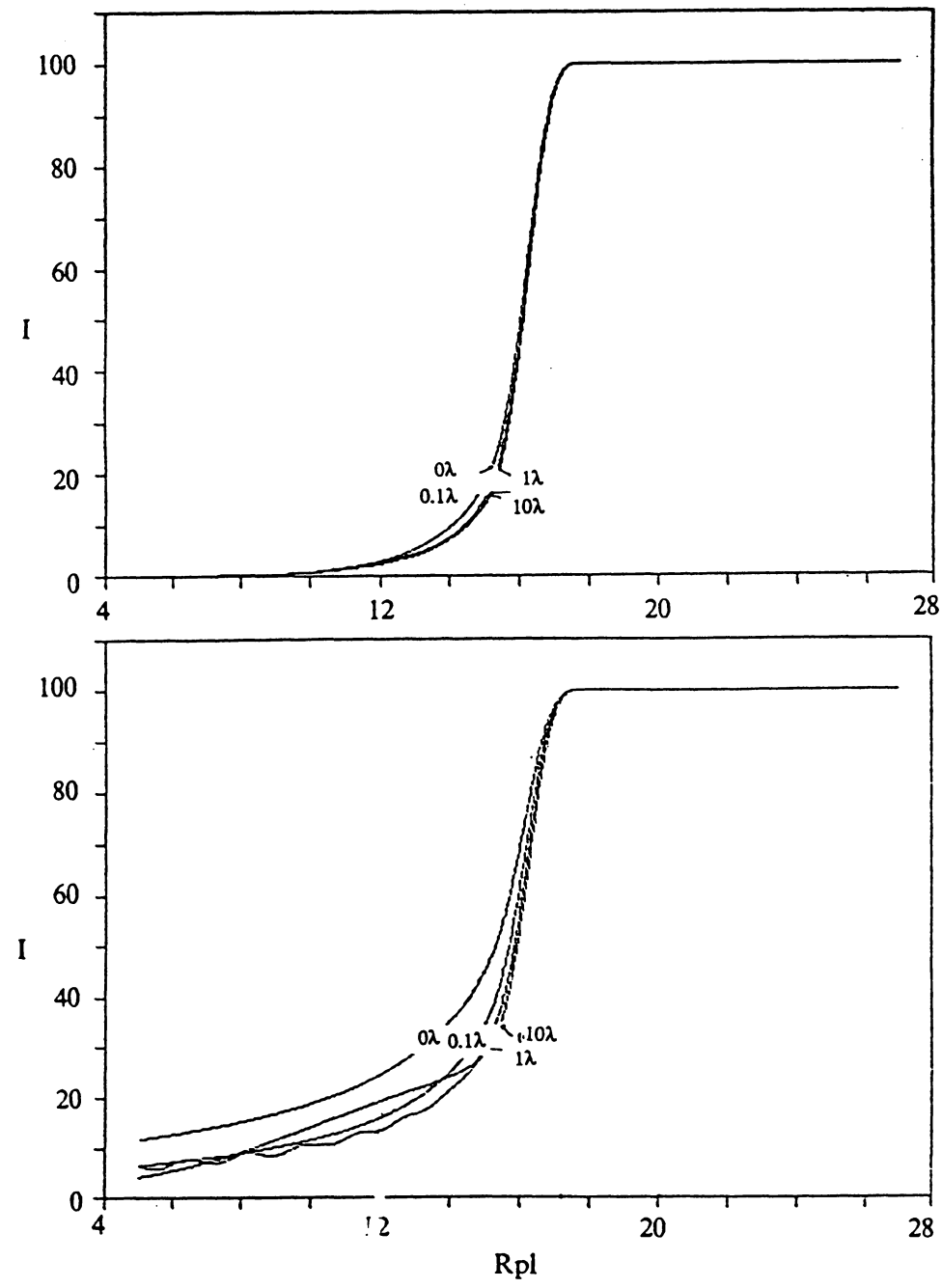

Figure 22. **Calculated Rpl-vs-I curves for different samples and liquid thicknesses:** a) (top) The incident light is in the p-state. The sample's refractive index is 1.5, the liquid's 1.7, a cone angle of 2° was used and the calculation performed for four different thicknesses of liquid; 0λ, 0.1λ, 1λ, and 10λ. b) (bottom) Similar to Figure 22a except the light is in the s-state.

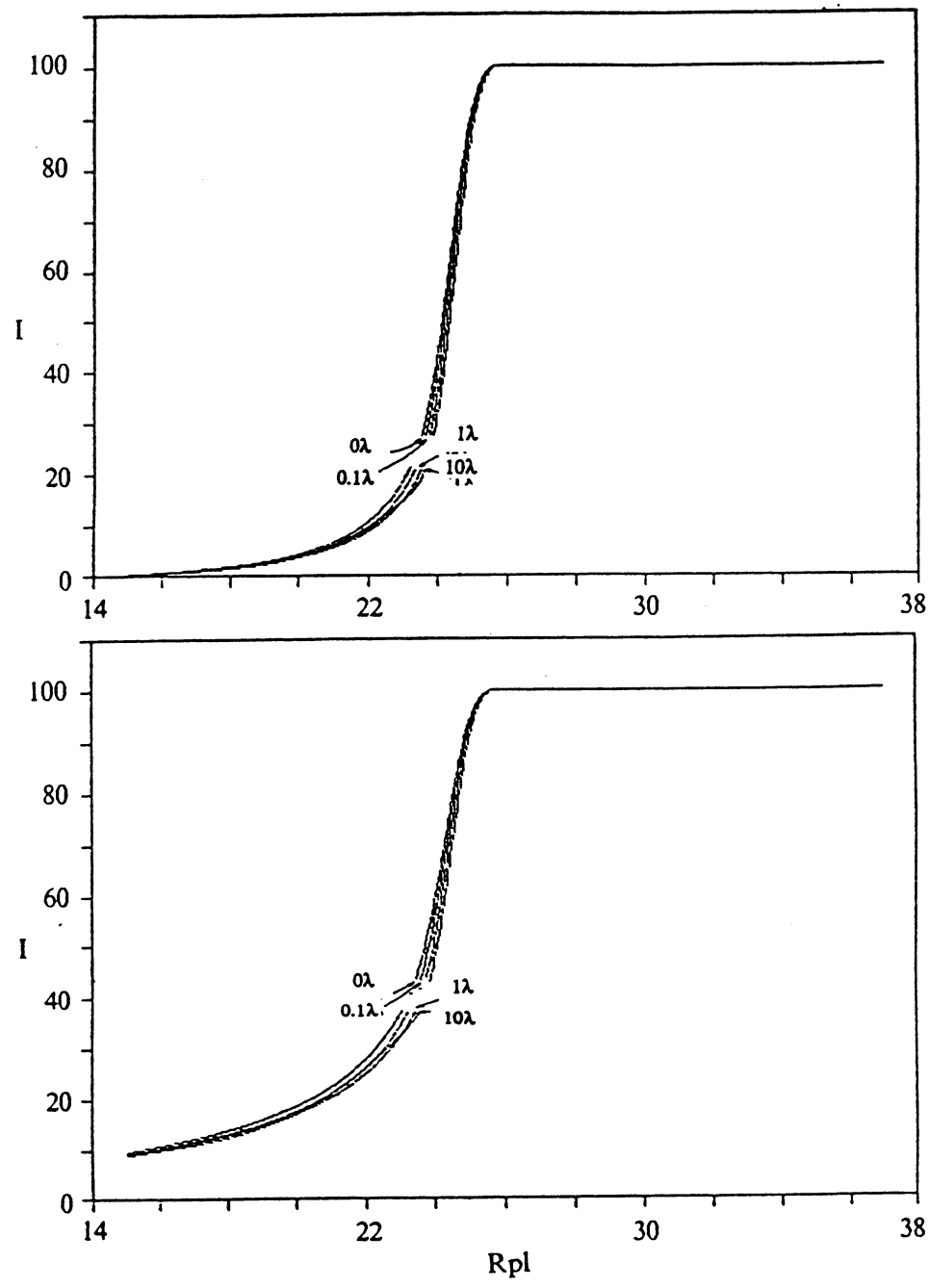

Figure 23. **Calculated Rpl-vs-I curves for different samples and liquid thicknesses:** a) (top) Rpl-vs-I curves similar to Figure 22a except the refractive index of the sample has been changed to 1.69. b) (bottom) Similar to Figure 22a except the light is in the s-state.

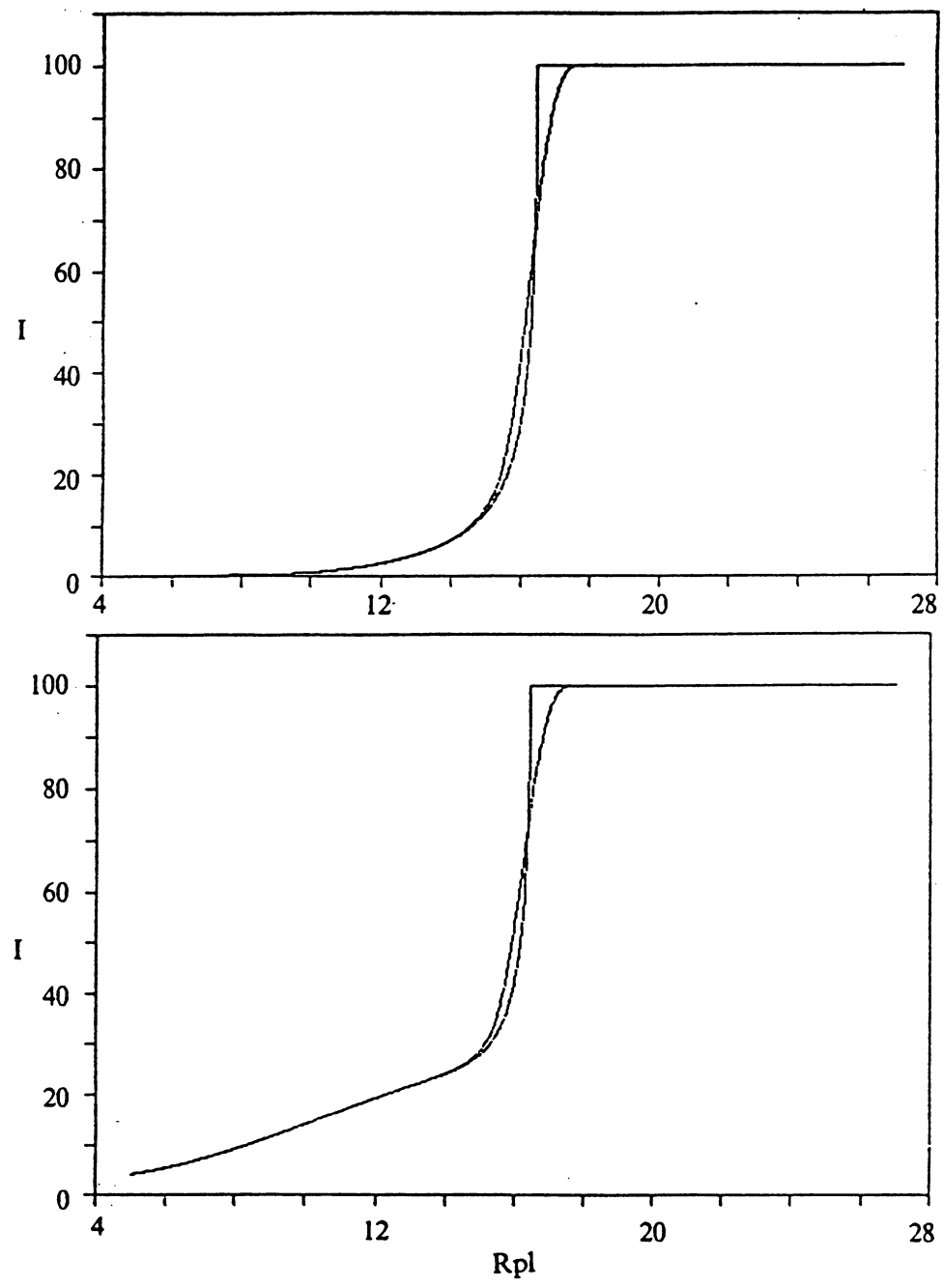

Figure 24. Calculated Rpl-vs-I curves for different samples and liquid thicknesses: a) (top) The two curves represent calculated Rpl-vs-I curves for an liquid thickness of 1λ. The curve with the sharp inflection has a cone angle of 0° the other curve has a cone angle of 2°. The incident light is in the p-state. b) (bottom) Similar to Figure 24a except the light is in the s-state.

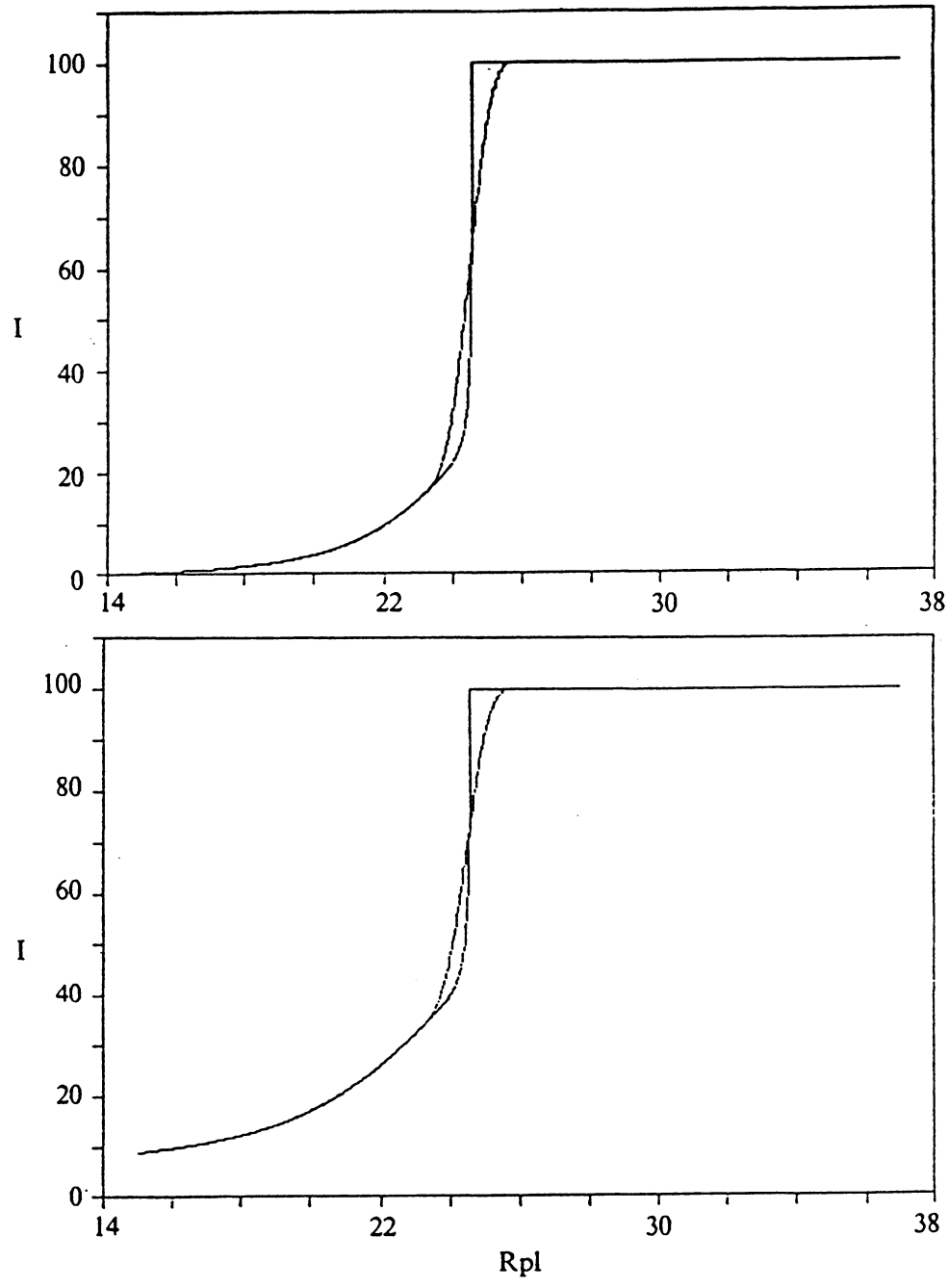

Figure 25. Calculated Rpl-vs-I curves for different samples and liquid thicknesses: a) (top) Similar to Figure 24a except the refractive index of the sample has been changed to 1.69. b) (bottom) Similar to Figure 24b except the refractive index of the sample has been changed to 1.69.

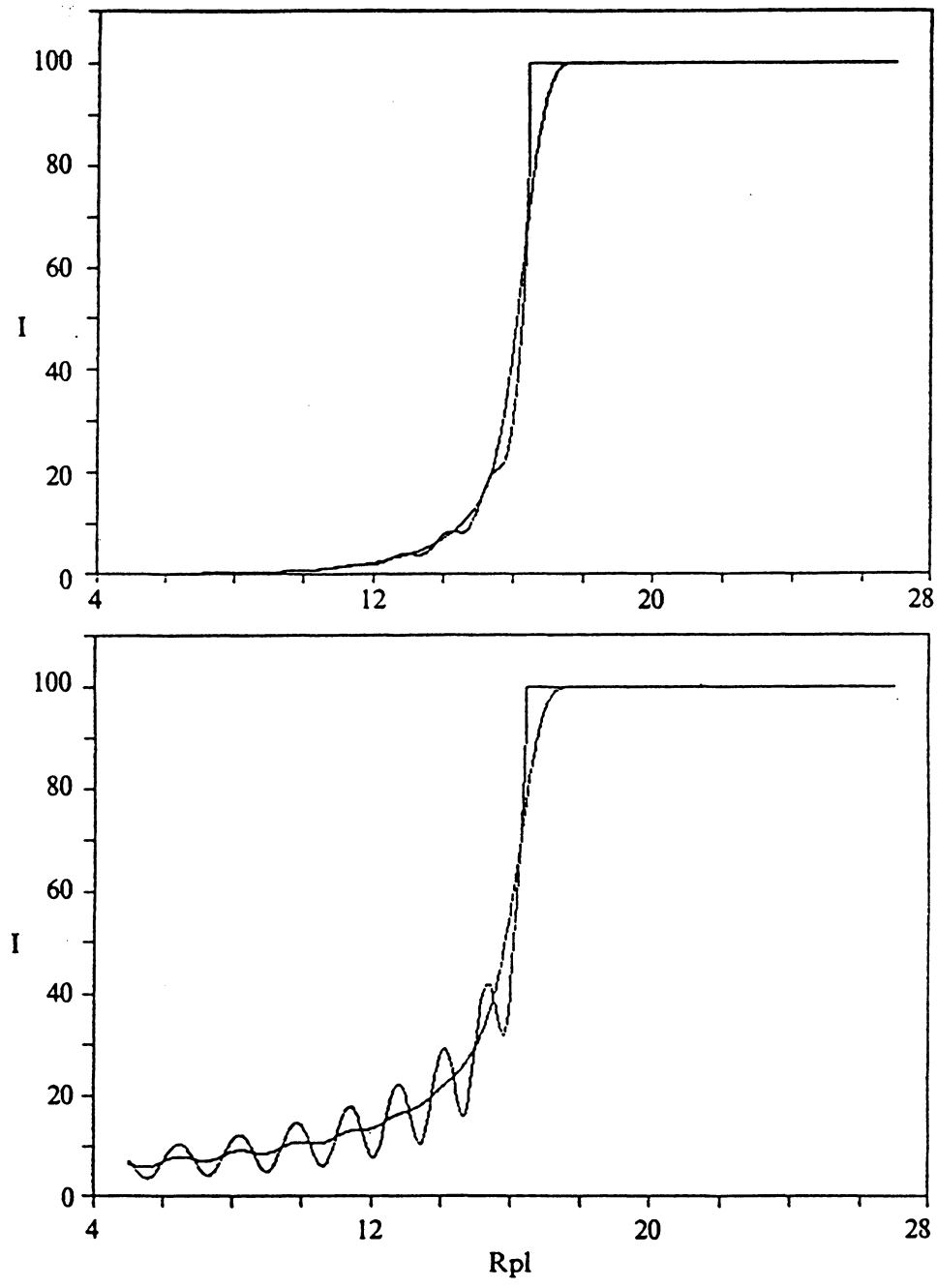

Figure 26. Calculated Rpl-vs-I curves for different samples and liquid thicknesses: a) (top) Similar to Figure 24a except the liquid thickness has been changed to 10λ. b) (bottom) Similar to Figure 24b except the liquid thickness has been changed to 10λ.

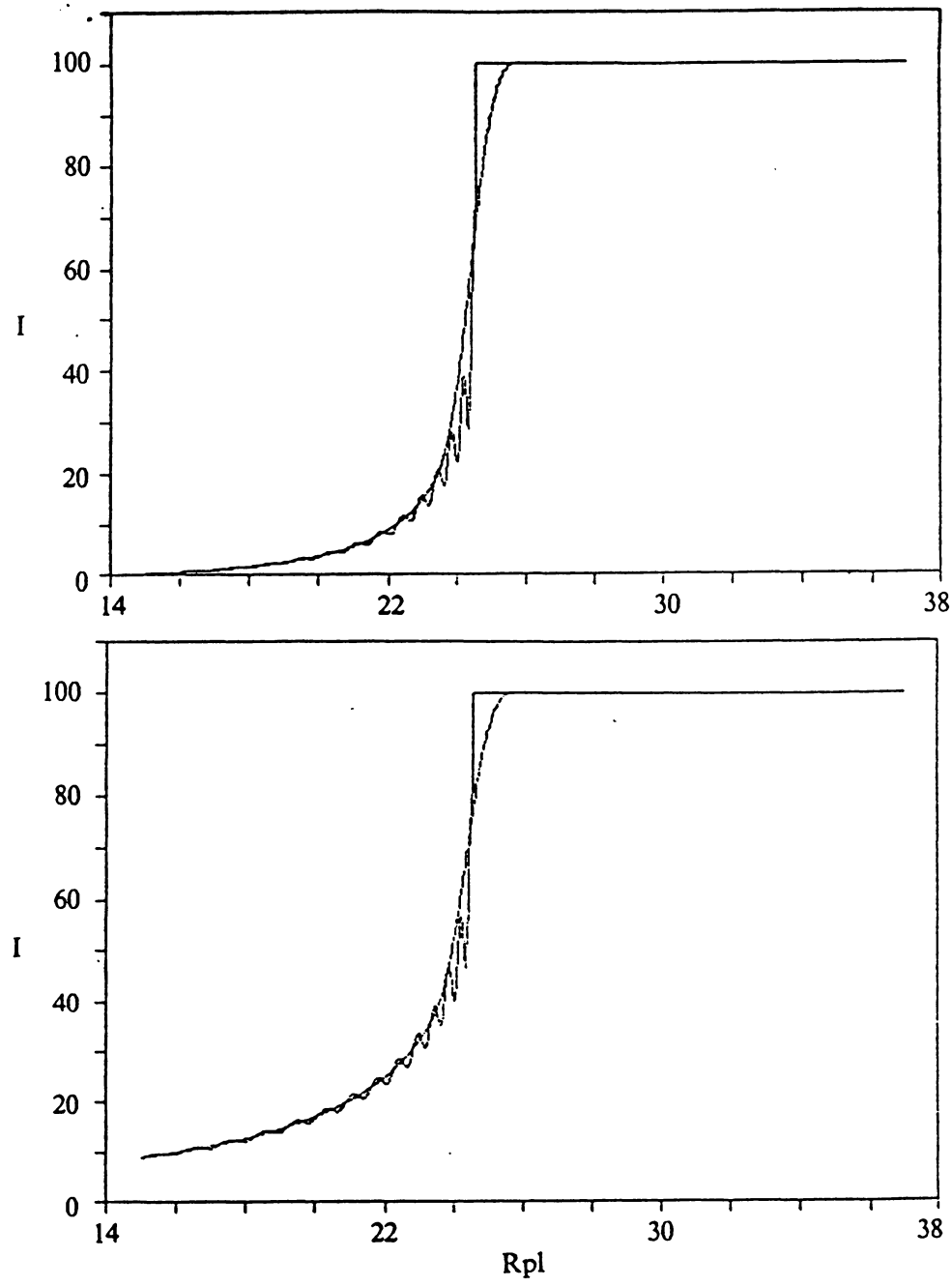

Figure 27. Calculated Rpl-vs-I curves for different samples and liquid thicknesses: a) (top) Similar to Figure 25a except the liquid thickness has been changed to 10λ. b) (bottom) Similar to Figure 25b except the liquid thickness has been changed to 10λ.

The contact liquid significantly affects the Rpl-vs-I scans when: 1) the contact liquid is very thick (on the order of 10 to 100 λ) 2) the cone angle is reduced to zero, an impossibility if the laser beam is focused onto the sample; furthermore, the resulting intensity changes occur in portions of the Rpl-vs-I scans too distant from the critical angle to be required for refractive index determination. The liquid film thickness was estimated to be approximately 1λ, probably less. Four liquid thicknesses were chosen to calculate Rpl-vs-I scans based upon this estimate; 0λ, 0.1λ, 1λ, and 10λ. The calculations were performed with cone angles of 0° and 2°. These calculations show that the effect of liquid thickness, especially 1λ and less, does not significantly affect the Rpl-vs-I scans at a cone angle of 2°. When the cone angle was set at 0° a sinusoidal intensity variation was calculated; non-zero cone angles tended to remove the contact liquid effect from the resulting curves. The effect of liquid thickness is more pronounced at Rpl angles well below the critical angle; thus, if these portions of the scans are not used for determining the refractive index of a material, then the contact liquid effect can be ignored. The calculated critical angles were the same for all four liquid thicknesses.

Other effects

In the two previous sections the effects of cone angle and contact liquid on the Rpl-vs-I scans from the BAR have been described. Three other phenomena contribute to a lesser extent to the form of the Rpl-vs-I scans: 1) particulate matter on the optical components of the BAR, 2) increased electronic noise at low signal levels, and 3) the "wave-guide" effect of the liquid film between the sample and the cubic zirconia hemicylinder. Each of these three factors will now be discussed individually, and then all factors known to contribute to the Rpl-vs-I scans will be reviewed and summarized.

The three additional effects on Rpl-vs-I scans discussed in this section were noticed from empirical observations and are presented graphically at the end of this section in Figure 28 through

Figure 31. To further support the validity of these observations references are made to Rpl-vs-I scans appearing in Automated Refractometer reports (Bloss, AR-1986a, AR-1987a; Bradley and Martin, AR-1986; and Gunter, AR-1986b, AR-1986c). The data presented in these reports and the new data presented here show the effects of 1) dust particles on the optical components, 2) increased electronical noise at low signal levels, and 3) the wave-guide effect of the liquid film.

Particulate matter on mirrors: Small dips have been observed in background scans (i.e., Rpl-vs-I scans with no sample) during past operation of the BAR. These dips disappeared after cleaning the reflecting components of the BAR's optical system; however, no documentation was kept on these small dips. To determine if these dips were dirt, hair, etc., a very simple experiment was devised. A cat hair, approximately 30 μm in diameter, was placed at several known Rpl positions on the first elliptical mirror. Next, scans were made with and without a sample (i.e., background scans) placed on the BAR. Figure 28a through Figure 30a show the results. Figure 28a is the control for the glass sample; it represents a normal scan with no hair. Figure 28b is a scan with a hair placed at 17.7° Rpl on the first elliptical mirror. A small deviation in intensity occurs in the circled area when compared to Figure 28a. Figure 29a contains two curves, the first (squares) is the background control, while the second (pluses) has a hair positioned at 17.7°. This sharp drop has been observed in past background scans. For the following scans only the hair was moved, the polarization state, sample position, etc. were not changed. Two more scans were made on the glass with the hair moved to different Rpl positions. In Figure 29b the hair is located at 21° Rpl, on the rapidly rising portion of the Rpl-vs-I curve. In Figure 30a the hair was moved to past the critical angle to an Rpl value of 24°.

The dips appearing in past Rpl-vs-I scans can be compared to those generated here. Here the size of the foreign body is approximately 30 μm; however, in past scans the size has been unknown and probably was much smaller, which would produce smaller dips, but dips of the same form. Dips occurring past the critical angle are more commonly observed in past data, probably because they are more pronounced than dips prior to the critical angle (compare Figure 30a to

Figure 28b and Figure 29b). Figures A1 through A3 in Gunter (AR-1986b) show dips at approximately 31.3°. Bradley and Martin's (AR-1986) Figure 16 shows two dips, 29° and 33.8°. From the generated data one can conclude these dips were caused by particulate matter on the optical elements of the BAR. In a more recent report by Bloss (AR-1987a) small dips occur in his scans of quartz and glass at the same Rpl value on the rapidly rising portion of the Rpl-vs-I scan. By comparing these scans to Figure 30a the same phenomenon appears to be producing the variation in intensity; thus some particulate matter caused the variation in intensity in his scans.

Electronic noise: Sinusoidal variations in past Rpl-vs-I scans in intensity were sometimes attributed to an interference phenomenon (Gunter, AR-1986b). The previous section showed that such interference may occur if the contact liquid is thick enough. However, another cause for sinusoidal variations exists. Scans taken with no signal reaching the detector (Figure 30b) show a distinct periodicity of approximately 1°. In Figure 31, a glass is scanned in both the p- and s-state; the p-state yielded a lower intensity than the s-state as expected. The periodicity of the sinusoidal intensity variation is approximately 1° which corresponds with the periodicity in Figure 30b. The s-state, receiving a higher intensity, also shows a similar periodicity, but the sinusoidal intensity magnitude is considerably less than the p-state. Those sinusoidal variations in intensity, because they occur at low signal levels, are attributed to electronic noise in the detector system. This sinusoidal variation differs from the contact liquid effect because: 1) it occurs when no light reaches the detector (Figure 30b), 2) no sample or liquid need be present for this variation to occur, and 3) the frequency matches for the no signal and very low signal cases (compare periodicity of low Rpl values in Figure 30 and Figure 31).

Past Rpl-vs-I scans support the assumption that the noise level increases as signal decreases. In Figure 5 the Rpl-vs-I scan shows that more noise occurs at lower values of Rpl for n than for N. The sinusoidal variation is also present, although not discernible, on the scale of this graph. If the graph is replotted at an expanded scale, the sinusoidal variation is seen to have a period of 0.05°. The periodicity is greater because of the slower sampling rate for this data (0.01° Rpl incre-

ments) as compared to Figure 30b and Figure 31 which have sampling rates of 0.1° Rpl. In Figure 8 of Bradley and Martin (AR-1986) the same tread occurs; the lower intensity portions of their curves contain more noise. This effect is not visible in the scans of Gunter (AR-1986b) even after these scans are expanded and replotted, possibly because a different photodetector system was used.

Wave-guide effect of liquid film: During the baseline testing of the BAR, intensity dropped significantly after the critical angle for the sample had been reached, but prior to the critical angle for the liquid. This intensity drop, believed to result from the wave-guide effect produced by the contact liquid film, was first explained by Indebetouw (AR-1986d). The wave-guide effect is caused by multiple reflections within the the liquid film. The laser beam is first reflected from the bottom surface of the sample toward the hemicylinder; next a portion is reflected back toward the sample. The proportions of the beams reflected back and forth between the sample and the hemicylinder is a function of the angle of incidence and refractive index of the reflecting media. As the angle of incidence and refractive index values increase, a larger portion of the beam is reflected. At large angles of incidence, which occur after the critical angle for the sample and before the critical angle for the liquid, enough of the beam's energy is multiplely reflected to produce the wave-guide effect.

Bradley and Martin's (AR-1986) Figure 4 showed the position of the intensity decrease to be related to the refractive index of the contact liquid. Examining past Rpl-vs-I scans, using the glass hemicylinders and the cubic zirconia hemicylinder, significant wave-guide effects occur only in the versions of the BAR containing the cubic zirconia hemicylinder. Bloss (AR-1985, Figure 7) and Gunter (AR-1986c, Figures 2-7) contain Rpl-vs-I scans when the leaded glass hemicylinder was in use. For Bloss' data the critical Rpl for the liquid is 30.3° (ca.), while in Gunter's scans the critical Rpl for the liquid is 35.7° (ca.); no intensity drop occurs in these regions, thus no wave-guide effect is present. Examples of recent scans appear in Figure 31 and Figure 8 (Bradley and Martin, AR-1986). These scans show a change in intensity after the critical angle for the sample but before the critical angle for the contact liquid; this change is caused by the wave-guide effect.

A significant wave-guide effect can occur only if the sample and the hemicylinder are flat and parallel. Only under these conditions could the light beam be "guided" out, through multiple reflections between the sample and hemicylinder, thus reducing the reflected intensity. There are two reasons the wave-guide effect occurred after replacing the leaded glass hemicylinder with the cubic zirconia hemicylinder: 1) the cubic zirconia hemicylinder is harder than the leaded glass hemicylinder and 2) the cubic zirconia hemicylinder has a higher refractive index. The increased hardness of the cubic zirconia results in a flatter surface, a requirement for the wave-guide effect, and an absence of scratches, which were common in the leaded glass hemicylinder and would cause beam scattering and reduce the possibility for multiple reflection; the higher refractive index increases the intensity of the reflected rays.

Summary Rpl-vs-I scans

Particulate matter (i.e., dirt, hair, etc.) on the elliptical mirrors produces a small local decrease in the intensity values at Rpl angles corresponding to the location of the particulate matter on the elliptical mirror. If the optical components are kept clean, these small changes will not occur. Electronic noise may produce sinusoidal variations in the intensity at low signal levels and at Rpl values well below the critical Rpl. Fortunately Rpl-vs-I data in these regions will not be used to refine the refractive index of an unknown. Thus the noise will not affect the critical angle determination. A wave-guide effect is produced by the liquid film. This effect causes the laser light to be "guided" by multiple reflections through the liquid film and not reflected into the detector, thus causing a decrease in intensity in the Rpl-vs-I scan. This effect occurred after replacement of the leaded glass hemicylinder with the cubic zirconia hemicylinder. The wave-guide effect, like the above noise effect, should not present problems because it occurs after the critical angle for the sample and the data in this region of the Rpl-vs-I scans need not be used to refine refractive index. However, care must be taken to keep the refractive index of the liquid at least 0.1 above the refractive index of the sample.

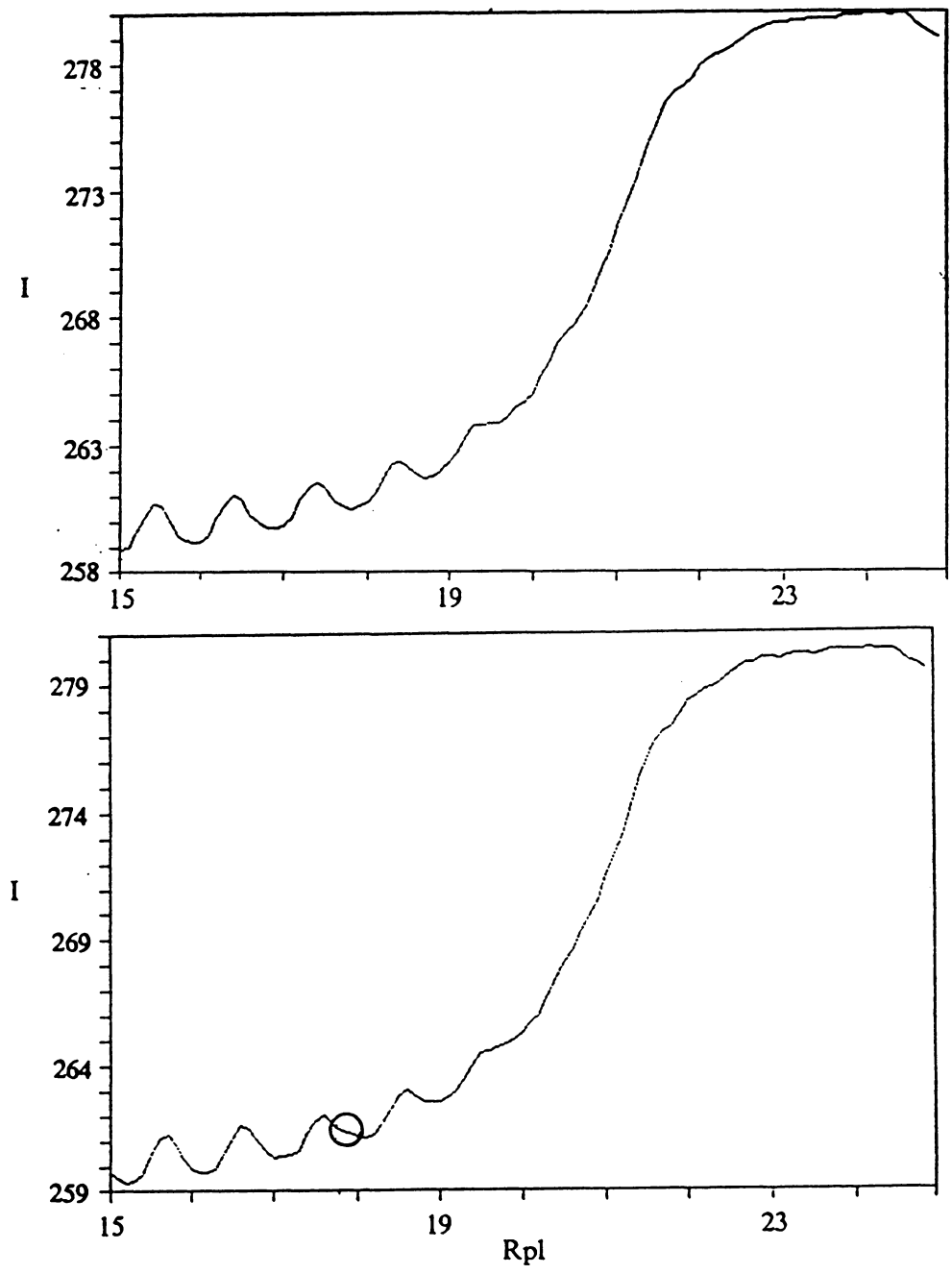

Figure 28. **Scans of a glass showing effects of particulate matter on the first elliptical mirror:** a) (top) This scan is the control; all the particulate matter was cleaned from the BAR's optical elements. b) (bottom) Same as Figure 28a, except a hair has been placed on the first elliptical mirror at 17.7°. The addition of the hair causes the intensity to be slightly modified in circled area.

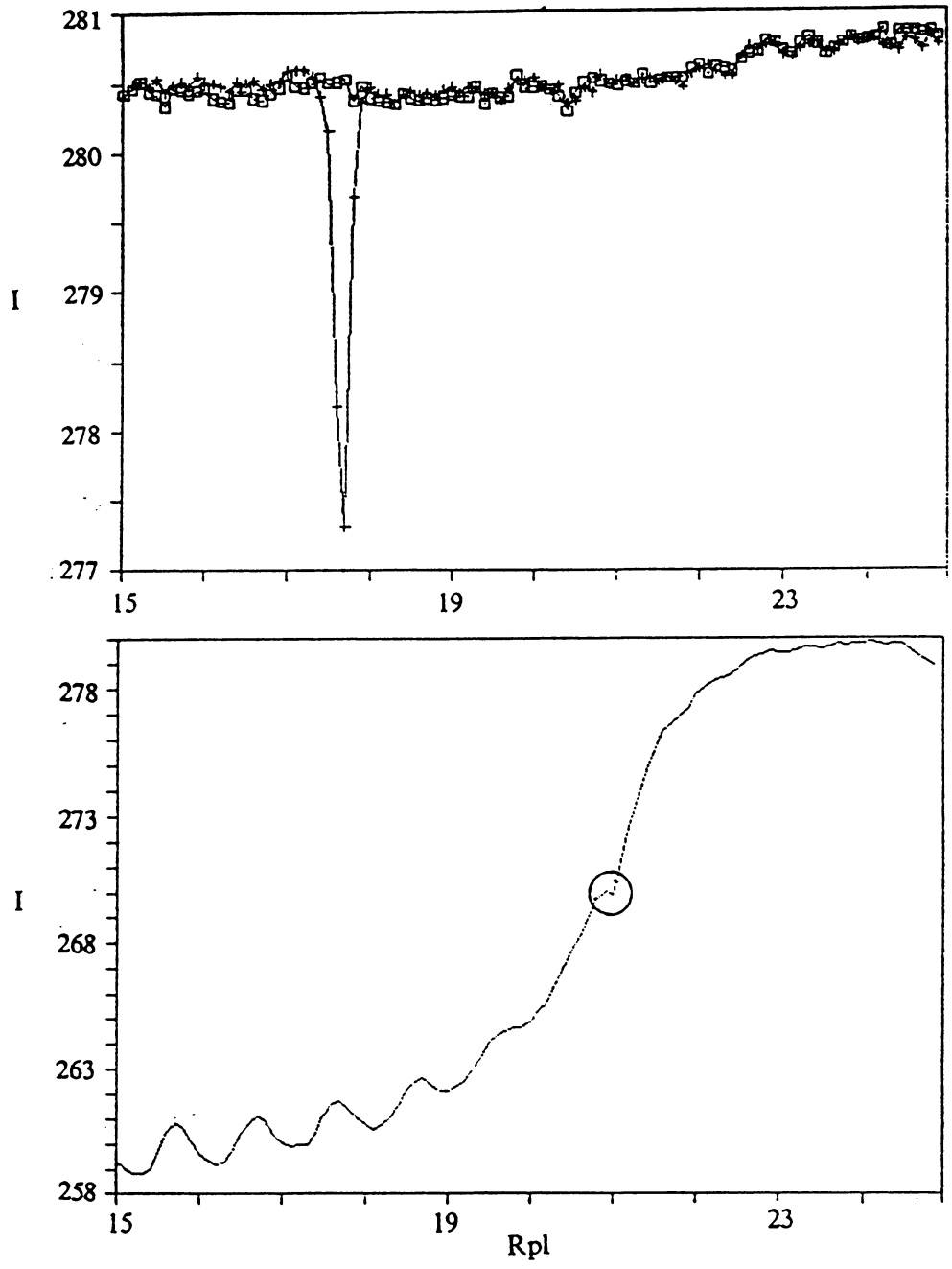

Figure 29. **Scans of a glass showing effects of particulate matter on the first elliptical mirror:** a) (top) Two scans appear on this graph, both are background scans, the first (squares) was performed as normal and the second (pluses) was performed after a hair was placed at 17.7° on the first rotatable mirror. b) (bottom) This scan is similar to Figure 28a except the hair has been moved to 21°, an Rpl value prior to the critical angle on the rapidly rising portion of the Rpl-vs-I scan.

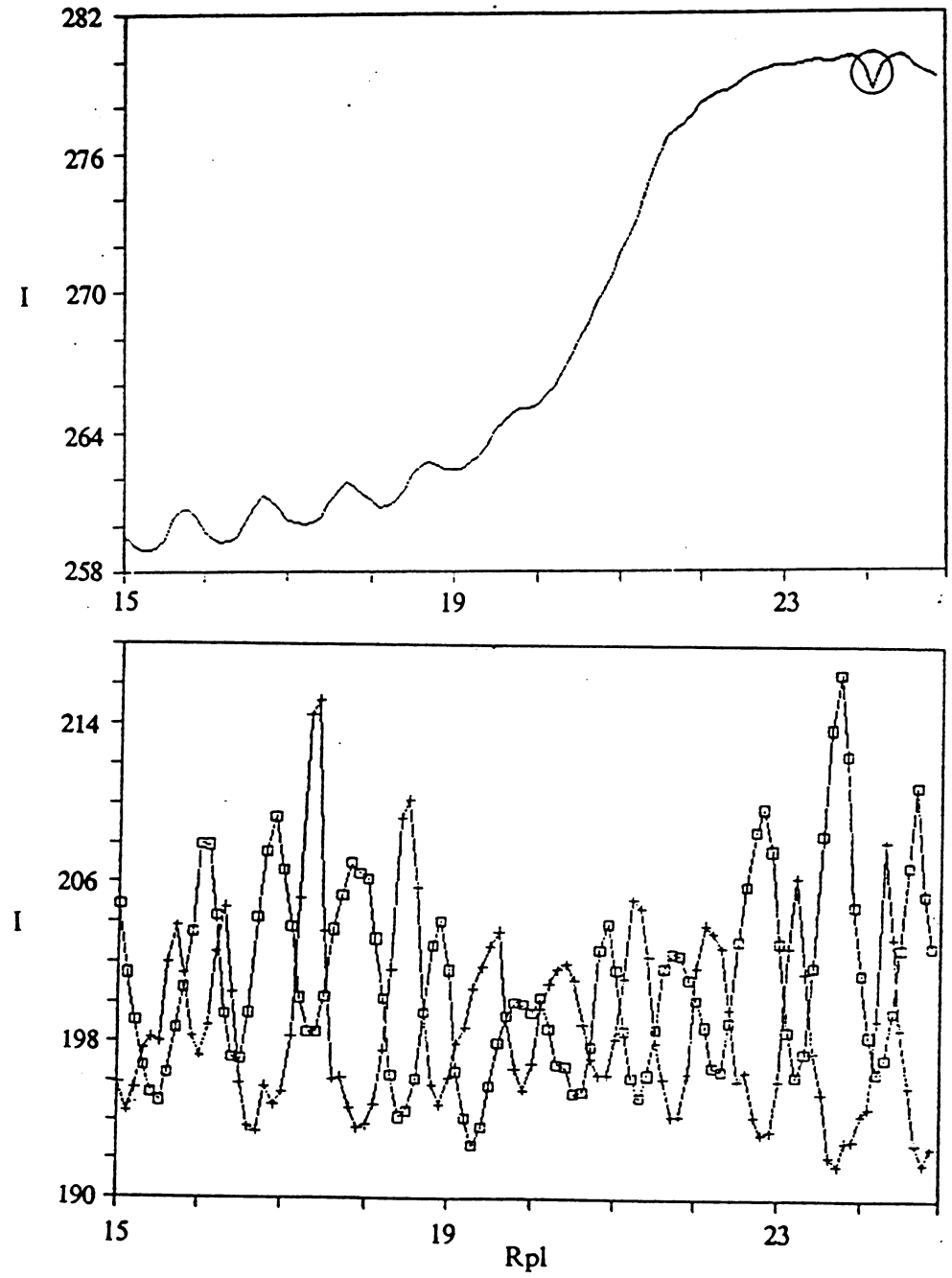

Figure 30. Scans of a glass showing effects of particulate matter on the first elliptical mirror: a) (top) This scan is similar to Figure 28a, except the hair has been moved to 24°, an Rpl value past the critical angle. b) (bottom) These two scans represent background runs with no detector signal. Their periodicity is approximately 1°.

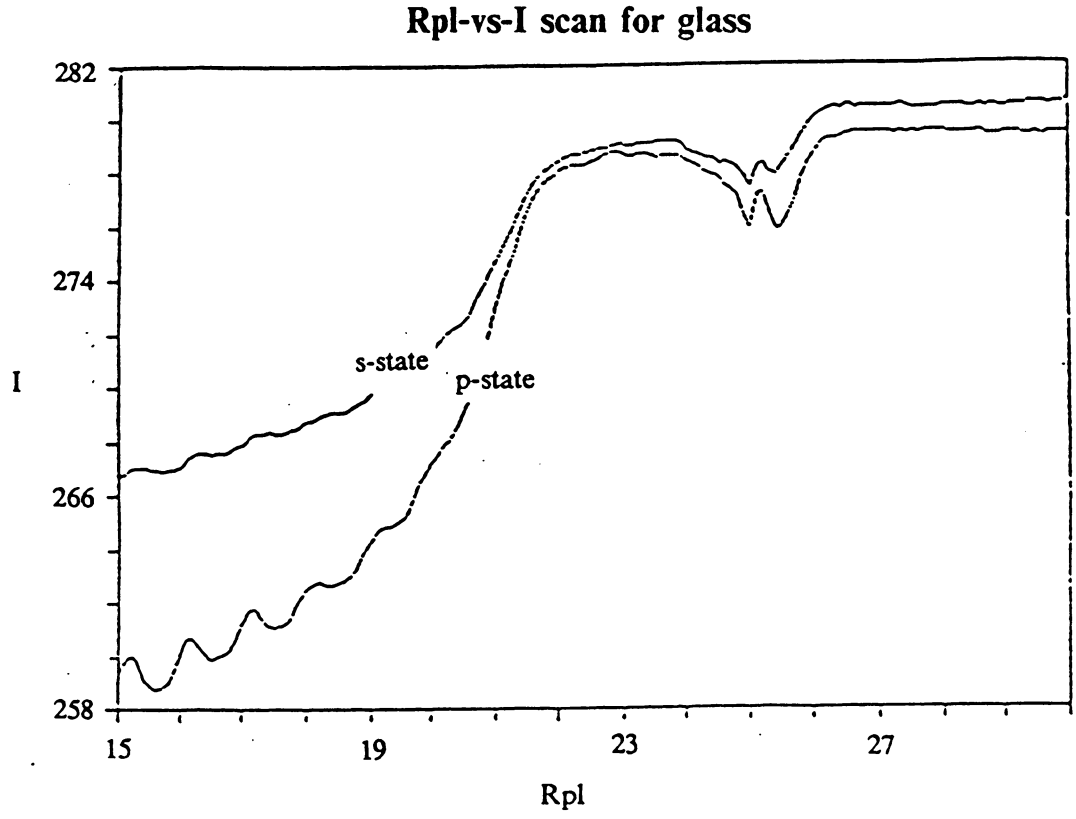

Figure 31. **A glass measured over an extended Rpl range in both the p- and s-states:** The scan shows: 1) sinusoidal noise at low signal levels (p-state) and 2) the wave-guide effect of the liquid film. The noise has a periodicity of approximately 1°, which agrees with the periodicity observed from Figure 30b.

Rpl-vs-I scans taken on the BAR involve at least six separate phenomena: 1) basic reflection as explained by the Fresnel equations, 2) the cone angle effect, 3) the contact liquid effect, 4) particulate matter on the BAR's optical components, 5) increasing electrical noise at low signal levels, and 6) the wave-guide effect of the hemicylinder/sample combination. Of these six the first two are the most significant and can easily be mathematically modeled and programmed into algorithms to refine refractive index measurements on the BAR. The other four factors cannot be mathematically modeled to determine their effects on the algorithms to determine refractive index. Moreover, they cannot be easily incorporated into the routine operation of the BAR, because their occurrences are either random (e.g., dirt on the mirrors) or impossible to maintain at a known fixed value (e.g., the liquid thickness). However, these factors, except for particulate matter, appear to produce significant intensity changes only in regions of the Rpl-vs-I scans that are not required to determine the refractive index of material analyzed by the BAR.

Obtaining a refractive index from the Rpl-vs-I scans

The purpose of this section is two-fold: 1) to use the information from the previous three sections to computer-model Rpl-vs-I scans for isotropic samples and 2) to devise a non-empirical method to determine the refractive index from Rpl-vs-I scans for isotropic samples. Rpl-vs-I scans were generated and analyzed by the modified Fresnel-fit (MFF) method for eleven different combinations of cone angle, noise level, polarization state, Rpl range, and Rpl increment. The noise was added from a random number generator which produced random numbers from a Gaussian distribution with specified mean and standard deviation. Two other data sets were created by 1) smoothing the I values and 2) calculating average I values based upon five scans. Each data set contained 100 observations to provide sufficient data for statistical analysis.

The ASYST language[8] was used to generate simulated Rpl-vs-I scans for isotropic samples with different cone angles, noise levels, Rpl ranges, Rpl increments, and polarization states based upon the recommendations in Gunter (AR-1987a). Also a modified Fresnel-fit (MFF) method was developed and programmed in the ASYST language. Thirteen Rpl-vs-I data sets, of 100 observations each, were generated under various combinations of the above parameters, and the refractive index values were calculated for each by use of the MFF method. These data were then analyzed to determine variability in calculated refractive indices. Three different techniques were chosen to increase precision of the MFF method. As a further check on this method, five data sets for the same glass obtained from the BAR were analyzed and the refractive index results compared to those obtained by the residual method (Gunter, AR-1986b).[9]

Computer generated Rpl-vs-I scans: Rpl-vs-I scans were generated by use of a computer program written in the ASYST language. With this program the following parameters could be modified: 1) cone angle, 2) polarization state, 3) noise level, 4) Rpl increment, and 5) Rpl range. Four cone angles were chosen 0°, 2°, 4°, and 8°. The 2° cone angle closely approximates the current BAR (Gunter, AR-1987a), while the 8° angle will more closely approximates the future Crystallographic BAR (Gunter, AR-1986j). Two noise levels were chosen, one set generated from a Gaussian distribution with mean 0 and standard deviation 1 (= N(0,1)) and the second from a N(0,5). Some 68.3% of the random numbers from an N(0,1) distribution will fall in the range of ± 1 s.d. unit of the mean. In other words 68.3% of the numbers will be between ± 1, likewise 95.4% will fall within ± 2 s.d. units and 99.7% within ± 3 s.d. units. This noise was added to intensity values ranging from 0 to 100%; thus, when a random number with a value of 1 was added to the intensity values it produced a change of 1% in the intensity. For the N(0,1) distribution, 68.3% of the generated

---

[8] ASYST is a specialized high-level scientific computer programming language developed by Macmillan software.

[9] The residual method was an empirical method to determine the refractive index from an Rpl-vs-I scan (Gunter, AR-1986b). In the method the intensity data was regressed on the Rpl data and the Rpl value corresponding to the maximum residual value, resulting from this linear regression, was presumed to be the critical Rpl and from it the refractive index was calculated. Details of the residual method are given in the Appendix.

random numbers would cause changes in intensity of 1% or less. The N(0,1) distribution was chosen to represent the current BAR; however, during the analysis it became obvious an N(0,0.3) to N(0,0.5) distribution may have been a better choice. (An explanation for the reduced noise level appears later in this section.) Scans were generated in both the p- and s-states to determine which orientation produced better results. Two Rpl increments were chosen, 0.1°, and 0.05°. All previous precise refractive index measurement were done at 0.01° by use of the residual method, but it would be highly desirable to formulate a method to find refractive index from scans made at a greater Rpl increment so as to decrease data collection and processing. A sample refractive index of 1.5 was chosen for the computer generated data.

Modified Fresnel-fit: The Fresnel-fit method, as first proposed by Bloss and Su (AR-1986), is an algorithm used to determine the refractive index of a sample based upon the Fresnel equations. The method minimizes the sum of squares of the differences between a calculated curve, based on the Fresnel equations, and the observed curve (i.e., the Rpl-vs-I scan). Their method met with only marginal success because, at that time, we did not fully understand the Rpl-vs-I scans obtained on the BAR for isotropic samples; thus we had no good method to arrive at the calculated curve. By adding to the Fresnel equations the cone angle effect, as described in an earlier section, actual data acquired on the BAR could be more closely modeled.

The modified Fresnel-fit (MFF) method permits calculation of Rpl-vs-I scans which closely resemble, for Rpl values close to the critical Rpl, those obtained from the BAR. The MFF method requires an initial guess of the refractive index of the unknown which can be obtained from the residual method. Then the refractive index used for the calculated curve is varied until the sum of the squares of its differences relative to the observed curve reaches a minimum. The refractive index which minimized the sum of squares is then assigned to the unknown. In detail, the sum of squares is calculated by finding the difference between the observed and calculated intensity at each Rpl setting (= residual), next the difference is squared and summed. This method has the advantage that it uses all the data of the Rpl-vs-I scan to minimize a sum, instead of a single intensity reading

as does the residual method. Another advantage of this method is scans can be taken at larger Rpl increments because precision is no longer directly based upon the Rpl increment, as with the residual method. This method is discussed in more detail in the Appendix.

Test of modified Fresnel-fit on computer generated Rpl-vs-I scans: One of the main purposes in generating Rpl-vs-I scans on the computer is the ability to analyze the performance of the BAR under different algorithms and operating conditions (i.e., different noise levels, Rpl increments, etc.). The ability of the MFF method to perform under varying operating conditions was determined by creating 13 different data sets each composed of 100 observations. To attain one of these data sets from the BAR, 100 Rpl-vs-I scans would need be made on the same material with operating conditions remaining constant. Then all 100 scans would have to be saved and analyzed; this would be a very time consuming process. The computer modeling performs the same task with only a minimum amount of time. Also, we do not have the ability to change empirically certain parameters of the BAR, for example, the cone angle or noise level. On the other hand, these are easily changed in the computer program and their effect on the algorithm can be ascertained. Table 2 lists the characteristics of the 13 computer-generated data sets and the parameters used by the MFF method to determine a refractive index from the Rpl-vs-I scan.

For each of the thirteen data sets presented in Table 2, descriptive statistics were calculated and are presented in Table 3; also Figure 32 contains a set of side-by-side boxplots of the data. The first 5 data sets differ only in the range about the critical Rpl used by the MFF method. Run 1 uses a range of -2° to + 1° Rpl relative to the approximate critical Rpl; this range corresponds to 3° of Rpl and thus, for 0.1° increment of Rpl, contains 30 data points (#obs, Table 2). The total number of intensity observations used in the MFF procedure, namely the #obs entry in Table 2, thus equals the Rpl range divided by the Rpl increment. For any statistical method as the number of observations decreases, the precision of the estimates will decrease; this explains the slight increase in the s.d. in run 2, whose range is 0° to -2° Rpl and contains only 20 data points. After observing the first 5 runs, a decision was made to chose the range of -1.5° to + 0.5° for further runs,

Table 2. Summary of computer generated Rpl-vs-I scan variables

	polar. state	Rpl increment(°)	Rpl range(°)	cone angle(°)	s.d. for noise	#obs
run 1	p	0.1	-2+1	2	1	30
run 2	p	0.1	-1+1	2	1	20
run 3	p	0.1	-1	2	1	10
run 4	p	0.1	-2	2	1	20
run 5	p	0.1	-1.5+0.5	2	1	20
run 6	s	0.1	-1.5+0.5	2	1	20
run 7	p	0.1	-1.5+0.5	0	1	20
run 8	p	0.1	-1.5+0.5	2	5	20
run 9	p	0.1	-1.5+0.5	4	1	20
run 10		same as run 9 except data was smoothed				
run 11	p	0.1	-1.5+0.5	8	1	20
run 12		same as run 11 except intensities based on 5 scan average				
run 13	p	0.05	-1.5+0.5	8	1	40

the decision was based upon the small s.d. and IQR (interquartile range = 0.75 percentile - 0.25 percentile) and following the recommendation of Gunter (AR-1987b) of minimizing the Rpl range used in determination of refractive indices.

Runs 5 and 6 are similar except they differ in polarization state; run 5 is p-state, run 6 s-state. From the s.d. in Table 3 it appears the p-state may provide more precise results, however the difference in s.d. is very small and more testing would be required to confirm this hypothesis. More importantly, as calculated by the MFF method, runs 5 and 6 yield the same refractive index; in previous work the residual method calculated different refractive indices for the p- and s-state, depending upon the chosen Rpl ranges. Runs 5 and 8 differ only in the noise level. Run 5 contains noise from an N(0,1) distribution while run 8 contains noise from an N(0,5) distribution. From statistics in Table 3 or the boxplots in Figure 32 the increase in noise significantly decreases the precision of the MFF method.

Four different cone angles were chosen: 0° (run 7), 2° (runs 1-6, and 8), 4° (runs 9-10), and 8° (runs 11-13). From the boxplots of Figure 32 the increase in the spread of the results is positively correlated to the increase in cone angle. Three methods were chosen to increase the precision for the higher cone-angle data sets. The first method was tested on runs 9 and 10 which are similar

Table 3. Descriptive statistics for modified Fresnel-fit computer generated Rpl-vs-I data

	mean	s.d.	min.	max.	median	IQR
run 1	1.49999	0.00016	1.4996	1.5004	1.5000	0.0002
run 2	1.50004	0.00035	1.4993	1.5009	1.5000	0.0005
run 3	1.50001	0.00038	1.4993	1.5010	1.5000	0.0006
run 4	1.50002	0.00015	1.4997	1.5005	1.5000	0.0002
run 5	1.50000	0.00022	1.4995	1.5006	1.5001	0.0003
run 6	1.50004	0.00029	1.4994	1.5007	1.5000	0.0003
run 7	1.50002	0.00009	1.4998	1.5003	1.5000	0.0001
run 8	1.50019	0.00080	1.4980	1.5016	1.5002	0.0014
run 9	1.50008	0.00054	1.4990	1.5009	1.5000	0.0009
run 10	1.50076	0.00042	1.4996	1.5014	1.5009	0.0004
run 11	1.49988	0.00172	1.4965	1.5043	1.4999	0.0022
run 12	1.50010	0.00074	1.4987	1.5017	1.4999	0.0012
run 13	1.49979	0.00117	1.4965	1.5027	1.4999	0.0016

with a cone angle of 4°, but the intensity data for run 10 was smoothed using the built-in smoothing function of the ASYST language. The smoothing decreased the s.d. in run 10 when compared to run 9; however, the median (or mean) was biased to a higher value because of the smoothing. For all runs, other than the smoothed run 10, the calculated mean and the median values are within ± 0.0002 of 1.5, the refractive index used to generate the data.

Run 11, with an 8° cone angle, yielded the highest variability. The second method to increase precision was tested on run 12 which was generated under the same conditions as run 11 except the intensity data were based upon an average of 5 scans. This compares to performing five scans of the same material on the BAR and averaging the intensity values. By performing 5 scans the variability was cut in half; the more scans performed the more the variability could be reduced. The third method to increase precision was to obtain intensity readings at smaller increments of Rpl. Run 13 was taken with an Rpl increment of 0.05°, thus it contains twice as many observations as run 11 taken at 0.1°. Run 13 shows a slight improvement in precision from run 11. By a combination of smoothing, multiple scans, and finer Rpl increments the precision of the refractive index values can be increased. The actual combination of these variables will need to be tested on the Crystallographic BAR or can be computer-modeled once the noise level of the detector system is known.

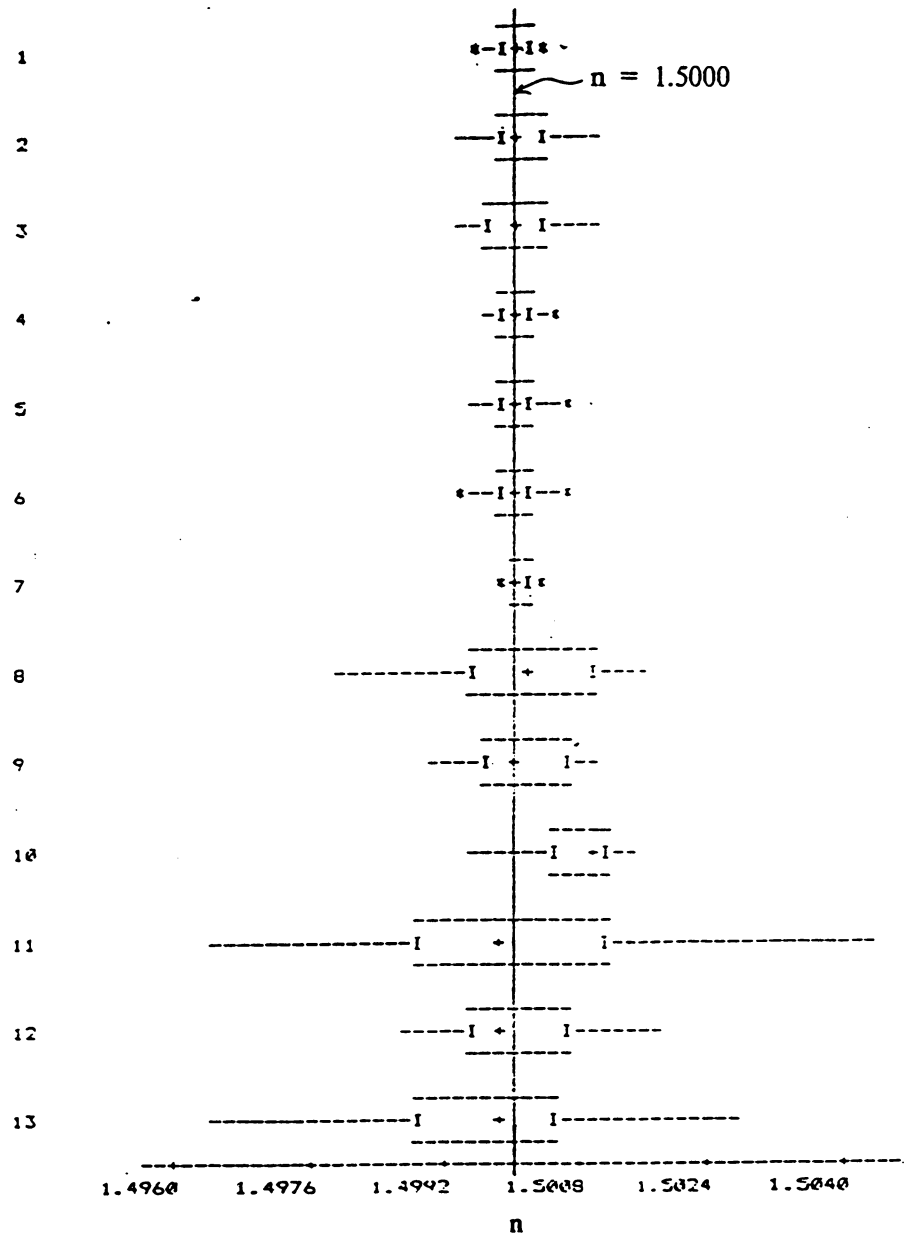

Figure 32. Boxplots for each of the 13 data sets listed in Table 2 and Table 3: Width of the boxes represent spread of the center portion of the data, the tails represent spread of the outer regions of the data, the asterisks represent outliers, and the pluses represent the median. Refer to Table 2 and Table 3 for a complete description of each data set's parameters and descriptive statistics.

Test of modified Fresnel-fit on BAR Rpl-vs-I scans: All of the above results are based upon computer generated data. To determine if the method used to generate Rpl-vs-I scans was correct and the MFF method sound for refractive index determination for actual BAR Rpl-vs-I scans, a set of 5 scans on a glass sample, taken 1-Dec-86, was analyzed. These scans were taken at $\pm 5°$ from the approximate critical Rpl at 0.01° Rpl increment. When the data was originally collected the refractive index values obtained from the residual method were calculated (Table 4, column 1).

To test the MFF method the intensity data from the BAR must be scaled; zero intensity will occur at the Brewster angle and 100% intensity occurs after total reflection. This knowledge was used to scale the raw intensity readings as follows: 1) 2499.8, the intensity at the Brewster angle empirically determined from a BAR scan, was subtracted from each intensity value, 2) the maximum intensity was found for each scan and all intensity values divided by it, and 3) the resulting values multiplied by 100. This scaling produced data sets with intensity values from approximately 50% to 100% over the 10° Rpl range measured. A -1.5° to + 0.5° Rpl range about the approximate critical Rpl was chosen to use the MFF method. Next the MFF method was applied to each of the five data sets using only data at 0.1° Rpl increments; the results appear in Table 4, column 2. Comparing the s.d. values in Table 4, the MFF method is superior to the residual method in precise determination of refractive index from Rpl-vs-I scans. The means of the values in Table 4 were adjusted to equal that the glass (1.5783), because comparison of the s.d. is the important point; calibration of the BAR will take care of the adjustment of the means.

Earlier it was stated an N(0,1) noise level may be higher than that of the BAR. This conclusion was reached after analysis of the above data. The MFF method produced an s.d. value of 0.00009 for actual data from the BAR, while the modeled data (#5, Table 2 and Table 3) has an s.d. of 0.00022. A sample size of 5 is too small to yield sound descriptive statistics, but the s.d. is nevertheless significantly smaller from data obtained on the BAR than the data obtained from computer modeling. A second reason to assume lower noise levels is based upon the intensity range for the glass data sets being approximately 200 intensity units. The random noise from the A/D converter is approximately 1 unit, thus when scaled the noise would be reduced by 50%.

Table 4. Comparison of residual method and modified Fresnel-fit methods for observed data.

	Residual method	Modified Fresnel-fit
scan 1	1.5771	1.5782
scan 2	1.5764	1.5784
scan 3	1.5782	1.5782
scan 4	1.5806	1.5783
scan 5	1.5792	1.5782
s.d.	0.00167	0.00009

Summary of MFF

From the previous work of Gunter (AR-1987a, AR-1987b, AR-1987c), Rpl-vs-I scans can be computer-modeled by use of the ASYST language. The addition of noise to the scans closely simulates the actual data collected from the BAR. Analysis of the thirteen computer-generated data-sets by the MFF method yielded standard deviations (s.d.) from 0.00009 to 0.00172. By smoothing the intensity data, performing multiple scans, or collecting intensity values at finer Rpl increments the precision can be increased. However data smoothing introduces a systematic error in the refractive index values; the other techniques used to increase precision do not. The methods currently being developed by Bloss and Su to determine the refractive indices and orientation for biaxial crystals require an s.d. of 0.0005 or less. From this study the MFF method will meet this criteria. The MFF method was also tested on data sets collected on the BAR; the s.d. for 5 scans was 0.00009, while for the residual method the s.d. was 0.00167.

Conclusions

A thorough understanding of the Rpl-vs-I scans has been developed and used to computer-model these scans for isotropic samples. From this modeling a refractive index determination algorithm was developed and tested, under various simulated operating conditions of the BAR, for robustness, precision, and accuracy. The application of this algorithm to current BAR data yielded a precision of better than ± 0.0001 for five scans of a glass.

Chapter 7. Automated RTR: successes, limitations, conclusions

Introduction

The ability to precisely measure refractive indices by RTR was clearly demonstrated in the late 1800s and early 1900s. The method of precise RTR, however, fell out of use by the early 1900s. Measurements made in the 1980s in Professor Bloss' lab led to a rekindling of interest in this method and resulted in the development of the Bloss Automated Refractometer (BAR). The goal, in developing the BAR was to measure the optical properties and sample orientation for anisotropic materials as small as 100 μm. During development of the BAR several areas arose which required further research to fully understand what would be required to meet these goals: 1) the Rpl-vs-intensity scans, 2) the behavior of reflected light from isotropic and anisotropic samples, 3) precision and accuracy which measurements could be made, and 4) the development of algorithms to perform the necessary calculations for determining refractive indices and optical indicatrix orientation.

Discussion

History and current state of RTR: RTR flourished in the late 1800s and early 1900s. With this method, researchers made refractive index measurements with a precision of ± 0.0002 or better. In the early 1900s the jeweler's refractometer, a less precise and much simpler instrument than that normally used in RTR, was developed. With it was ushered in the age of ± 0.002 precision or worse. The method of RTR not only waned during this century, as did optical crystallography in general, but was almost forgotten. Fortunately the gemologists, although not as quantitative as the early mineralogists, maintained the use of refractometers in the identification of anisotropic gemstones.

Modeling anisotropic samples and Jones calculus: Modeling of anisotropic samples is far more difficult than isotropic samples. For isotropic samples all that is required for modeling are the Fresnel equations, as modified by the cone angle, and the material's single refractive index. The required mathematics need only be written in simple algebraic forms. For an anisotropic sample in a random orientation, linear algebraic techniques must be employed along with Jones calculus. To model Rpl-vs-I scans for anisotropic samples, the two or three refractive indices and their orientation must be known. From this information a dielectric tensor is written. Next by a lengthy series of mathematical manipulations, the reflected light intensity can be calculated. If the cone angle is significantly greater than the birefringence, the form of the Rpl-vs-I scan will appear similar to that for an isotropic sample, however if the cone angle is too small the scan will have a "knee", which represents n prior to total reflection of N.

Rpl-vs-Intensity: Although the theoretical base for the Rpl-vs-I scans lies in the well known Fresnel equations, the actual scans departed significantly from them. Four causes were found for this departure: 1) the cone angle effect, 2) contact liquid effect, 3) the wave-guide effect, and 4) particulate material on the BAR's optical components. The cone angle effect is the most significant of the four

and also the easiest to model. The contact liquid effect becomes important only in Rpl regions of the Rpl-vs-I scans that are not used in calculating the refractive index of the sample or when the liquid film becomes very thick or the cone angle equals zero, two conditions which do not occur. Only if the critical angle is exceeded will the wave-guide effect become significant; thus it too does not have an effect on refractive index determination for the Rpl-vs-I scans. Lastly, particulate matter on the BAR's optics can have an effect on the refractive index determination, however if the optics are kept clean this problem can be avoided.

Modeling isotropic samples: From the knowledge gained by an understanding of the Rpl-vs-I scans isotropic samples could be easily modeled. The Fresnel equations plus the cone angle effect can be used to calculate Rpl-vs-I scans. Monte Carlo studies can then be performed to determine how the Rpl-vs-I scans behave under different conditions, such as: 1) changes in the cone angle, 2) use of different orientations of the incident polarized light (e.g., the p- vs. the s-state), 3) changes in scan increments and lengths, and 4) differing noise levels. By varying these parameters, the robustness of different algorithms used to determine refractive index from Rpl scans can be statistically studied.

Precision: Before major contributions can be made to RTR, the precision of refractive index determination should be at least ± 0.0005. One of the major advantages of the BAR is its ability to determine the refractive indices of small samples, on the order of 100 μm as compared to the jeweler's refractometer which requires 1 mm size samples. To obtain results on smaller samples the BAR uses a focused laser beam; smaller samples can be studied by focusing the laser to smaller spot sizes. However, as was determined in the Monte Carlo study for isotropic samples, the larger the cone angle (= the smaller the spot size) the lower the precision, or repeatability, of the refractive index determined from an Rpl-vs-I scan. Several methods exist to increase precision, but they all require more time; thus some compromise must be reached between spot size, precision, and time. Modeling has indicated that a precision of ± 0.0005 can be easily achieved with a spot size of approximately 100 μm.

Algorithms: Two basic algorithms are required for the BAR to automatically determine optical properties and orientations of unknowns: 1) an algorithm to determine the refractive index from an Rpl-vs-I scan, for example, the modified Fresnel-fit and 2) a second algorithm to use the results of the first to determine the principal refractive indices and optical orientation for anisotropic materials, for example, the Julian-Bloss method. The MFF has been applied to computer-generated data and data collected from the BAR; in both cases it performs very well and determines refractive indices from Rpl-vs-I scans to within ± 0.0005 or better. The Julian-Bloss method has only been applied to computer-generated data. The data, containing errors commensurate with those expected in empirical data, yielded principal refractive indices within ± 0.0005 for anisotropic crystals.

Refractive index range: The refractive index range of the BAR is governed by three factors: 1) mechanical constraints, 2) refractive index of the hemisphere, and 3) refractive index of the contact liquid. Mechanical constraints affect both the high and low end of the range while the others affect the high range. Refractive indices cannot be determined which are greater than that of the hemisphere; however, the limiting factor for the upper end of the range is not the hemisphere's refractive index but that of the contact liquid. Materials exist, and can be used, which have refractive indices above 2.00; however, no satisfactory contact liquid exists above approximately 1.80. So for routine RTR the upper range is approximately 1.8.

Optical design constraints: A series of mirrors is employed on the BAR to control the angle of incidence of the laser beam onto the sample. Reflection of linearly polarized light from a mirror (a non-dielectric) at non-normal incidence, in general, will rotate the plane of polarization and impart a small ellipticity to the polarized light. For work with anisotropic samples these phenomena are undesirable. Jones calculus techniques were used to quantify the amount of polarization alteration by the reflecting components. These calculations showed the effects to be small but significant for orientation measurements - on the order of a degree of two.

Initially the BAR was being designed as a catoptric system (an optical system composed only of mirrors). With this design refractive indices could be measured at any wavelength within the hemisphere's transmission range. However, to obtain small spot size and control the laser beams, polarization-altering optical elements were added to the BAR that will not perform over as broad a wavelength range. Because of these constraints the BAR, without modification, will only be able to measure refractive indices in a range of a few 100 nm.

Conclusions

1. A review of the literature showed RTR flourished at the turn of the century; the review also disclosed that these earlier precise methods and even the earlier theories were not understood or even referred to in this century.

2. We independently, and accidentally, discovered that all principal refractive indices could be obtained to ± 0.0005, or better, from a single random polished section through a crystal.

3. From this discovery an automated refractometer (the BAR) capable of measuring smaller samples than normal refractometers was designed.

4. In normal refractometers the critical angle is measured and converted into the refractive index, but in the BAR the intensity data before total reflection is used to determine the refractive index.

5. Methods to calculate the polarization characteristics, phase, and intensity of reflected light from isotropic and anisotropic dielectrics and metals were developed by use of Jones calculus.

6. A complete understanding of all the factors contributing to the form of the Rpl-vs-I scans taken on the BAR for isotropic and anisotropic samples was established.

7. The necessary algorithms and methods were developed to collect and reduce the Rpl-vs-I scans into principal refractive indices for isotropic and anisotropic samples. These methods were tested both with BAR data and computer-generated data.

8. Measurements were made on isotropic samples and their refractive index could be determined with a precision of ± 0.0002, or better.

9. Measurements were made on anisotropic samples and the variation in refractive index correlated with the sample's birefringence and orientation.

References

Abbe, E. (1874) New instruments for the determination of refractive and dispersion properties of solid and liquid substances.[10] Jenaishe Zeitschrift für Naturwissenschaften, 8.

Anderson, B.W., Payne, C.J. and Pike, J. (1940) New refractometers employing diamond and other minerals. Mineralogical Magazine, 25, 579-582.

Azzam, R.M.A. and Bashara, N.M. (1977) Ellipsometry and Polarized Light. North-Holland, Amsterdam.

Bennett, J.M. (1964) Precise method for measuring the absolute phase change on reflection. Journal of the Optical Society of America, 54, 612-624.

Bennett, J.M. and Bennett, H.E. (1978) Polarization. Handbook of Optics. Eds. W. G. Driscoll and W. Vaughan, McGraw-Hill, New York.

Berreman, D.W. (1972) Optics of stratified and anisotropic media: 4x4 - matrix formulation. Journal of the Optical Society of America, 62, 502-510.

Berreman, D.W. (1973) Optics in smoothly varying planar structures: Application to liquid-crystal twist cells. Journal of the Optical Society of America, 63, 1374-1380.

Bertrand, E. (1885) Title unknown. Bulletin de la Sociètè française de Minèralogie, 8, 375-377.

Billard, J. (1966) Unpublished Thesis. University of Paris.

Bloss, F.D. (1961) An Introduction to the Methods of Optical Crystallography. Holt, Rinehart, and Winston, New York.

Bloss, F.D. (1971) Crystallography and Crystal Chemistry. Holt, Rinehart, and Winston, Inc. New York.

Bloss, F.D. (1981) The Spindle Stage: principles and practices. Cambridge University Press, Cambridge.

Bloss, F.D. (1985) Automated Refractometer. United States Patent Office.

Brill, A. (1889) Bestimmung der optischen Wellfläche aus einem ebenen Centralschnitte derselben. Mathematische Annalen, 34, 297-305.

[10] Translated title.

Burbage, E.J. and Anderson, B.W. (1941) An analysis of the movements of shadow-edges on the refractometer in the case of biaxial gemstones. Mineralogical Magazine, 26, 246-253.

Clarke, D. and Grainger, J.F. (1971) Polarized Light and Optical Measurement. Pergamon Press, Oxford.

Cornu, M.A. (1901) Dètermination des trios paramètres optiques principaux d'un cristal, en grandeur et en direction, par le rèfractomètre. Comptes Rendus, 133, 125-131.

Cornu, M.A. (1902) Dètermination des trios paramètres optiques principaux d'un cristal, en grandeur et en direction, par le rèfractomètre. Bulletin de la Sociètè française de Minèralogie, 25, 7-30.

Davis, L.E. (1985) Pegmatitic muscovites: effect of composition on optical and lattice parameters. Masters thesis, Virginia Tech, Blacksburg, Va.

DeSmet, D.J. (1975) Ellipsometry of a biaxial surface. Journal of the Optical Society of America, 65, 542-547.

DeSmet, D.J. (1976) Generalized ellipsometry and the 4x4 matrix formalism. Surface Sciences, 56, 293-306.

Drude, P. (1959) The Theory of Optics. Dover Publications, Inc. New York.

Duardo, J.A., Wang, S.C., and Hug, W. (1976) Polarization properties of internal mirror He-Ne lasers. SPIE, 88, 34-49.

Graves, R.H.W. (1969) Determination of the optical constants of anisotropic crystals. Journal of the Optical Society of America, 59, 1225-1228.

Hecht, E. and Zajac, A. (1979) Optics. Addison-Wesley, Reading.

Höfert, H.J. (1962) Abbe refractometer. Carl Zeiss, West Germany.

Hunter, W.R. (1965) Errors in using reflectance vs angle of incidence method for measuring optical constants. Journal of the Optical Society of America, 55, 1197-1204.

Hurlbut, C.S. and Switzer, G.S. (1979) Gemology. John Wiley and Sons, New York.

Hurlbut, C.S. (1981) A cubic zirconia refractometer. Gems and Gemology, 17, 93-95.

Hurlbut, C.S. (1984) The jeweler's refractometer as a mineralogical tool. American Mineralogist, 69, 391-398.

Hurwitz, H. and Jones, R.C. (1941) A new calculus for the treatment of optical systems: II. Proof of three general equivalence theorems. Journal of the Optical Society of America, 31, 493-499.

Jenkins, F.A. and White, H.E. (1976) Fundamentals of Optics. McGraw-Hill, New York.

Jones, R.C. (1941) A new calculus for the treatment of optical systems: I. Description and discussion of the calculus. Journal of the Optical Society of America, 31, 488-492.

Jones, R.C. (1941) A new calculus for the treatment of optical systems: III. The Sohncke theory of optical activity. Journal of the Optical Society of America, 31, 500-503.

Jones, R.C. (1942) A new calculus for the treatment of optical systems: IV. Journal of the Optical Society of America, 32, 486-493.

Jones, R.C. (1947) A new calculus for the treatment of optical systems: V. A more general formulation, and description of another calculus. Journal of the Optical Society of America, 37, 107-110.

Jones, R.C. (1947) A new calculus for the treatment of optical systems: VI. Experimental determination of the matrix. Journal of the Optical Society of America, 37, 110-112.

Jones, R.C. (1948) A new calculus for the treatment of optical systems: VII. Properties of the N-matrices. Journal of the Optical Society of America, 38, 671-685.

Jones, R.C. (1956) A new calculus for the treatment of optical systems: VIII. Electromagnetic theory. Journal of the Optical Society of America, 46, 126-131.

Lavenir, M.A. (1891) Sur la dètermination de l'orientation optique dans un cristal quelconque. Bulletin de la Sociètè française de Minèralogie, 14, 100-120.

Lin-Chung, P.J. and Teitler, S. (1984) 4x4 matrix formalism's for optics in stratified anisotropic media. Journal of the Optical Society of America A, 1, 703-705.

Kerr, P.F. (1977) Optical Mineralogy. McGraw-Hill, New York.

McKague, H.L. (1979) The refractometer in mineralogy instruction. Journal of Geology Education, 19, 67-72.

Moreels, C. de Greef and Finsy, R. (1984) Laser light refractometer. Applied Optics, 23, 3010-3013.

Nye, J.F. (1986) Physical Properties of Crystals. Claredon Press, Oxford.

Perrot, M.L. (1889) Vèrification expèrimentale de la mèthode de M. Charles Soret, pour la mesure des indices de rèfraction des cristaux à deyx axes. Comptes Rendus, 108, 137-138.

Phillips, W.R. (1971) Mineral Optics: principles and techniques. W.H. Freeman and Company, San Francisco.

Pockels, F. (1906) Lehrbuch der Kristalloptik. Leipzig.

Pulfrich, C. (1899) Ueber die Anwendbarheit der Methode der Totalreflexion auf kleine und mangelhafte Krystallfla'chen. Zeitschrift für Kristallographie und Mineralogie, 30, 568-586.

Ramachandran, G.N. and Ramaseshan, S. (1961) Crystal Optics. In Encyclopedia of Physics, 25, 1-217.

Schulz, L.Z. (1954) The optical constants of silver, gold, copper, and aluminum. I. The absorption index k. Journal of the Optical Society of America, 44, 357-362.

Schulz, L.Z. and Tangherlini, F.R. (1954) The optical constants of silver, gold, copper, and aluminum. II. The index of refraction n. Journal of the Optical Society of America, 44, 362-368.

Shurcliff, W.A. (1962) Polarized Light; Production and Use. Harvard University Press, Cambridge.

Shurcliff, W.A. and Ballard, S.S. (1964) Polarized Light. D. Van Nostrand Company, Princeton.

Smith, G.F. (1905a) An improved form of refractometer. Mineralogical Magazine, 14, 83-86.

Smith, G.F. (1905b) A new model refractometer. Mineralogical Magazine, 14, 354-359.

Sosnowski, T.P. (1972) Polarization mode filters for integrated optics. Optics Communications, 4, 408-412.

Soret, M.C. (1888a) Sur la mesure des indices de rèfraction des cristaux à deux axes, par l'observation des angles limites de rèflexion totale sur des faces quelconques. Comptes Rendus, 107, 176-178.

Soret, M.C. (1888a) Sur la mesure des indices de rèfraction des cristaux à deux axes, par l'observation des angles limites de rèflexion totale sur des faces quelconques. Comptes Rendus, 107, 479-482.

Soret, M.C. (1889) Ueber die Anwendung der Erscheinungen der Totalreflexion zur Messung der Brechungsexponenten zweiaxiger Krystalle. Zeitschrift für Kristallographie und Mineralogie, 15, 45-59

Su, S.C., Bloss, F.D. and Gunter, M.E. (1987) Procedures and computer programs to refine the double variation method. American Mineralogist, 72, 1011-1013.

Szivessy, G. (1928) Kristalloptik. In Geiger and Scheel Handbuch der Physik, 20, 635-904.

Teitler, S. and Henvis, B.W. (1970) Refraction in stratified, anisotropic media. Journal of the Optical Society of America, 60, 830-834.

Tilton, L.W. (1942) Testing and accurate use of Abbe-type refractometers. Journal of the Optical Society of America, 32, 371-381.

Tilton, L.W. (1943) Sources of error in precise commercial refractometry. Journal Research National Bureau of Standards, 30, 311-328.

Tully, B.J. (1927) A new model refractometer for determining the refractive indices of gem-stones, crystals, and liquids. Mineralogical Magazine, 21, 324-328.

Tutton, A.E.H. (1922) Crystallography and Practical Crystal Measurement. MacMillion and Co., Limited.

Viola, C. (1899a) Ueber die Bestimmung der optischen Constanten eines beliebig orientation zweiaxigen Krystallschnittes. Zeitschrift für Kristallographie und Mineralogie, 31, 40-48.

Viola, C. (1899b) Ueber einge im mineralogischen Institute zu München ausgeführte Untersuchungen. Zeitschrift für Kristallographie und Mineralogie, 30, 417-442.

Viola, C. (1902) Die Bestimmung der optischen Constanten eines Krystalles aus einem einzigen beliebigen Schnitte. Zeitschrift für Kristallographie und Mineralogie, 36, 245-251.

Wahlstrom, E.E. (1969) Optical Crystallography. John Wiley and Sons, Inc., New York.

Winchell, A.N. (1937) Elements of Optical Mineralogy: Part I - Principles and Methods. Braunworth and Co., Inc., Bridgeport.

Wollaston, W.H. (1802a) A method of examining refractive and dispersive powers, by prismatic reflection. Philosophical Transactions of the Royal Society, 92, 365-380.

Wollaston, W.H. (1802b) On the oblique refraction of Iceland crystal. Philosophical Transactions of the Royal Society, 92, 381-386.

Wright, F.E. (1908) Die Justierung des Abbe-Pulfichschen Kristallrefraktometers. Zeitschrift für Instrumentenkunde, 28, 201-206.

Wright, F.E. (1911) The methods of petrographic-microscopic research. Carnegie Institution of Washington, Publication No. 158.

Automated Refractometer References

Bloss, F.D. (1986a) Operational procedures for the BAR. Automated Refractometer Report 1.

Bloss, F.D. (1985) BAR progress report, September 20, 1985: Results of the on-line BAR and mathematics of the angular BAR. Automated Refractometer Report 2.

Gunter, M.E. (1985a) Error analysis results for the angular BAR. Automated Refractometer Report 3.

Gunter, M.E. (1985b) Comparison of on-line and angular BAR and methods to increase precision of angular BAR. Automated Refractometer Report 4.

Gunter, M.E. (1986a) Possible hemicylinder materials for the BAR. Automated Refractometer Report 5.

Gunter, M.E. and Walsh, K. (1985) Procedure for angular BAR alignment. Automated Refractometer Report 6.

Indebetouw, G. (1986a) Preliminary study of the optical system of the BAR: Its effect on a small spot size and its sensitivity of misalignment. Automated Refractometer Report 7.

Indebetouw, G. (1986b) Theoretical light output intensity of the BAR. Automated Refractometer Report 8.

Martin, A. (1986a) Survey of laser systems. Automated Refractometer Report 9.

Indebetouw, G. (1986c) Brief report and recommendations regarding the usefulness of an optical design program for the BAR analysis and optimization. Automated Refractometer Report 10A.

Martin, A. (1986b) Review of optical design program. Automated Refractometer Report 10B.

Gunter, M.E. (1986b) Three computational techniques for refractive index determination with the BAR. Automated Refractometer Report 11.

Gunter, M.E. (1986c) Locating the principal vibration directions of anisotropic materials with the BAR. Automated Refractometer Report 12.

Bloss, F.D. (1986b) The three possible modes of operation of the BAR. Automated Refractometer Report 13.

Bloss, F.D. (1986c) Standardization, standard symbols, and routine operation of the BAR. Automated Refractometer Report 14.

Indebetouw, G. (1986d) Comments on the performance of the Version A BAR. Automated Refractometer Report 15.

Bradley, R.S. and Martin, A. (1986) Baseline evaluation of BAR Version A. Automated Refractometer Report 16.

Bloss, F.D. (1986d) Report on four patents called to our attention by the (U.S.) patent examiner. Automated Refractometer Report 17.

Speer, J.A. (1986) Work necessary to design a crystallographic, production-model BAR. Automated Refractometer Report 18.

Bloss, F.D. (1986e) Report on the four patents cited by the British Patent Office. Automated Refractometer Report 19.

Gunter, M.E. (1986d) Application of antireflection coatings to the BAR's optical system. Automated Refractometer Report 20.

Gunter, M.E. (1986e) Linear polarization angle control by half-wave retarders. Automated Refractometer Report 21.

Bradley, R.S. (1986a) Optical coupling media. Automated Refractometer Report 22.

Gunter, M.E. (1986f) Optical characterization of the Version A BAR. Automated Refractometer Report 23.

Gunter, M.E. (1986g) Laser beam expansion and focusing. Automated Refractometer Report 24.

Martin, A. (1986c) Possible configurations for automating the BAR. Automated Refractometer Report 25.

Bradley, R.S. (1986b) Elliptical mirror optimization. Automated Refractometer Report 26.

Bradley, R.S. (1986c) Addendum to elliptical mirror optimization. Automated Refractometer Report 26a.

Gunter, M.E. (1986h) Tolerance analysis of the Version A BAR. Automated Refractometer Report 27.

Gunter, M.E. (1986i) Improved optical design for the crystallographic BAR. Automated Refractometer Report 28.

Gunter, M.E. (1986j) Addendum to improved optical design for the crystallographic BAR. Automated Refractometer Report 28b.

Bloss, F.D. and Su, S.C. (1986) The Fresnel-fit method for determining refractive indices from Rpl scans of isotropic data. Automated Refractometer Report 29.

Gunter, M.E. (1986k) Polarization characterization of the optical components of the BAR. Automated Refractometer Report 30.

Bloss, F.D. (1987a) Methods of operation of the BAR and related computations. Automated Refractometer Report 31.

Martin, A. (1986d) Light sources for the BAR. Automated Refractometer Report 32.

Bloss, F.D. (1986g) Calculating E_x,E_y,E_z from S_x,S_y,S_z. Automated Refractometer Report 33.

Bloss, F.D. (1986h) Optical coupling liquids revisited. Automated Refractometer Report 34.

Gunter, M.E. (1987a) Rpl vs. intensity: Cone angle effect. Automated Refractometer Report 35.

Gunter, M.E. (1987b) Rpl vs. intensity: Oil effects. Automated Refractometer Report 36.

Gunter, M.E. (1987c) Rpl vs. intensity: Miscellaneous effects and summary of all effects. Automated Refractometer Report 37.

Martin, A. (1987a) BAR Version B software functional specifications. Automated Refractometer Report 38.

Gunter, M.E. (1987d) Computer modeling of isotropic data and a revised Fresnel-fit. Automated Refractometer Report 39.

Bloss, F.D. and Su, S.C. (1987) Smoothing HBV data. Automated Refractometer Report 40.

Bloss, F.D. (1987b) Effects of random errors in HBV data on the Julian-Bloss solutions for biaxial crystals. Automated Refractometer Report 41.

Martin, A. and Bradley, R.S. (1987) Linear photodetector for the BAR. Automated Refractometer Report 42.

Gunter, M.E. (1987e) Polarization light reflection from dielectrics. Automated Refractometer Report 43.

Gunter, M.E. (1987f) Basic algorithm for the Julian-Bloss method. Automated Refractometer Report 44.

Bloss, F.D. (1987c) Broad details of program involving use of the Julian-Bloss method. Automated Refractometer Report 45.

Gunter, M.E. (1987g) Review of French articles on refractometry of anisotropic samples. Automated Refractometer Report 46.

Gunter, M.E. (1987h) A procedure to evaluate the crystallographic BAR's ability to determine optical parameters of isotropic and anisotropic samples. Automated Refractometer Report 47.

Appendix: Sample calculations and derivations

Derivation of Rpl-vs-n relationship

Given the refractive index of the hemicylinder, n_i, and the angle of incidence, θ, for a ray undergoing total reflection upon entering a material of unknown refractive index, n_t ; n_t can be found by application of Snell's law. For the BAR, however, the angle which can be controlled is not θ, but Rpl. This angle is defined as the angle between the normal to the first rotatable mirror for the BAR and the incident laser beam (Figure 33a), and is mathematically related to θ by use of the geometrical properties of an ellipse. Figure 33a shows these relationships, which can be expressed as follows:

$$\theta = \alpha + \beta \qquad [A.1]$$

where,

θ = angle of incidence

α = angle which is a function of Rpl

β = angle which is an instrument constant

To find θ, the angle α must be written in terms of Rpl. Equation A.2 provides the relationship, which is shown in Figure 33b that relates α and 2Rpl.

$$\cos\alpha = \frac{k_1 + k_2 \cos 2Rpl}{k_2 + k_1 \cos 2Rpl} \qquad [A.2]$$

where,

$k_1 = 2ac$

$k_2 = a^2 + c^2$

a = semi-major axis of elliptical mirror

b = semi-minor axis of elliptical mirror

$c = \sqrt{a^2 - b^2}$

Recall Snell's law, which can be written as follows:

$$n_i \sin\theta = n_t \sin\theta_t$$

where,

n_i = refractive index of incident media

θ = angle of incident ray

n_t = refractive index of transmitting media (i.e., unknown)

θ_t = angle of refracted ray

and for $\theta_t = 90°$,

$$n_t = n_i \sin\theta_{CA}$$

where,

θ_{CA} = critical angle

Substituting $\alpha + \beta$ of Eqn. A.1 for θ in the above expression of Snell's law, at total reflection, results in

$$n = nhc \times \sin(\cos^{-1}\frac{[k1 + k2\ \cos 2Rpl]}{[k2 + k1\ \cos 2Rpl]} + \beta) \qquad [A.3]$$

where,

n = refractive index of unknown, n_t in Snell's law

nhc = refractive index of the hemicylinder, n_i in Snell's law.

It would also be convenient to express Rpl as a function of the refractive index, n (i.e., write an expression in the form Rpl = f(n)). By algebraic rearrangement Eqn. A.3 can be expressed as:

$$\sin^{-1}\frac{n}{nhc} - \beta = \cos^{-1}\frac{k1 + k2\ \cos 2Rpl}{k2 + k1\ \cos 2Rpl}$$

The $\sin^{-1}\frac{n}{nhc}$ is equal to θ; thus because $\theta = \alpha + \beta$, the above equation can be reduced to:

$$\cos\alpha = \frac{k_1 + k_2 \cos 2Rpl}{k_2 + k_1 \cos 2Rpl}$$

Next, this equation is algebraically manipulated as follows:

$$(k_2 + k_1 \cos 2Rpl)\cos\alpha = k_1 + k_2 \cos 2Rpl$$

and,

$$k_1 \cos\alpha \cos 2Rpl = k_1 + k_2 \cos 2Rpl - k_2 \cos\alpha$$

and,

$$\cos 2Rpl(k_1 \cos\alpha - k_2) = k_1 - k_2 \cos\alpha$$

finally,

$$Rpl = \frac{\cos^{-1}\frac{k_1 - k_2 \cos\alpha}{k_1 \cos\alpha - k_2}}{2} \qquad [A.4]$$

After a critical Rpl value has been observed, Eqn. A.3 (Eqn. 3.1a in the text) is required to calculate the refractive index. Equation A.3 is plotted in Figure 34 showing the relationship between Rpl and n. Three different curves appear on this figure showing how the Rpl-vs-n relation changes as the geometry of the elliptical mirror is varied.

Jones matrix calculation for isotropic dielectric

To find the intensity and polarization characteristics of a linearly polarized beam reflected from a dielectric, Eqn. 5.10 can be solved. To calculate the Jones matrix for the sample, the angle of incidence, θ, and the refractive indices for n_i and n_t must be specified. Then any polarization vector can be written and multiplied by the Jones matrix; the resulting vector can be analyzed to

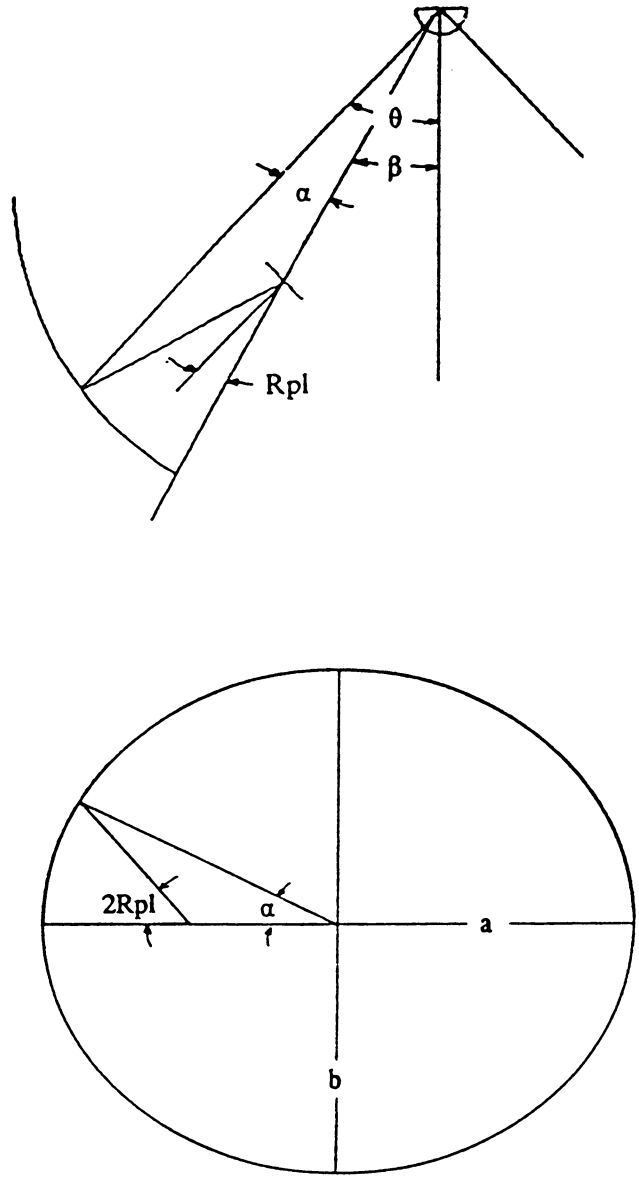

Figure 33. **Geometrical relations between the elliptical mirror and the angle of incidence:** a) (top) This figure shows the nomenclature used to relate the Rpl angle of the BAR, to the angle of incidence, θ. θ is the sum of β, an instrument constant, and the angle α, which is a function of the Rpl angle. b) (bottom) Angles α and 2Rpl are inscribed in an ellipse with semi-major axis a and semi-minor axis b. Equation A.2 gives the relationship between these two angles.

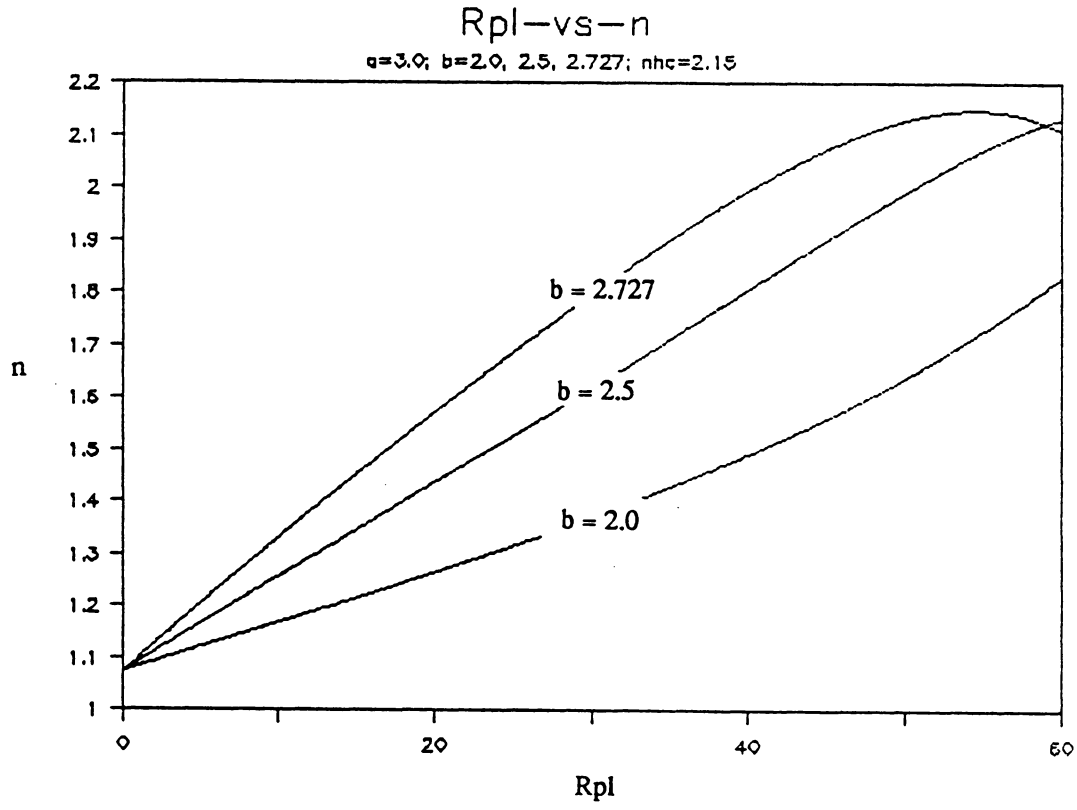

Figure 34. Relationship of the Rpl angle and observable refractive index: Three different choices of b in Eqn. A.3 are shown in the above plot. For b = 2.727 the curve is concave down. When b is changed to 2.0 the Rpl-vs-n curve becomes concave up. If b is changed to 2.5 a near linear relationship exists between Rpl and n.

determine the polarization characteristics of the reflected beam. By choosing θ to be 35°, n_i and n_t to be 2.0 and 1.5, then for incident linearly polarized light with α = 45°, the following results:

$$\begin{bmatrix} -0.024 & 0.000 \\ 0.000 & 0.258 \end{bmatrix} \begin{bmatrix} 0.707 \\ 0.707 \end{bmatrix} = \begin{bmatrix} -0.017 \\ 0.182 \end{bmatrix}$$

With the above results, the intensity and polarization orientation can be calculated from the resultant by Eqns. 5.8 and 5.9. Table 5 lists results for three different angles of incidence and three different orientations of the linearly polarized beam. For α = 0° and 90°, the p- and s-states, there is no rotation of the beam after reflection. The p- and s-state are thus the two orthogonal eigenpolarization states, because the polarization characteristics for the incident and reflected beams are equivalent. However, for α = 45° the reflected beam's polarization direction is rotated. The amount of rotation is dependent upon the angle of incidence.

Jones matrix calculation for isotropic metal

The Jones matrix for an isotropic dielectric is a simplified form of the calculation for a metal. The optical properties of a metal cannot be solely defined by its refractive index, n. To fully define the metal its extinction coefficient, k, must be used with n. Because k is non-zero for a metal, a non-π phase shift occurs. The Jones matrix must use contain these phase shifts. Equations 3.7, the generalized Fresnel equations, and 3.8, the phase angle equations, must be used to calculate the amplitude and phase that enters the Jones matrix. If θ, is chosen to be 60° and n and k set equal to 0.97 and 6.00 (the optical properties of Al) solution of Eqn. 5.10 yields the following:

$$\begin{bmatrix} 0.907\,(323.6°) & 0.000\,(0.0°) \\ 0.000\,(0.0°) & 0.975\,(170.5°) \end{bmatrix} \begin{bmatrix} 0.707\,(0.0°) \\ 0.707\,(0.0°) \end{bmatrix} = \begin{bmatrix} 0.641\,(323.6°) \\ 0.689\,(170.5°) \end{bmatrix}$$

The above Jones matrix can be multiplied by a vector describing linearly polarized light with α = 45°. By Eqn. 5.8 the intensity of the reflected beam is 88.6%. Equations 4.7 and 4.8 are used to

Table 5. **Reflection intensity and polarization rotation for a dielectric**

	$\alpha_i = 0°$		$\alpha_i = 90°$		$\alpha_i = 45°$	
	I	α_r	I	α_r	I	α_r
$\theta = 35.0°$	0.06%	0.0°	6.66%	90.0°	3.34%	-84.7°
$\theta = 40.0°$	0.29%	0.0°	10.82%	90.0°	5.57%	80.7°
$\theta = 45.0°$	33.18%	0.0°	54.32%	90.0°	43.79%	51.9°

calculate the polarization characteristics of the reflected beam. Solving these equations yields α = -42.7° and ε = 13.39. Thus the incident linearly polarized light has become elliptically polarized with the major axis of the ellipse oriented at -42.7°. For linearly polarized light incident upon a metal at α = 0° or 90°, the reflected beam will be linearly polarized. Thus the p- and s-state for an isotropic metal correspond to the metal eigenpolarization states.

Jones matrix calculation for randomly oriented anisotropic dielectric

The Jones reflection matrix for a randomly oriented anisotropic dielectric can be found by solution of Eqns. 5.1 through 5.7. First a randomly oriented sample must be chosen and the values and orientations of its three principal refractive indices known. Table 6 lists the required data for this example.

The S,E spherical coordinates of Table 6 are transformed by Eqn. 5.1 into the following cartesian coordinates:

	x	y	z
α	0.6054	-0.7928	0.0779
β	-0.1568	-0.0226	0.9874
γ	0.7810	0.6091	0.1379

Next the dielectric tensor (DT) is found by Eqn. 5.3 as follows:

Table 6. Optical properties of Tiburon albite

α = 1.52890	S_x = 174.39°	E_x = 52.81°
β = 1.53291	S_y = 91.31°	E_y = 99.02°
γ = 1.53929	S_z = 12.76°	E_z = 38.64°

$$DT = \begin{bmatrix} 2.3570 & 0.0153 & 0.0015 \\ 0.0153 & 2.3497 & 0.0024 \\ 0.0015 & 0.0024 & 2.3501 \end{bmatrix}$$

The optical matrix is formed from the dielectric tensor, magnetic permeability tensor, and optical rotation tensors by Eqn. 5.4. The magnetic permeability tensor is the identity matrix for this example and the optical rotation matrices become null matrices for reflection; thus OM can be written as:

$$OM = \begin{bmatrix} 2.3570 & 0.0153 & 0.0015 & 0.0000 & 0.0000 & 0.0000 \\ 0.0153 & 2.3497 & 0.0024 & 0.0000 & 0.0000 & 0.0000 \\ 0.0015 & 0.0024 & 2.3501 & 0.0000 & 0.0000 & 0.0000 \\ 0.0000 & 0.0000 & 0.0000 & 1.0000 & 0.0000 & 0.0000 \\ 0.0000 & 0.0000 & 0.0000 & 0.0000 & 1.0000 & 0.0000 \\ 0.0000 & 0.0000 & 0.0000 & 0.0000 & 0.0000 & 1.0000 \end{bmatrix}$$

The propagation matrix (PM) is formed by mathematical manipulation of OM by use of Eqn. 5.5 as follows:

$$\mathbf{PM} = \begin{bmatrix} -0.0008 & 0.3441 & -0.0013 & 0.0000 \\ 2.3570 & -0.0008 & 0.0153 & 0.0000 \\ 0.0153 & 2.3497 & 0.0024 & 1.0000 \\ 0.0153 & -0.0013 & 0.8082 & 0.0000 \end{bmatrix}$$

The next step requires computing the four eigenvalues and their corresponding eigenvectors of PM. Two of these eigenvectors correspond to the reflected component of the incident light, the other two to the transmitted. The eigenvalues and eigenvectors for PM are listed below.

Four eigenvalues and eigenvectors of PM

1	2	3	4
-0.9063	-0.8940	0.9033	0.8954
0.2952	-0.2587	0.3583	-0.3261
-0.7755	0.6736	0.9434	-0.8471
0.4135	0.5367	0.5544	0.6128
-0.3748	-0.4798	0.5008	0.5487

The two eigenvectors with positive eigenvalues correspond to the reflected beam: #3 and #4. These two eigenvectors are substituted into S_1 and S_2 of Eqn. 5.6. Solving Eqn. 5.6 results in the Jones matrix (RM) for Tiburon albite at a 35° angle of incidence with n_i equal to 2.1646 (the value of the hemicylinder).

$$S1 = \begin{bmatrix} 1.5682 & 2.0172 \\ -1.3963 & 2.1622 \end{bmatrix}$$

$$S1 = \begin{bmatrix} 1.5896 & 1.0151 \\ -1.4031 & 1.1029 \end{bmatrix}$$

$$RM = \begin{bmatrix} 0.0048 & -0.0032 \\ 0.0021 & -0.3272 \end{bmatrix}$$

Given RM, the characteristics of any polarized light beam reflected from the sample can be found. For example if linearly polarized light with $\alpha = 90°$, the s-state, is reflected from the sample and the following calculation would be performed:

$$\begin{bmatrix} 0.0048 & -0.0032 \\ 0.0021 & -0.3272 \end{bmatrix} \begin{bmatrix} 0 \\ 1 \end{bmatrix} = \begin{bmatrix} -0.0032 \\ -0.3272 \end{bmatrix}$$

Analysis of the reflected beam discloses that it is not equivalent to the incident beam as in the early calculations for isotropic samples. Table 7 lists calculations performed at two angles of incidence for three different input orientations for linearly polarized light. For all three input orientations, there is a rotation of the reflected beam. The rotation also changes with differing angles of incidence. As discussed in Chapter 1, it was originally assumed that reflection would have no effect on polarized light. However, as seen form the above calculations, polarization changes are an inherent part of light reflection for both isotropic and anisotropic samples.

Julian-Bloss method

For each stage setting S of the BAR, refractive index values of N and n can be determined for an anisotropic crystal. Curves of refractive index vs S can be obtained from this data (Viola, 1899, Burbage and Anderson, 1941, and Hurlburt, 1984). From these curves the principal refractive indices of an anisotropic crystal can be visually determined. A more quantitative method to determine the refractive indices, and also the orientation of the optical indicatrix, was discussed in Bloss (AR-1987a, Appendix). This method has become known as the Julian-Bloss method (JB method) and the purpose of this section is to explain its basic algorithm.

The JB method can be used to determine the orientation and shape (i.e., the refractive indices) of the optical indicatrix of an anisotropic crystal. The method requires, as input values, N, n, and E for at least three non-duplicate stage settings. The E angles are calculated from the N and n values. If measurements are made at more than three S settings the system is over determined. This system of equations can then be solved using least squares to increase the precision and accuracy of the method.

Table 7. **Reflection intensity and polarization rotation from Tiburon albite**

	$\alpha_i = 0°$		$\alpha_i = 90°$		$\alpha_i = 45°$	
	I	α_r	I	α_r	I	α_r
$\theta = 35.0°$	0.003%	23.6°	10.71%	89.4°	5.28%	-89.7°
$\theta = 44.9°$	52.12%	0.5°	72.72%	88.6°	64.52%	49.1°

In the JB method a matrix A is found. The A matrix describes a triaxial ellipsoid, which is geometrically equivalent to the biaxial indicatrix. The A matrix has been called the index tensor (Ramachandran and Ramaseshan, 1961) and is equal to the inverse of the dielectric tensor. The inverses of the square roots of the eigenvalues of A equal the three principal refractive indices, while their associated three eigenvectors define the orientation of the principal vibration directions X,Y, and Z of a biaxial crystal. The A matrix can be formed by determination of the N and n values at various S settings. Next the E angles are calculated based upon Eqn. 1, Bloss (1987b). The A matrix can now be formed from calculation of the following two 2x2 matrices: B and C (Bloss, 1987a, Appendix).

$$B = \begin{bmatrix} L_N \cos^2 E_s + L_n \sin^2 E_s & (L_N - L_n) \sin E_s \cos E_s \\ (L_N - L_n) \sin E_s \cos E_s & L_N \sin^2 E_s + L_n \cos^2 E_s \end{bmatrix} \quad [A.5]$$

$$C = \begin{bmatrix} a_{11} & a_{12} \cos S + a_{13} \sin S \\ a_{12} \cos S + a_{13} \sin S & a_{22} \cos^2 S + a_{33} \sin^2 S + 2a_{23} \cos S \sin S \end{bmatrix} \quad [A.6]$$

where,

$L_N = \frac{1}{N^2}$

$L_n = \frac{1}{n^2}$

E_s = the angle between the BAR's x axis and N in the crystal

a_{ij} = the individual elements of the A matrix

S = the stage position at which the n, N, and E_s were determined.

The A matrix is found by equating b_{ij} with c_{ij} of Eqns. A.5 and A.6 above. If three sets of N and n values have been obtained at three non-duplicate S settings, S settings which do not rep-

resent the same sections through the crystal (e.g., S = 0° and S = 180° would not be non-duplicate), then the following set of equations, formed by equating the matrix B (Eqn. A.5) and the matrix C (Eqn. A.6), can be solved to find matrix A, whose terms are:

$$a_{11} = L_N \cos^2 E_s + L_n \sin^2 E_s \qquad [A.7a]$$

$$a_{12} \cos S + a_{13} \sin S = (L_N - L_n) \sin E_s \cos E_s \qquad [A.7b]$$

$$a_{22} \cos^2 S + a_{33} \sin^2 S + 2a_{23} = L_N \sin^2 E_s + L_n \cos^2 E_s \qquad [A.7c]$$

The right-hand sides of Eqns. A.7a-c represent numerical values calculated from BAR-determined S, E, N, and n values. Solutions of Eqns. A.7a-c for a_{ij} values yield the A matrix. The a_{11} value can be determined from a single S setting. The values for a_{12} and a_{13} require information from two non-duplicate S settings. Thus, after data for two S settings have been collected, Eqn. A.7b can be written for each S setting to produce two equations from which the two unknowns, a_{12} and a_{13}, can be calculated. The remaining three values, a_{22}, a_{33}, and a_{23} , are found by making measurements at a third S setting and then obtaining three different values for the right-hand side of Eqn. A.7c and solving this set to find a_{22}, a_{33}, and a_{23}.

Once the A matrix has been formed the refractive indices and orientation of the biaxial indicatrix are easily determined. The inverse square root of the three eigenvalues of A correspond to the three principal refractive indices. The three corresponding eigenvectors give the orientation of the three principal refractive indices.

The above method was simplified in Bloss (1987a, Appendix) by choosing two of the three S settings to be 0° and 90°. From this simplification several of the terms in Eqn. A.2 became zero; thus given these two special S settings all the elements of the A matrix, except a_{23}, could be found without resorting to solving systems of simultaneous equations. However, to find a_{23}, a set of equation based upon Eqn. A.7c must still be solved.

Numerical Example

To proceed in the example we will take a biaxial crystal whose refractive indices and orientation are known. From this data we can generate the necessary values of E, N, and n for three S settings, then this data can be used in Eqns. A.5-A.7 above. This example is based, in part, on Bloss (1987a, Appendix).

Table 6 describes the optical properties of the crystal used in this example. From the data in Table 6, the necessary values for N, n, and E at three S settings (Table 8) can be calculated from Bloss (1981, Eqn. 4-9a, p.146).

Equations A.7a-c can be solved to find the elements for the A matrix from the data in Table 8. At each S setting Eqn. A.7a can be solved and a value of a_{11} found. In general two S settings are required to find a_{12} and a_{13} because there are two unknowns in Eqn. A.7b. To find a_{22}, a_{33} and a_{23}, three S settings are needed so Eqn. A.7c can be written three times and then solved for its three unknowns. The following shows solution of each equation at the required S settings.

Eqn. A.7a: S = 0°: $b_{11} = c_{11}$: --> a_{11} = 0.424333

Eqn. A.7b: S = 0°: $b_{12} = c_{12}$: --> a_{12} = -0.002745
Eqn. A.7b: S = 90°: $b_{12} = c_{12}$: --> a_{13} = -0.000273

Eqn. A.7c: S = 0°: $b_{22} = c_{22}$: --> 0.425663
Eqn. A.7c: S = 50°: $b_{22} = c_{22}$: --> 0.425142
Eqn. A.7c: S = 90°: $b_{22} = c_{22}$: --> 0.425510

By solving the three equations based on Eqn. A.7c at three different S settings from above, the following a_{ij} values are found:

a_{22} = 0.425663
a_{33} = 0.425142
a_{23} = -0.000437

Table 8. Values for N, n, and E at S = 0°, 50°, and 90°

S	E	N	n
0°	37.701°	1.53917	1.52893
50°	38.489°	1.53819	1.53084
90°	11.606°	1.53541	1.53291

In the above example only the set of equations for Eqn. A.7c would require solution of a set of simultaneous equations. The two equations based upon Eqn. A.7b, for the case of S = 0° and S = 90°, have explicit solutions for a_{12} and a_{13} because Eqn. A.7b simplifies under these conditions. The A matrix can now be given as follows:

$$A = \begin{bmatrix} 0.424333 & -0.002745 & -0.000273 \\ -0.002745 & 0.425663 & -0.000437 \\ -0.000273 & -0.000437 & 0.425510 \end{bmatrix}$$

The eigenvalues and eigenvectors appear in Table 9.

The values appearing in Table 9 can be transformed into the values appearing in Table 6, which can in turn be transformed into refractive indices and spherical orientation of the optical indicatrix. Refractive indices are obtained from the eigenvalues in Table 9 by taking their inverse square root; the results of this transformation appear in Table 10 and agree, within round off error, to the values in Table 6. The x,y,z cartesian coordinate's for the eigenvectors in Table 9 are transformed by Eqns. 5.2 into the S and E spherical coordinate system; the values resulting from this transformation appear in Table 10 and agree, within round-off error, to those values in Table 6.

Table 9. Eigenvalues and eigenvectors for the A matrix

eigenvalue	eigenvector
0.427836	x = 0.611342 y = -0.787686 z = 0.076243
0.425566	x = -0.158099 y = -0.027165 z = 0.987050
0.422104	x = 0.775413 y = 0.615478 z = 0.141139

Modified Fresnel-fit calculation

The MFF method can be used to determine the refractive index, n, from an Rpl-vs-I scan. The method is based upon the Fresnel equations as modified by the cone angle effect. The following six step method can be used to perform the modified Fresnel-fit (MFF).

1. Collect data: Collect Rpl-vs-I (= I_{obs}) over the entire BAR Rpl range at user defined Rpl increments and polarization angle (= α, defined as the angle between the BAR's x direction and the orientation of the incident linearly polarized light).

2. Normalize data: The I_{obs} data must be normalized from 0 to 100%, instead of the relative intensity readings obtained from the BAR. The following procedure is recommended:

A. Determine a zero for the BAR by intensity measurement of Brewster's angle (= I_{BA}), from earlier Rpl-vs-I scans this value was determined to be 2499.8.

B. Subtract I_{BA} from each I_{obs}.

Table 10. Calculated optical properties of Tiburon albite

α = 1.52884	S_x = 174.47°	E_x = 52.31°
β = 1.53291	S_x = 91.58°	E_x = 99.10°
γ = 1.53918	S_x = 12.92°	E_x = 39.16°

C. Locate the maximum I_{obs} and divide all I_{obs} by it, then multiply all values by 100 to place intensities on a percent scale.

3. Approximate refractive index: Determine an approximate refractive index (=n.guess), for example by use of the residual-method (Gunter, 1986a).

4. Create calculated data: Based upon n.guess calculate Rpl-vs-I ($=I_{calc}$) by use of the Fresnel equations as modified by the cone angle as follows.

Fresnel equations: Define n_t equal to n.guess, then find:

$$r_s = \frac{n_i \cos\theta_i - n_t \cos\theta_t}{n_i \cos\theta_i + n_t \cos\theta_t} \qquad [A.8a]$$

$$r_p = \frac{n_t \cos\theta_i - n_i \cos\theta_t}{n_t \cos\theta_i + n_i \cos\theta_t} \qquad [A.8b]$$

$$R = (r_p^2 \cos^2\alpha + r_s^2 \sin^2\alpha) \times 100 \qquad [A.8c]$$

where,

r_s = amplitude coefficient normal to plane of incidence
r_p = amplitude coefficient parallel to plane of incidence
n_i = refractive index of hemisphere
n_t = refractive index of unknown
θ_i = angle of incidence, mathematically related to Rpl
θ_t = angle of transmitted beam, mathematically related to θ_i by Snell's law
R = calculated intensity ($= I_{calc}$), in percent
α = the angle between the polarization direction and x

Cone angle modification:

$$I_r = I_0 e^{-2\frac{r^2}{w^2}} \qquad [A.9]$$

where,

I_r = the resultant intensity

I_o = the original intensity, R from Eqn. A.8c

r = the distance from the beam center

w = the beam radius

Snell's law is used to calculate the critical angle, and all intensities equal to or greater than this angle are assigned 100. The cone angle effect, discussed at length in Gunter, 1987b, is used to model a focused laser beam incident upon the sample. Each I_{calc} is modified by a weighting factor scheme determined from a Gaussian distribution (Eqn. A.9) and the physical parameters of the BAR (i.e., the cone angle, Rpl increment, and laser beam radius). Recall that the cone angle is a function of focusing the laser; more tightly focused laser beams will have a higher cone angle. The following series of numbers represent the values for weighting the beam in Eqn. A.9 given a cone angle = 1°, Rpl increment = 0.1°, and a beam radius of 1 mm:

0.1353 0.2780 0.4868 0.7261 0.9231 1.000 0.9231 0.7261 0.4868 0.2780 0.1353

The number of weights will be equal to the cone angle divided by the Rpl increment plus one. Once the weights are established they are convoluted into the I_{calc} values as follows (using the above BAR parameters):

I_{calc}		weights
I_{calc1}	×	weight 1
I_{calc2}	×	weight 2
I_{calc3}	×	weight 3
I_{calc4}	×	weight 4
I_{calc5}	×	weight 5
I_{calc6}	×	weight 6 ----> new value for I_{calc6}
I_{calc7}	×	weight 7
I_{calc8}	×	weight 8
I_{calc9}	×	weight 9
I_{calc10}	×	weight 10
I_{calc11}	×	weight 11

This single calculation yields a new value for I_{calc6}, by summing all eleven of the above terms and normalizing. In general the above procedure is represented in Eqn. A.10 as follows:

$$\sum_{j=1}^{m}\sum_{i=1}^{n}(I_{calc(i,j)} \times weight_{(i)}) / NF \qquad [A.10]$$

where,

$I_{calc(i,j)}$ = the i^{th} calculated intensity at the j^{th} Rpl value

$weight_{(i)}$ = the i^{th} weight

n = the number of weights, which equals the cone angle divided by Rpl increment plus one

m = the number of Rpl values, which equals the Rpl range divided the Rpl increment

NF = a normalization factor dependent upon the values of the weights

Next, the entire calculation is repeated with the weights "slid" to the next higher I_{calc} value - increment j in Eqn. A.10. The process is continued until all the I_{calc} values have been modified by the cone angle effect. In the procedure the ends of the I_{calc} values are lost, (I_{calc1} through I_{calc5} in the above example, or in general one half the cone angle divided by the Rpl increment will be lost at each end). This presents no problem for the calculation; one simply extends the Rpl range used in the calculation to compensate for the lost values.

5. Compare observed and calculated: Compare I_{obs} to I_{calc} by computing the value of Eqn. A.11.

$$\sum_{i=1}^{n}(I_{obs(i)} - I_{calc(i)})^2 \qquad [A.11]$$

where,

$I_{obs(i)}$ = the observed intensity at the i^{th} Rpl value.

$I_{calc(i)}$ = the calculated intensity at the i^{th} Rpl value.

n = the number of intensity readings, which is the Rpl range divided by the Rpl increment.

6. Minimize Eqn. A.11: Proceed with minimization of Eqn. A.11 by iterating upon n.guess and recalculating I_{calc}. When a value of n.guess is found to within 0.0001 that minimizes Eqn. A.11, assign this n.guess to be the observed refractive index.

Residual method

The data obtained from the BAR appear as in Figure 35. Given this data, we must locate the point at which the reflected beam's intensity first reaches a maximum (the point marked approximate critical angle on Figure 35). From this Rpl-vs-I scan the residual method can be used to determine an approximate critical Rpl as follows:

A. Collect a data set.

B. Perform a simple linear regression (SLR) on the Rpl-vs-I scan to obtain a linear equation of the form

$$\hat{I} = b_0 + b_1 Rpl \qquad [A.12]$$

where,

$\hat{I}$ = predicted intensity

Rpl = observed Rpl

b_0 and b_1 = estimated parameters for the linear equation's intercept and slope.

C. Calculate the residuals based on Eqn. A.12 and the following

$$r_i = I_i - \hat{I}_i \qquad [A.13]$$

where,

$r_i = i^{th}$ residual

$I_i = i^{th}$ observed intensity

$\hat{I}_i = i^{th}$ predicted intensity

D. Locate the maximum residual.

E. Denote the Rpl associated with this maximum residual as the Rpl value at which total reflection occurs.

The above procedure is shown graphically in Figure 35.

Given the approximate critical angle as determined by the residual-method, we can proceed to refine on this approximation. First, a new data set is collected by scanning over a $\pm 5°$ (this $\pm 5°$ appears satisfactory but could be refined upon) Rpl range from the approximate critical angle at 0.01° increments. Next, the above steps are repeated to obtain a more accurate value for the critical angle. The residual method was tested on samples of quartz and calcite. The results appear in Table 11.

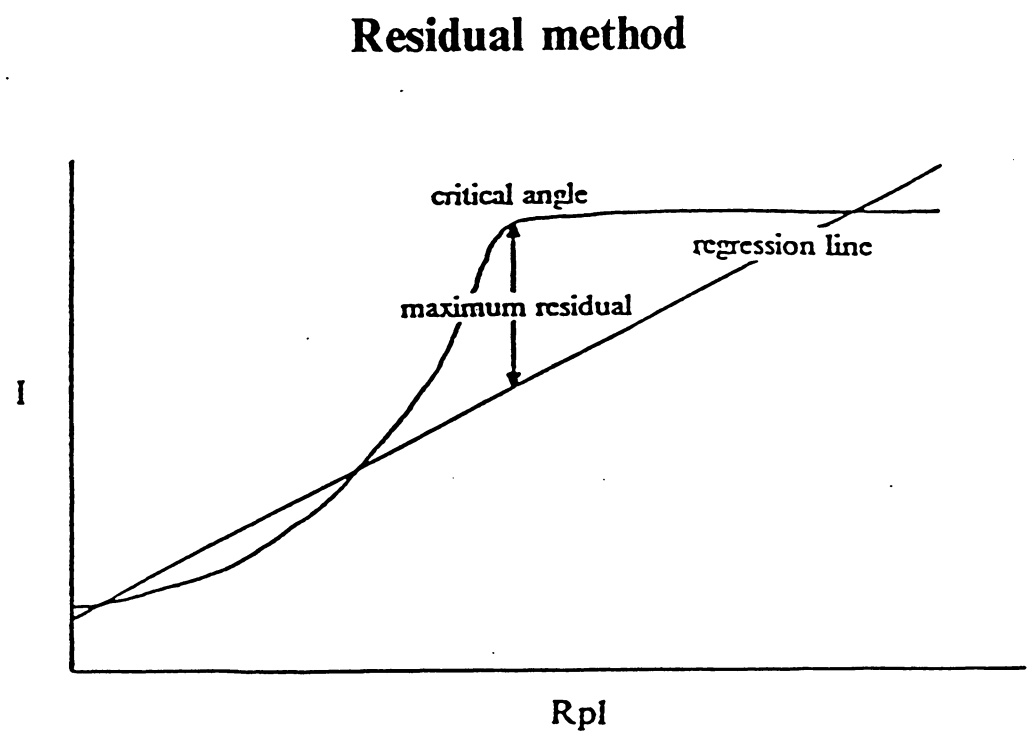

Figure 35. Graphical representation of the residual-method: The residual-method yields an approximate critical Rpl angle. A simple linear regression is performed on the Rpl-vs-I scan. From this analysis a straight line similar to the one in the above graph would result. The residuals for each Rpl value are calculated and the maximum residual corresponds to an approximate critical Rpl.

Table 11. **Refractive indices for quartz and calcite by the residual-method**

Polarizer Orientation	Quartz	Calcite
none	1.552	1.564
0°	$\omega = 1.544(-1)$*	$\omega = 1.656(0)$
30°	1.546	1.655
45°	1.549	1.564
60°	1.551	1.563
90°	$\varepsilon = 1.551(+1)$	$\varepsilon' = 1.562(0)$

* number in brackets represents actual minus - predicted value

** for quartz; $\omega = 1.543$, $\varepsilon = 1.552$: for calcite; $\omega = 1.656$, $\varepsilon' = 1.562$

The three page vita has been removed from the scanned document. Page 1 of 3

The three page vita has been removed from the scanned document. Page 2 of 3

The three page vita has been removed from the scanned document. Page 3 of 3